

**The E3 ligase CHIP as an initiator of cellular adaptation
during early proteostasis stress.**

Dissertation
zur Erlangung des Doktorgrades
der Naturwissenschaften

vorgelegt beim Fachbereich
Biochemie, Chemie und Pharmazie (FB14)
der Johann Wolfgang-Goethe Universität
in Frankfurt am Main

von
Yannick Kopp
aus Dudweiler Saarbrücken

Frankfurt 2018

(D30)

vom Fachbereich Biochemie, Chemie und Pharmazie (FB14)
der Johann Wolfgang-Goethe Universität als Dissertation angenommen.

Dekan: Prof. Dr. Clemens Glaubitz

Gutachter: Dr. Martin Vabulas
Prof. Dr. Volker Dötsch

Datum der Disputation: 29.05.2019

Abstract

All lifeforms have to sense changes in their environment and adapt to possibly detrimental conditions. On a cellular level, the highly elaborate proteostasis network (PN) consisting of housekeeping and stress-induced proteins, confers this tolerance against stress and maintains cellular protein homeostasis. This is essential for survival, as an accumulation of stress-induced protein aggregation will eventually affect the functionality of crucial cellular components and ultimately lead to cell death. The guardians of this balance are the molecular chaperones and their activity-regulating co-chaperones. They are engaged in all aspects of protein biogenesis, maintenance and degradation, especially during stress. The heat shock proteins (HSPs) are the major chaperones in mammals and encompass constitutive and stress-induced isoforms. Among them, the HSP70 and the HSP90 family are the most abundant HSPs and their activity is involved in a great variety of homeostasis and stress-induced tasks.

As part of the protein triage the E3 ligase CHIP (C-terminal HSC70-interacting protein) is an essential activity regulating co-chaperone of HSP70 and HSP90 which provides a link between chaperone mediated protein-folding and various degradation pathways. Due to its decisive function, CHIP is involved in a wide array of cellular processes, especially in clearing misfolded HSP70 client proteins that are prone to aggregate. As a consequence, CHIP was reported to confer protection against many aggregation-induced pathologies of the neuronal system. Additionally, CHIP has been identified as a critical factor in various types of cancer and is implied to affect the development and the longevity of mammals. Despite the significant progress in the understanding of CHIP's structure and function, many aspects surrounding its chaperone dependency and its substrate recognition remain unclear. Moreover, due to the variety of substrates in diverse cellular pathways, there are yet many connections to elucidate between CHIP and components of the cellular proteostasis network.

The work of this thesis was focused on the role of CHIP in acute stress response and the corresponding status of chaperone association. Moreover, it was investigated if CHIP, as the connecting ligase of folding and degradation systems, might also provide a link between the PN and the reorganisation of the cellular architecture upon stress exposure. This has become of increasing interest as recent reports highlight the importance of spatial sequestration in protein quality control.

To this end, subcellular distribution of CHIP was analysed by live-cell microscopy during heat stress. It became obvious that during the heat-induced challenge of the chaperone system, CHIP migrated to new cellular sites. Further experiments suggested that the observed migration to the plasma membrane is a chaperone-independent process and *in vitro* reconstitution of membrane association confirmed the competitive nature of membranes and chaperones for CHIP binding. A detailed *in vivo* and *in vitro* analysis of the newly observed membrane association of CHIP revealed a distinct lipid specificity and a novel direct association with lipids. Binding experiments with recombinantly purified deletion mutants of CHIP identified the TPR domain and a positive patch in the coiled-coil domain as main determinants for the lipid association. Through biochemical and biophysical approaches, the structural integrity and functionality of CHIP upon membrane binding was confirmed and further characterised.

Moreover, mass spectrometry analysis provided a high confidence identification of chaperone-free interactors of CHIP at the plasma membrane and other membranous compartments. In accordance with the lipid specificity, the Golgi apparatus was one of these sites. Only chaperone-free CHIP had a significant effect on the morphology of the organelle, again confirming the competitive role of chaperones and lipids. With respect to the physiological consequences of the changed localisation of CHIP, preliminary results indicated increased cell death when the ligase localises to cellular membranes. The results lead to the conclusion that CHIP acts as an initiator of early stress adaptation and as a sensor for the severity and strength of the stress reaction.

Zusammenfassung

Alle Lebewesen müssen Veränderungen in ihrer Umgebung wahrnehmen und widrigen Umständen ausweichen oder sich anpassen um zu überleben. Auf zellulärer Ebene ist diese Reaktion auf schädliche Stressfaktoren durch einen evolutionär stark konservierten Mechanismus gesteuert. Die zelluläre Stressreaktion wird durch stressinduzierte Proteine vermittelt, deren Homologe sich in allen Domänen der Lebewesen (Eucarya, Archaea, Bacteria) finden. Die Signalwege um eine Beeinträchtigung der zellulären Makromoleküle (Lipide, Proteine, DNS) zu erfassen und eine entsprechende Reaktion hervorzurufen sind komplex und zahlreich, weshalb sich diese Arbeit mit der Reaktion von Säugerzellen auf eine Beeinträchtigung des zellulären Proteomes beschäftigt.

In Säugerzellen überwacht ein kompliziertes Netzwerk, das sogenannte „proteostatische Netzwerk“, bestehend aus kooperativ-vernetzten Proteinen verschiedener Funktionalitäten, die Reaktion auf eine Beeinträchtigung der zellulären Proteine durch schädliche Einflüsse. Äußere Einflüsse, wie Temperatur, Strahlung, toxische Agenzien oder eine Fehlfunktion des „proteostatischen Netzwerks“, können die Stabilität von Proteinen in der Zelle zerstören oder deren empfindliche Synthese beeinträchtigen. Dadurch kann es zu einer Akkumulation von toxischen Proteinaggregaten kommen, die die Funktionen der Zelle stören und schlussendlich zu ihrem Tod führen können. Die Ursache vieler neurodegenerativer Erkrankungen ist in einer Akkumulation solcher toxischer Proteinaggregate zu finden. Bedingt wird dies häufig durch eine verringerte Kapazität oder Fehlfunktion der Proteinqualitätskontrolle des „proteostatischen Netzwerks“, wie sie mit dem Altern von Organismen oder in diversen Pathologien einhergeht. In vielen Formen von Krebs ermöglicht eine Hyperaktivität der Proteinqualitätskontrolle in Tumorzellen deren Überleben und Verbreitung, trotz der andernfalls nachteiligen Umgebungsumstände im Tumor oder in Metastasen.

Die zentralen Knotenpunkte des „proteostatischen Netzwerks“ sind die Chaperone. Diese speziellen Proteine überwachen und erhalten das Gleichgewicht zwischen Synthese und Abbau, sowie die strukturelle Unversehrtheit zellulärer Proteine. Chaperone ermöglichen die dreidimensionale Faltung neusynthetisierter Proteine, verhindern unspezifische Interaktionen ihrer Substrate mit anderen Bestandteilen des Zytosols und halten fehlgefaltete oder beschädigte Proteine in einem metastabilen Zustand, indem sie entweder ihre native Struktur wiedererlangen können oder an zelluläre Abbaumaschinerien weitergeleitet

werden können. Die größte Gruppe von Chaperone sind die sogenannten „heat shock proteins“ (HSP), die entsprechend ihrem Molekulargewicht in die Familien HSP40, HSP60, HSP70, HSP90 und HSP110 klassifiziert werden.

Die Mitglieder der HSP70 und HSP90 Familie bilden den Großteil der HSPs in Säugern, wobei HSP70s ubiquitär vorhanden sind und unterschiedliche Funktionen erfüllen. HSP90 ist hauptsächlich an der Bildung der nativen Struktur und der Aktivierung von Substratproteinen beteiligt. Die dreizehn Mitglieder der HSP70 Familie bilden den Großteil der HSPs im Menschen und erfüllen eine Vielzahl von Funktionen in der Proteinsynthese, Komplexbildung, Qualitätskontrolle, dem Proteintransport und der Stressreaktion. Die stressinduzierten Isoformen HSPA1A und HSPA1B sind die am häufigsten exprimierten Chaperone unter Stressbedingungen und reduzieren die Bildung von toxischen Aggregaten. Um diese Vielfalt an Funktionen zu bewältigen, interagieren HSPs mit einer Vielzahl von Co-chaperonen, die Substrate identifizieren oder die Aktivität des Chaperons regulieren, um die weitere Prozessierung entsprechend zu steuern. Kann ein Chaperonsubstrat seine native Struktur nicht einnehmen, wird es an Abbaumaschinerien weitergeleitet. Eine dieser Abbausysteme ist das Ubiquitin-Proteasome-System (UPS), in dem nicht-funktionale oder irreparabel beschädigte Proteine vom 26S Proteasom in kleine Peptide abgebaut werden. Um das Substratprotein an das Proteasome weiterzuleiten, interagiert das Chaperon mit substratspezifischen E3 Ubiquitinligasen, die in einer zyklischen Reaktion zusammen mit zwei weiteren Enzymen (E1: Ubiquitin aktivierendes Enzyme und E2: Ubiquitin konjugierendes Enzym) das Signalprotein Ubiquitin, über eine Isopeptidbindung, an ein Lysin des Substratproteins binden. Der zyklische Ablauf dieser Reaktion erzeugt Polymerketten aus Ubiquitin, deren spezifisches Verknüpfungsmustern als Signal für die weitere Prozessierung dient.

CHIP (C-terminal HSC70-interacting protein) ist ein Co-chaperon von HSP70 und HSP90, das im Zytosol der meisten Säugerzellen exprimiert wird. Aufgrund seiner Aktivität als E3 Ligase stellt es den zentralen Verbindungspunkt zwischen der chaperon-gesteuerten Proteinfaltung und verschiedenen zellulären Abbausystemen dar. Aufgrund seiner zentralen und entscheidenden Position in der Proteinqualitätskontrolle, konnte eine regulatorische Funktion von CHIP in diversen zellulären Prozessen wie Autophagie, Signaltransduktion, Apoptose, Seneszenz und der Entwicklung von Organismen nachgewiesen werden.

CHIP ist von besonderer Bedeutung in der Stressreaktion, da es essenziell für den Abbau von potenziell aggregierenden und partiell entfalteten Proteinen ist. Daher ist es nicht verwunderlich, dass eine protektive Funktion von CHIP gegen neurodegenerative Erkrankungen, wie Parkinson und Alzheimer, gezeigt werden konnte. Außerdem konnte CHIP als kritischer Faktor in vielen Krebsarten identifiziert werden, der Verlauf und Bösartigkeit der Tumore maßgeblich beeinflussen kann. Aufgrund dessen ist CHIP ein vielversprechender Kandidat für zukünftige therapeutische Ansätze zur Bekämpfung

lebensbedrohlicher Krankheiten.

Trotz zahlreicher Fortschritte in der Strukturaufklärung und Funktionsweise von CHIP bleiben viele Fragen über seine regulatorischen Funktionen in diversen zellulären Prozessen, sowie seine Abhängigkeit von der Assoziation mit HSP70/90 ungeklärt. Neuere Forschungen deuten auf eine zusätzliche chaperon-unabhängige Funktion von CHIP in der Qualitätskontrolle bestimmter Substrate hin. Diese Funktion könnte von besonderer Bedeutung bei einer Stressreaktion der Zelle sein, bei der das Chaperonsystem mit dem steigenden proteotoxischen Druck ausgelastet ist, wie etwa bei diversen humanen Krankheiten oder dem Alterungsprozess.

In dieser Arbeit wurde deshalb die Rolle von CHIP während akuter Stressbelastung, im Hinblick auf Chaperonassoziation und im Besonderen auf die subzelluläre Lokalisation der E3 Ligase während der Stressexposition, untersucht. Die subzelluläre Lokalisation ist von großer Bedeutung, da jüngste Studien der räumlichen Separation bei der Bewältigung von proteotoxischem Stress hohe Bedeutung beimessen. Es erscheint sinnvoll anzunehmen, dass CHIP aufgrund seiner Substratvielfalt in diversen zellulären Prozessen und seiner verbindenden Funktion von Proteinfaltung und Abbau, auch eine Verbindung zur Stressadaptation zellulärer Strukturen darstellt. Dabei wurde von der Hypothese ausgegangen, dass Chaperone unter akuter Stressbelastung destabilisierte Proteine binden, um deren Aggregation zu verhindern oder abzuschwächen. Folglich würde ein Teil der gebundenen regulatorischen Proteine, wie CHIP, dissoziieren und eine kompartiment-spezifische Bindung an anderen Lokalisationen in der Zelle ermöglichen. Das neue kompartiment-spezifische Interaktom könnte dann, hinsichtlich einer Stressadaptation, modifiziert werden oder es könnten andere Signalwege, wie beispielsweise die Apoptose, initiiert werden.

In Übereinstimmung mit dieser These konnte, mithilfe von Live-cell Imaging, eine neue Lokalisation von CHIP an der Plasmamembran von hitzestressexponierten Zellen beobachtet werden. Es konnte gezeigt werden, dass diese Migration von einem Chaperondefizit abhängig ist, da die Co-expression zusätzlicher Chaperone die Lokalisation an die Membran inhibierte. Des Weiteren lösten eine spezifische Inhibition von HSP70 und HSP90 dieselbe Lokalisationsveränderung aus. Eine CHIP Mutante (CHIP-K30A), die eine stark verringerte Affinität zu HSP70 aufweist, zeigte unter physiologischen Bedingungen ebenfalls eine subzelluläre Lokalisation an der Plasmamembran. Die verringerte Affinität von CHIP-K30A zu HSP70 konnte in ITC Experimenten bestätigt werden. Außerdem konnten eine Destabilisierung der Sekundärstruktur der Mutante mittels CD Spektroskopie und Schmelzpunktbestimmung ausgeschlossen werden.

Eine *ex vivo* Fraktionierung konnte eine Membranlokalisation eines Teils des zellulären CHIP pools, auch unter physiologischen Bedingungen, bestätigen. Weiterführende Crosslinking Experimente unter Zusatz des C-terminalen HSP70 Peptides zeigten außerdem, dass ein Teil des membranlokalisierten endogenen CHIPs nicht an ein Chaperon

gebunden ist. Diese Ergebnisse legen eine neuartige direkte Assoziation von CHIP mit der Membran nahe.

In Lipid Overlay Experimenten konnte eine Lipidspezifität für Phosphatidsäure (PA) und Phosphatidylinositol-4-phosphat (PI4P) nachgewiesen werden. CHIP-K30A zeigte dieselbe Spezifität wie das Wildtyp Protein, wodurch eine mutationsinduzierte Lipidspezifität ausgeschlossen werden konnte. Beide Lipide sind in der Plasmamembrane von Säugerzellen zu finden. Eine Modulation der jeweiligen Lipidlevel *in vivo*, durch Inhibition ihrer Synthesewege, initiierte eine Relokalisation von CHIP-K30A ins Zytosol. Mithilfe von PA und PI4P enthaltenden Liposomen konnte die Lipidbindung *in vitro* rekonstruiert werden. In Bindungsexperimenten an Liposomen und Lipid-strips konnte durch die Zugabe von HSP70 erneut der kompetitive Charakter der Assoziation von CHIP mit Lipiden und Chaperonen bestätigt werden. Durch massenspektrometrischen Vergleich des Interaktoms von membranlokalisiertem CHIP-K30A und des durch Inhibitorzugabe ins Zytosol relokalierten CHIP-K30As konnte die mikroskopisch beobachtete Lokalisationsänderung bestätigt werden. Darüber hinaus konnte ein erstes Interaktom von membrangebundenem CHIP identifiziert und quantifiziert werden.

Um die Determinante der Lipidinteraktion in CHIP zu identifizieren, wurden Deletionsmutanten in Bindungsexperimenten mit Liposomen eingesetzt. Dabei zeigte sich, dass die TPR Domäne von essentieller Bedeutung für die Bindung an Lipide ist. Zusätzlich konnte ein positiv geladener Bereich (m2) in der coiled-coil Domäne von CHIP identifiziert werden, der ebenfalls zu Lipidbindung von CHIP beiträgt. Der exakte Mechanismus der Interaktion, sowie in welchem Maße die TPR Domäne und m2 Lipidspezifität vermitteln, bleibt jedoch unklar.

Durch biochemische und biophysikalische Methoden, konnte die Bindung von CHIP an Liposome weiterführend charakterisiert werden und die Resultate deuten auf eine transiente Assoziation hin, die die Struktur und Aktivität von CHIP nicht beeinträchtigt. Vorläufige Ergebnisse zur Oligomerisierung von CHIP konnten Tetramere und Hexamere in Lösung identifizieren. Eine membranabhängige Akkumulation höherer Oligomere wurde ebenfalls beobachtet, bedarf allerdings weiter Verifikation. Die Aktivität als Ubiquitinligase wurde durch die Liposombindung nicht signifikant beeinträchtigt. Es konnte jedoch gezeigt werden, dass eine Beeinträchtigung der nativen Struktur von NOQ1, einem natürlichen Substrat von CHIP, zu einer erhöhten Ubiquitylierung mit K48 Ubiquitinketten, in Abhängigkeit von der spezifischen Assoziation von CHIP mit PA versetzten Liposomen, führte.

Im Hinblick auf die physiologischen Konsequenzen der stressinduzierten Membranlokalisierung von CHIP wurde der Einfluss auf den Golgi-Apparat untersucht, da dieser sich durch eine hohe Konzentration von PI4P auszeichnet. Chaperon-freies CHIP fragmentierte die Cristae des Golgi-Apparats, während Co-expression von HSP70 die Fragmentierung inhibierte. Dies bestätigt erneut die Kompetitivität der Bindung von Chaperonen

und Lipiden an CHIP. Eine Fragmentierung des Golgi-Apparats steht oft in Verbindung mit Apoptose, weshalb ein dahingehender Einfluss von CHIP untersucht wurde. Tatsächlich zeigten CHIP knock-out Zelllinien eine erhöhte Resistenz gegen hitzeinduzierten Zelltod, während eine Expression des membranlokalisierten CHIP-K30A zu erhöhtem Zelltod führte. Ein weiterer Hinweis auf eine Verbindung von membranlokalisiertem CHIP und dem programmierten Zelltod, war die Migration von CHIP zur Plasmamembran unter Staurosporin Behandlung. Staurosporin ist ein bakterieller Wirkstoff, der als Initiator für Apoptose bekannt ist.

Zusammenfassend konnte eine neue Interaktion von CHIP mit spezifischen Lipiden gezeigt werden, die der Chaperonbindung kompetitiv gegenübersteht. Diese Interaktion wird durch eine temporäre Auslastung des Chaperonsystems erzeugt, wodurch CHIP dissoziiert und die lipidbindenden Eigenschaften der TPR Domäne freigesetzt werden. Dies eröffnet CHIP den Zugang zu kompartiment-spezifischen Interaktomen, die entsprechend der Stärke der Stressreaktion modifiziert werden können.

Acknowledgements

First of all, I would like to thank Dr. Martin Vabulas for giving me the opportunity to do my PhD in his laboratory and being an excellent supervisor. I gratefully acknowledge his scientific guidance and generous support during my thesis. His open-minded character and enthusiasm about science generated an inspiring atmosphere which greatly benefited my work. Moreover, I want to thank him for the many opportunities to follow new ideas and learn new techniques, as well as the chance to participate at the exciting EMBO conference "Protein quality control: Success and failure in health and disease" 2017 in Girona and the Frankfurt Conference on Ubiquitin and Autophagy 2016.

I am especially grateful for the work of Dr. Giulia Calloni. Her processing and analysis of my mass spectrometry data greatly advanced my work and enabled the final publication. Special thanks go to Dr. Robert Ernst and his group for their introduction to liposome preparation. I am much indebted to Dr. Harald Hofbauer for the support in measuring my liposomes at the NanoSight and the continuous helpful discussions on lipids and liposomes.

Further, I want to thank Dr. Nina Morgner for the opportunity to explore CHIP oligomers with native mass spectrometry. Thanks go to Mr. Kudratullah Karimi for his readiness and time to measure my samples.

I also want to thank Dr. Tobias Schuster for this initial introduction at the start of my thesis and the plasmids I could continue to use for my work. In this regard, I want to mention Wei-Han Lang for providing the knockout cell lines and additional plasmids.

I am equally grateful for the pleasant working atmosphere generated by the other members of the Vabulas group. I much appreciated the enjoyable conversations and scientific discussions with Marion Alriquet, Adrian Martínéz-Limon and Haotian Wang.

Last, I am thankful for the support of my parents and my girlfriend who always had time and patience to help me through struggles and motivated me throughout the entire time.

Contents

Abstract	I
Zusammenfassung	III
Acknowledgements	VIII
1 Introduction	1
1.1 The cellular stress response	1
1.2 The role of chaperones during folding and heat shock response	5
1.2.1 Heat shock protein 70 structure and function	7
1.2.2 Heat shock protein 90 structure and function	10
1.3 The ubiquitin-proteasome-system	12
1.3.1 Ubiquitin	12
1.3.2 Ubiquitylation cascade	14
1.3.3 E3 ligases	16
1.4 The E3 ligase CHIP	18
1.4.1 Canonical and non-canonical activity of CHIP	18
1.4.2 CHIP structure	22
1.4.3 CHIP regulation	26
1.4.4 CHIP in physiology and disease	27
1.5 Objectives of this thesis	29
2 Material and Methods	31
2.1 Materials	31
2.1.1 Chemicals	31
2.1.2 Equipment	33
2.1.3 Kits	34
2.1.4 Plasmids and primer	34
2.1.5 Cell lines and bacteria strains	36
2.1.6 Inhibitors	36
2.1.7 Lipids	36
2.1.8 Media, buffers and solutions	37
2.1.9 Special consumables	39

2.1.10	Antibodies	40
2.2	Methods	41
2.2.1	Cloning	41
2.2.2	Cell culture and transfection	41
2.2.3	Confocal fluorescence microscopy	44
2.2.4	Brightfield microscopy	45
2.2.5	TIRF microscopy	45
2.2.6	Immunofluorescence	45
2.2.7	Fluorescence-activated cell sorting (FACS)	46
2.2.8	SDS-PAGE and immunoblotting	46
2.2.9	Recombinant protein purification	46
2.2.10	Subcellular fractionation and chemical crosslinking	48
2.2.11	Liposome preparation	48
2.2.12	Nanoparticle tracking analysis	49
2.2.13	Liposome leakage assay	49
2.2.14	Lipid binding assay	50
2.2.15	Preparation of lipid strips	50
2.2.16	Flotation assay	50
2.2.17	Co-sedimentation assay	51
2.2.18	Chemical crosslinking <i>in vitro</i>	51
2.2.19	<i>In vitro</i> ubiquitylation assay	51
2.2.20	CD spectroscopy	52
2.2.21	Protease sensitivity assay	52
2.2.22	Isothermal titration calorimetry	52
2.2.23	Thermal denaturation assay	52
2.2.24	Secreted placental alkaline phosphatase assay	53
2.2.25	Luciferase reporter assay	53
2.2.26	XTT cell proliferation assay	53
2.2.27	Mass spectrometry	54
3	Results	56
3.1	Chaperone-free CHIP interacts with cellular membranes <i>in vivo</i> and <i>ex vivo</i>	56
3.2	Lipid specificity of CHIP	63
3.3	Contact interfaces for lipid binding	71
3.4	CHIP structure and stability on membranes	75
3.5	CHIP oligomerization on membranes	78
3.6	CHIP activity on membranes	82
3.7	Physiological consequences of CHIP association with membranes	88
3.7.1	CHIP influences cellular architecture	88

3.7.2	Membrane localisation of CHIP is linked to cell survival	92
4	Discussion	95
4.1	Research question and working hypothesis	95
4.2	Chaperone independent CHIP recruitment to cellular membranes	96
4.3	Structural determinants for CHIP binding to membranes	102
4.4	Physiological implications of CHIP localisation to cellular membranes . .	106
5	Appendix	130
5.1	Vector maps	130
5.2	Recombinant Protein Purifications	132
5.3	FACS	134
5.4	Microscopy quantification	135

Abbreviations

ATP	Adenosine triphosphate
BMLS	Buchmann Institute for Molecular Life Science
CD	Circular dichromatism
ER	Endoplasmatic reticulum
ESI	Electronic spray ionisation
HBSS	Hanks's buffer saline solution
HSP	Heat shock protein
HSR	Heat shock response
LB	Lysogeny broth
m/z	Mass-per-charge ratio
MEF	Murine embryonic fibroblasts
MS	Mass spectrometry
OD	Optical density
PN	Proteostasis network
RT	Room temperature
SD	Standard deviation
SDS	Sodium dodecyl sulphate
SEC	Size exclusion chromatography
TIRF	Total internal refelction fluorescence
UPR	Unfolding protein response
v/v	Volume per volume
w/v	Weight per volume
WT	Wild-type

List of Figures

Fig.1	The proteostasis network	4
Fig.2	The ATP-driven HSP70 cycle	8
Fig.3	The HSP90 cycle	11
Fig.4	The ubiquitin chain diversity	13
Fig.5	The ubiquitylation cascade	15
Fig.6	Structures and mechanisms of E3 ligases	18
Fig.7	Chaperones and CHIP mutually influence their activity	22
Fig.8	CHIP sequence alignment	23
Fig.9	Crystal structures of the symmetric and asymmetric CHIP dimer	25
Fig.10	The impact of CHIP on various diseases	29
Fig.11	Heat stress induces CHIP mobilisation to cellular membranes <i>in vivo</i>	56
Fig.12	HSP70 and HSP90 deficiency induces CHIP localisation to membranes	57
Fig.13	Chaperone abundance is linked to CHIP localisation <i>in vivo</i>	58
Fig.14	Arsenite treatment does not mobilise CHIP to membranes	59
Fig.15	CHIP localisation during severe starvation	59
Fig.16	A fraction of endogenous CHIP resides at membranes as chaperone-free dimer	60
Fig.17	CHIP-K30A resembles CHIP-WT structurally but not functionally	61
Fig.18	EGFP-CHIP-K30A localises to the plasma membrane of MEF cells	62
Fig.19	Distribution of EGFP-CHIP-K30A on the plasma membrane	63
Fig.20	CHIP specifically binds to a subset of cellular phospholipids	63
Fig.21	CHIP binds to phosphatidic acid spotted on nitrocellulose supported membranes	64
Fig.22	CHIP binds to liposomes spiked with phosphatidic acid (PA) and phosphatidylinositol-4-phosphate (PI4P).	65
Fig.23	CHIP binding to mixed liposomes	66
Fig.24	Depletion of PA and PI4P causes undocking of EGFP-CHIP-K30A from cellular membranes	67
Fig.25	Interactome of chaperone-free CHIP at cellular membranes	68
Fig.26	CHIP association to lipids is impaired by C-terminal HSP70 octapeptide	69
Fig.27	C-terminal HSP70 blocks CHIP association with liposomes	70
Fig.28	TPR domain mediates CHIP binding to lipids	71

Fig.29	The TPR domain is a determinant for liposome association of CHIP	72
Fig.30	Isolated TPR domain displays reduced global secondary structure upon liposome association	72
Fig.31	A positively charged patch in the middle domain is required for CHIP binding to membranes <i>in vivo</i>	73
Fig.32	m2 mutation affects binding of CHIP to specific phospholipids <i>in vitro</i> . .	74
Fig.33	Wild-type CHIP-m2Δ <i>in vivo</i> and <i>in vitro</i>	75
Fig.34	CHIP binding to liposomes is size dependent and does not induce fission or fusion of liposomes.	76
Fig.35	Characterisation of CHIP structure on liposomes	77
Fig.36	CHIP can not be released from liposomes by increasing ionic strength . . .	77
Fig.37	Oligomerization of CHIP in solution	79
Fig.38	Deoxycholate-induced oligomerization of CHIP	80
Fig.39	CHIP effects on membrane permeability <i>in vitro</i>	81
Fig.40	NF-κB activation is not influenced by CHIP-mediated K63 ubiquitylation .	83
Fig.41	CHIP maintains its ubiquitylation activity on liposomes	84
Fig.42	CHIP binding to lipids is enhanced by the presence of misfolded proteins .	85
Fig.43	CHIP ubiquitylates heat-treated BSA independently of lipids	86
Fig.44	CHIP ubiquitylates unfolded proteins on PA-containing liposomes	87
Fig.45	Label-free quantitative mass spectrometry shows specific proteome changes in MEFs upon overexpression of CHIP	88
Fig.46	Chaperone-free CHIP distorts Golgi morphology	89
Fig.47	Excessive HSP70 rescues Golgi apparatus from CHIP-induced distortion .	90
Fig.48	Overexpression of CHIP impairs SEAP secretion in MEF cells	91
Fig.49	The presence of CHIP negatively influences cell viability in MEF cells exposed to heat stress	92
Fig.50	Induction of apoptosis correlates with the plasma membrane localisation of CHIP in MEF cells	93
Fig.51	Membrane-localised CHIP-K30A induces cell death in Hek293T	94
Fig.52	Bacterial expression vectors	130
Fig.53	Mammalian expression vectors	131
Fig.54	Purification of GST-CHIP	132
Fig.55	Purification of GST-CHIP-K30A	132
Fig.56	Purification of the E2 Ube2W	133
Fig.57	Purification of HSP70	133
Fig.58	Purification of C-terminal HSP70	133
Fig.59	Cell death in CHIP transfected Hek293T	134
Fig.60	FACS sorting for MS interactome analysis of CHIP	134

List of Tables

Tab.1	Reagents	31
Tab.2	Laboratory equipment	33
Tab.3	Preparation and assay kits	34
Tab.4	Plasmids	34
Tab.5	Primer	35
Tab.6	Mammalian cell lines and bacteria strains	36
Tab.7	Inhibitors	36
Tab.8	Lipids	36
Tab.9	Media and ready-to-use solutions	37
Tab.10	Established Buffers	37
Tab.11	Resins and Columns	39
Tab.12	Membranes and Tools	40
Tab.13	Primary and secondary antibodies	40
Tab.14	Average cell numbers for quantification	135

Introduction

1.1 The cellular stress response

Organisms have to constantly sense and adapt to changes in their environment. If the conditions are excessive and detrimental, organisms need to increase their stress tolerance to survive. On a cellular level, this is realised by a strongly conserved mechanism, referred to as the cellular stress response [1]. It describes the defence reaction of cells, which monitors stress by two general principles: The degree of damage inflicted on macromolecules and the changes in the cellular redox-state. Thus, the cellular stress response is activated rather independent of the specific character of an environmental signal. Accordingly, it is not surprising that all cells in the three super-kingdoms of life (eukaryotes, bacteria and archaea) express stress-induced proteins and share a conserved set of proteins involved in key aspects of stress response. These key aspects mainly encompass the assessment and counter-action on a perturbation of membrane lipids, protein integrity, DNA damage, increase of reactive oxygen species and alteration of energy metabolism. The capacity of the cellular stress response is determined by the cell-specific proteome, which can also provide specificity depending on the type of damage inflicted on proteins, membranes or DNA [1]. In case of excessive stress, cells which are irreversibly damaged initiate a programmed cell death (apoptosis). This principle is especially important for multicellular organisms who can tolerate a certain threshold of cell death in exchange for the functional preservation of higher levels of biological organisation (e.g. tissues, organs) [2]. The details of pathways for sensing and adapting the reaction to damaged membranes, DNA and proteins are numerous and this study will focus on the response of mammalian cells to a disruption of protein integrity.

The proteome of an individual mammalian cell encompasses about 10,000 different functional proteins which are not only sensitive to stress-induced alterations, but have to overcome adverse conditions during synthesis. The nascent polypeptide chain, emerging from the ribosome, needs to attain a distinct three-dimensional structure in order to yield a biologically functional protein [3]. However, this folding process is intrinsically error-prone, as protein sequences are evolutionary selected by their functionality, not only by the sta-

bility of their folding-process. Thus, especially larger, multi-domain proteins have to navigate a complex thermodynamic energy landscape until they acquire their native structure [4]. The resulting folding intermediates are prone to expose hydrophobic residues to the solvent, rendering them susceptible for non-native interactions that have the propensity to accumulate into insoluble aggregates [3]. This is further enhanced *in vivo* by the protein density of the cytosol (300 to 400 g of total protein per litre in the cytosol), leading to a high probability of erroneous binding of the partially folded proteins to other cytosolic components [5]. The accumulation of such aggregates can tip the balance of protein homeostasis (proteostasis) and will eventually affect the functionality of crucial components in the cell and ultimately lead to a proteostatic collapse and cell death [6]. Thus, it is essential for cell survival to protect proteins during folding and continuously monitor the structural and functional integrity of the proteome. The proteostasis network (PN) is a highly elaborated system encompassing about 2,700 different, cooperating proteins which preserve the proteostasis in face of intrinsic or environmental stress [7].

Failure or imbalance of the proteostasis network by endogenous misfolding or exterior stress is involved in many human diseases. Especially during ageing, the capacity of the PN is thought to decline, which leads to an increasing accumulation of toxic aggregates and subsequently to the dysfunction of specific cell types and tissues [8]. This has become of increasing relevance in the understanding of neurodegenerative diseases like Parkinson's, Huntington's and Alzheimer's. A hallmark of these diseases is the accumulation of amorphous or amyloid-like aggregates that have been linked to onset and progression of the diseases [9]. In many types of cancer the PN is hyperactive in terms of the preservation of protein integrity, promoting the survival and proliferation of tumour and metastatic cells in an otherwise adverse environment. It is thus inevitable to gain a deeper understanding of the PN components and their interconnected regulation, in order to understand the network as a whole and to find targets for therapeutic approaches.

The central nodes of this system are the molecular chaperones and their regulating co-chaperones, participating in all aspects of protein biogenesis, maintenance and degradation. They assist kinetically trapped folding intermediates in acquiring their native structure and prevent the accumulation of misfolded proteins. Chaperones keep the client protein in a meta-stable state and cooperate with a variety of co-chaperones and cofactors to refold the client into its native state or, if misfolding is irreversible, recruit degradation machineries in order to dispose the potential harmful client agglomerates.

One of these degradation pathways is the ubiquitin-proteasome system (UPS), which is characterised by the proteolysis of non-functional or misfolded proteins through the 26S proteasome. The UPS is a cooperative pathway in which chaperones interact with ubiquitin ligases to recognize and target a client protein for proteasomal degradation. This is realized through the attachment of a variety of polymeric chains of ubiquitin, a small protein ubiquitously found in all eukaryotic organisms [10] [11].

These ubiquitin chains are then recognized by the 19S subunit of the 26S proteasome. The 20S subunit subsequently cleaves the misfolded protein into short peptides.

However, the UPS is mainly restricted to proteins that are kept in a partially folded state by chaperones. Already aggregated proteins are disposed by various, chaperone-dependent and -independent pathways of autophagy and lysosomal degradation. In general, the target aggregate or cell compartment is enclosed by a the phagophore membrane, which forms the vesicular autophagosome. By fusion with a lysosome, the autophagosome content is disassembled by the low pH of the lysosome lumen [12].

In addition to the classical containment and disposal of misfolded proteins by the UPS and autophagy, there is growing evidence that spatial sequestration of misfolded protein species, is an essential feature of cellular quality control, especially under stress conditions [13]. Inclusions are a hallmark of neurodegenerative diseases and were thought to be detrimental for cell survival. However, the recent understanding suggests that this sequestration to resiticted locations within the cell can be beneficial for cell survival in a number of settings. The local concentration restricts the propensity of misfolded proteins to interfere with native cell physiology and facilitates terminal degradation or secretion to the extracellular milieu. Misfoled proteins and insoluble aggregates are directed to a diverse range of compartments, like the aggresome, Q-bodies and the JUxtaNuclear Quality control (JUNQ) compartment. The active sorting process is mediated by chaperones (in mammals mostly by members of the HSP70, HSP90, HSP110 families) and their co-chaperones, which might play an important role in target recognition and determination of the terminal fate of the misfolded substrates [14]. The concept is supported by research results of the asymmetric distribution of inclusions between mother and daughter cell, rejuvenating the daughter cell by removal of the potentially harmful material [15]. Growing evidence suggests an involvement of cellular structures, like the cytoskeleton and organelles in the sequestration process, even though regulation and effects on cellular fate remain largely unknown [16] [14].

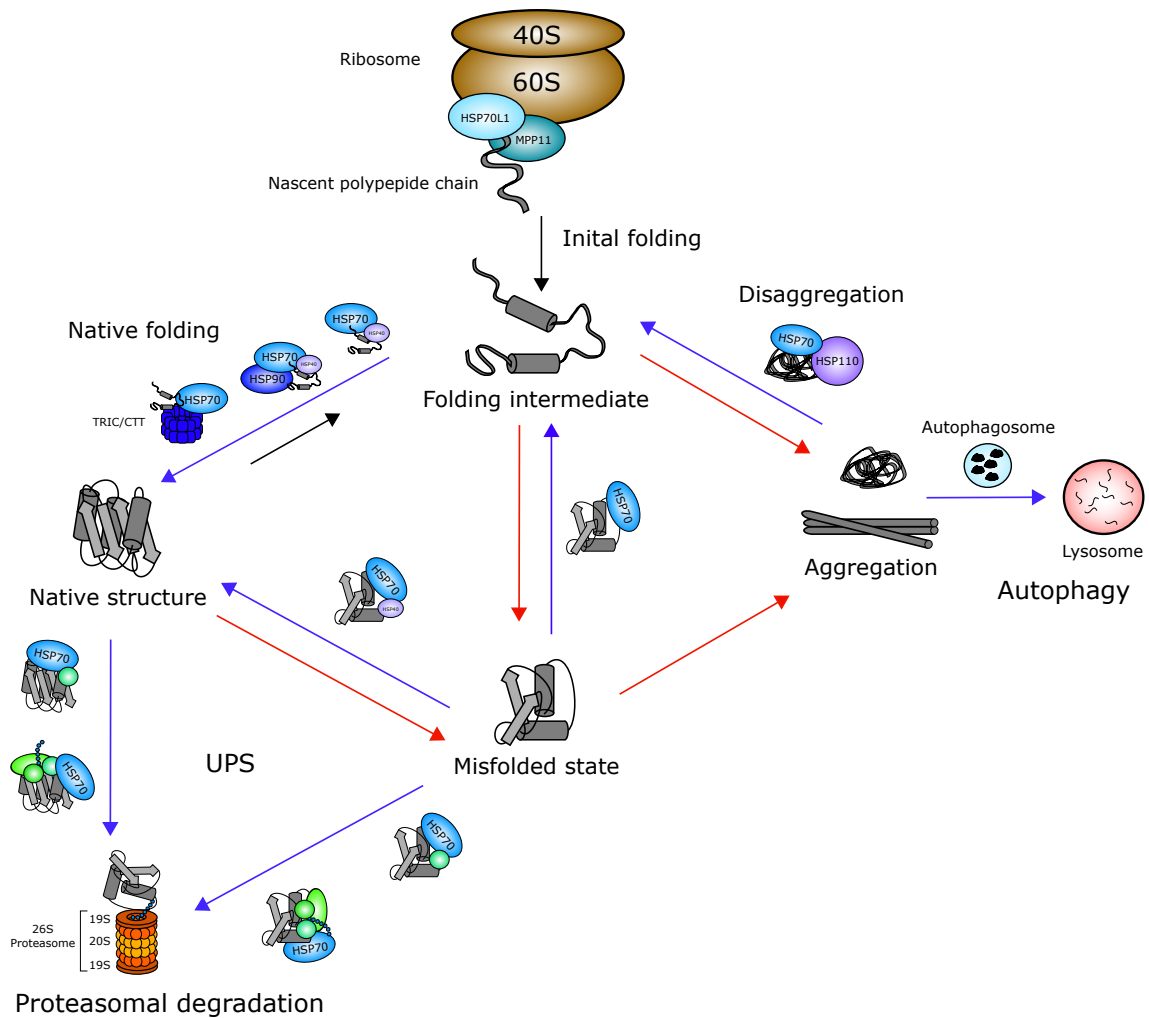


Figure 1. The proteostasis network monitors and maintains the functionality of the cellular proteome. Generalized depiction of the PN components in protein folding and degradation, starting with protein (grey) synthesis at the ribosome (brown). Blue arrows indicate chaperone assisted pathways, with examples of participating components in mammalian cells (chaperones in blue and violet). Arrows in red indicate undesirable pathways induced by intrinsic or environmental stress and fostering aggregation. The ubiquitin proteasome system (UPS) for native and misfolded proteins encompasses proteasomal degradation in a chaperone-assisted manner together with the E1-E2-E3 ubiquitylation complex (green). A second pathway of degradation encompasses several versions of autophagy in clearance of aggregates.

1.2 The role of chaperones during folding and heat shock response

Molecular chaperones are a key for maintenance of cellular homeostasis. They interact with a client protein during translation, help it to acquire its final structure by bridging energetically unfavoured folding intermediates and shield it from nonspecific interactions with surrounding cytosolic components. After folding is completed, they disembark yielding the native functional protein [3]. This is especially true for proteins of low abundance, which are frequently prone to misfold or aggregate while proteins of essential function have an evolutionary reduced need for chaperone mediated folding. Accordingly, it has been postulated that chaperones also act as a buffer on protein evolution, stabilizing proteins of potential functionality but reduced stability occurring due to spontaneous mutations [17].

When the nascent polypeptide chain emerges from the ribosome exit channel it can not immediately assume proper folding, as it underlies sterical and temporal restrictions by the translation process. Residues needed for folding of a protein domain might still be within the ribosome exit-channel and thus are not available for folding. Therefore ribosome binding chaperones receive the emerging polypeptide chain and prevent intra- and intermolecular, non-specific interactions. In mammals the nascent polypeptide-associated complex (NAC) receives the emerging polypeptide. MPP11 and HSP70L1 are examples of this first line of assistance by chaperones (Fig.1) [18].

In the co- or post-translational *de novo* folding process, intermediate structures are engaged by various chaperones of the HSP70 family (DnaK in bacteria, Ssa1–4 in yeast and HSC70 in mammals). If the native structure can not be obtained, the HSP70 chaperone system is cooperatively linked to downstream chaperones like HSP90 and chaperonins to finalize folding and activation of the client protein [3]. HSP90 is a conformationally flexible, ATP-driven machinery that assists in the assembly and activation of its clients. Chaperonins like GroEL in bacteria and the tailless complex polypeptide-1 ring complex (TRiC) in eukaryotes, are large double-ring complexes with a central cavity, which provide an isolated space for the folding of a specialized subset of proteins (TRiC: 5 %-10 % of eukaryotic proteins) (Fig.1) [19].

In addition to their translational folding capability, chaperones maintain protein structure especially under environmental stress conditions such as heat stress. Elevated temperatures destabilize the tertiary structure of proteins by disrupting hydrogen bonds and electrostatic interactions, increasing the propensity of mis- or unfolding and subsequent accelerate aggregation [20].

Cells react to this disturbance of proteostasis, not specifically to a change in temperature. Thus, their countermeasure commonly termed heat shock response (HSR) is an universal mechanism that can be applied to all sorts of stresses that elevate protein unfolding, such as heavy metal exposure, nutrient deprivation, infections and inflammation [21].

The HSR and the associated chaperones are a conserved machinery that can be found in all domains of life from archaia to mammals [1]. On a cellular level heat stress affects not only protein structures but also nuclear processes, leading to an accumulation of incorrectly processed mRNAs which aggregate together with associated proteins in the cytosol, forming stress granules. This corresponds to a decrease in overall translation, an early hallmark of the heat shock response [22]. Additionally, cellular structures are destabilized as increasing temperatures change membrane morphology and composition, enhancing membrane permeability and fission [23][24].

To compensate these multiple disruptions of homeostasis, cells enhance the expression of stress induced chaperones, especially chaperones of the heat shock protein (HSP) family, named after their initial discovery in heat-stressed *Drosophila melanogaster* in 1960 [25] [26]. Heat shock proteins are among the most conserved protein families in evolution, comprising members of significant homology in all organisms. Many of them are classified according to their respective molecular weight in kDa: HSP40s, HSP60s, HSP70s, HSP90s and HSP100s [3]. During stress conditions, stress-induced isoforms of HSPs interact with unfolding proteins, keeping them in a folding-competent state and preventing aggregation until the stress subsides and clients can be channelled to constitutively expressed chaperones for refolding or cleared via degradation pathways. For example, small heat shock proteins (sHSP) act as a first line of defence against aggregation, being optimized for the recognition of non-native proteins. The larger chaperones, like members of the HSP70 family, include stress inducible variants like HSPA1A and HSPA1B, which are the major stress induced chaperones in mammals. HSP90, which assists protein folding under physiological conditions, is also upregulated in HSR and changes its interaction to specific co-chaperones that stall substrate release, allowing HSP90 to contain non-native clients for an extended period [21]. Similar functionality is provided by the chaperonin GroEL from *E.coli* under stress conditions, containing aggregation-prone substrates in its cavity. Interestingly, the eukaryotic functional homologue TRiC is not heat induced, which might be due to its limited pool of potential substrates compared to GroEL (binding up to 50 % of the *E.coli* proteins) [19].

In single cell organisms, components of the degradation pathway are also induced during stress response to clear accumulated aggregates that could jeopardize survival of the organism. Multi-cellular organisms seem to focus more on refolding and repair mechanisms than up-regulating degradation pathways, possibly because they can tolerate a certain level of cell death [21]. The transcriptional up-regulation of HSPs depends on the activity of transcription factors σ^{32} in bacteria and heat shock factor 1 (HSF1) in eukary-

otes. They bind to a heat shock element on the DNA and initiate transcription of HSPs. The current model for HSF1 activation is that HSC70 and HSP90 bind monomeric HSF1 under physiological conditions, sequestering it into the cytosol and thereby preventing it from activating the transcription of heat shock genes. Under stress conditions HSPs are recruited to unfolding proteins, thus releasing HSF1 which initiates homotrimerization and transport into the nucleus, where further modification like phosphorylation and acetylation modulate the activity of the final transcription factor complex [27].

1.2.1 Heat shock protein 70 structure and function

In humans, members of the HSP70 family are the most ubiquitously occurring HSPs, comprising thirteen gene products differing in tissue-specific and intra-cellular expression levels as well as in subcellular localisation. Among the thirteen members, HSPA1A and HSPA1B (collectively referred to as HSP70) are the major stress-inducible chaperones while the constitutively expressed HSPA8 (HSC70) exhibits essential housekeeping functions in protein folding and polypeptide transport. Little is known about the other inducible and constitutive members of the HSP70 family. Some are thought to be involved in specialized functions like spermatogenesis (HSPA2, HSPA1L), endoplasmic reticulum protein transport (HSPA5), reaction to nutrient starvation (HSPA7) or promotion of specific cancer types (HSPA14: hepatocellular carcinoma). For the other members the function remains largely elusive and only sub-cellular localisation or tissue expression patterns are known [28].

All thirteen members share a common domain structure, consisting of a N-terminal nucleotide-binding domain (NBD) and a C-terminal substrate-binding domain (SBD), connected by a highly conserved, hydrophobic linker region. The SBD contains a β -sandwich subdomain where the hydrophobic substrate binding pocket is located and an α -helical lid that assumes open and closed conformations during the ATP-driven cycle (Fig.2). The movement of the SBD lid is allosterically linked to the nucleotide turnover in the NBD. In the ATP bound state the equilibrium is shifted towards an open conformation, in which the flexible interdomain linker is buried in a cleft of the NBD domain which subsequently triggers docking of the SBD and opening of the α -helical lid. This state is characterized by low substrate affinity and high dissociation rates. Substrates delivered by J-domain proteins (JDP) of the HSP40 family, which bind the C-terminal IEEVD motif, promote substrate binding to the β -sandwich subdomain and trigger closure of the α -helical lid. Subsequently, the JDP stimulates the hydrolysis of ATP, inducing a structural rearrangement of the NBD which frees the interdomain linker. Thus the SBD can detach from the NBD domain and the equilibrium in the ADP bound state, is shifted towards the closed conformation with high substrate affinities [29][30]. Substrate release is favoured by the binding of nucleotide exchange factors (NEF) to the NBD, releasing

ADP and thereby causing an opening of the α -helical lid, closing the active cycle by ATP binding to the vacant NBD. Eukaryotic cells possess several families of NEFs, including the Bcl-2-associated athanogene (BAG) domain proteins and HSP70 binding protein 1 (HSPBP1), which can act as positive and negative regulators of HSP70 [28].

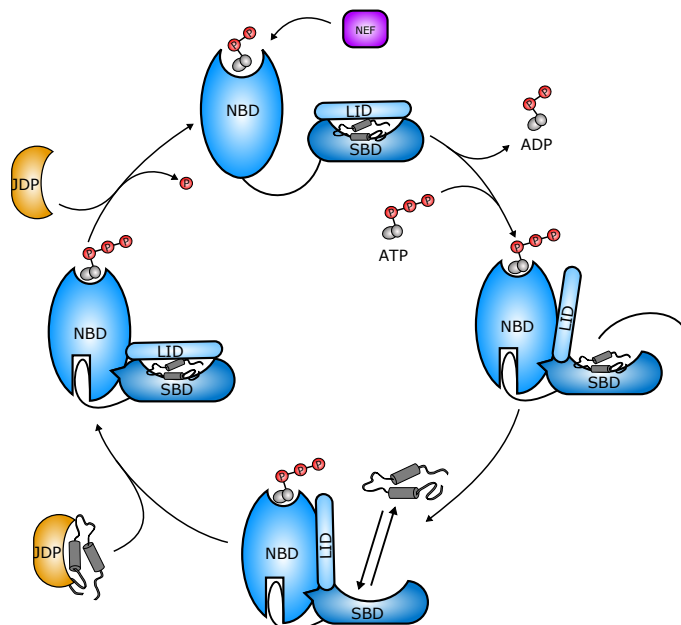


Figure 2. The ATP-driven HSP70 cycle. The HSP70 cycle is characterized by states of ATP or ADP association to the nucleotide-binding domain (NBD). In the ATP-bound state the hydrophobic linker is engulfed in the NBD, leading to a docking of the substrate binding domain (SBD) and favouring the open conformation of the α -helical lid domain (LID). Due to the open lid domain, substrates have high dissociation/association rates with low affinity toward the SBD. Substrate delivery by J-domain proteins (JDP) enhances substrate binding and triggers lid closure. Subsequent hydrolysis of ATP to ADP releases the hydrophobic linker, undocking the SBD with the tightly bound substrate. Substrate release is governed by the activity of nucleotide exchange factors (NEF), removing ADP from the NBD and enabling a new cycle through ATP binding.

HSP70s perform a great variety of homeostasis and stress-induced tasks, shifting substrate proteins between various folding states to prime them for *de novo* folding, complex assembly, refolding of stress-denatured proteins, protein transport, membrane translocation and protein degradation [3]. Additionally, they have been found to be potent anti-apoptotic proteins, blocking caspase dependent and independent pathways, facilitating single-strand break DNA repair and are implicated in the disassembly of protein aggregates in concert with HSP110 (Fig.1) [31][28]. To fulfil all of these different cellular tasks, members of the HSP70 family interact with other chaperones (HSP90/HSP110) and are assisted by a broad spectra of co-chaperones delivering substrates and regulating chaperone activity. Aside from JDP, tetratricopeptide repeat (TPR) containing proteins can recognize the C-terminal EEVD motif of HSP70 to regulate its activity. For example, HOP, a component of the progesterone receptor complex, stabilizes HSP70 client proteins and links HSP70 to HSP90, facilitating the substrate transfer for coordinated folding [32].

In contrast to HOP, the E3 ligase CHIP inhibits the ATPase cycle promoting substrate ubiquitination and subsequent degradation [33]. Due to the importance of HSP70 in maintaining proteostasis and enhancing cell survival, it also plays a crucial role in tumor invasion and metastasis. HSPA1A overexpression is frequently observed in many cancer types and connected to a poor patient prognosis. HSPs promote cancer cell survival and confer resistance to stress-induced apoptosis. Additionally, it has been found that tumors with high HSP70 expression are highly resistant to radiochemotherapy, most likely due to blockage of the NF- κ B, JNK, and ERK signaling pathways [28].

Surprisingly, despite the lack of a canonical transmembrane or lipid binding domain, various HSP70s localise to the plasma membrane or the extracellular milieu in tumor cells and viral or bacterial infected cells. Specifically, 15-20 % of HSPA1A was found in the plasma membrane of several tumor cells but not in corresponding normal cells [34]. In fact membrane density of HSP70A1A is considerably higher in metastases compared to primary and relapse tumors, making it a potent biomarker for aggressive tumors. The membrane association possibly protects the metastatic cell from environmental stress induced by the unfavorable milieu during migration [35]. The details of the insertion are still under discussion and several mechanisms for membrane insertion and export have been proposed, including exosomal and endolysosomal transport [28].

Two studies claimed that membrane insertion by the C-terminal SBD of HSP70 is the initial step in this export process, followed by oligomerization and release through vesicles [36][37]. However, there are also opposing opinions claiming a peripheral attachment to membranes by transient phospholipid anchorage [38]. Several works on HSP70 membrane interaction agree on the fact that the interaction is very specific for membranes containing negatively charged phospholipids, particularly phosphatidylserine (PS) [37][38]. Apart from the importance of membrane interaction in cancer, recent work has shed light on additional functions. PS-enriched membrane binding of constitutively expressed HSC70 has been reported during endosomal internalization of cytosolic proteins by endosomal microautophagy. However, membrane interaction is proposed to be of transient nature, mediated by positively charged residues at the C-terminus of the lid domain, revealing another possible membrane contact surface [39]. Furthermore, it has been reported that in a neuronal context Hsc70-4, a homolog from *Drosophila melanogaster*, can bind PS containing giant unilamellar liposomes (GUV) and cause membrane deformation needed for synaptic microautophagy [40].

1.2.2 Heat shock protein 90 structure and function

The human genome encodes two cytosolic HSP90s, a constitutively expressed HSP90 β and a heat shock induced HSP90 α [27]. Both proteins have 86 % sequence identity and form an active homodimer *in vivo* [41]. Each monomer comprises an amino-terminal domain (NTD), connected to a middle domain and a C-terminal domain (CTD) by a flexible linker region. During the ATP-driven cycle these domains undergo extensive structural rearrangements assuming open and closed functional states, ultimately releasing an active protein [3].

In the absence of ATP, HSP90 homodimer assumes a V-shape, with CTDs dimerized at the bottom [27]. Upon ATP binding to the NTD binding site, HSP90 adopts an intermediate state interacting with a variety of co-chaperones that broaden HSP90s functional range. Indeed, co-chaperones are the most important regulators of HSP90 functions during its entire active cycle, as different co-chaperones complexing HSP90 are integrated in the proceeding of the active cycle as well as in the selection, maturation and activation of the client proteins. They bind to specific conformational states of HSP90 in a sequential manner as they have overlapping binding sites on HSP90. One of these co-chaperones is HOP, a TPR containing protein that recognizes the C-terminal MEEV motif of HSP90 to bridge the binding of the HSP70:HSP40 complex to HSP90 during protein folding. Furthermore, it stabilizes the V-shape conformation of HSP90 to facilitate substrate binding. The partially folded, inactive polypeptide is transferred from the HSP70:HSP40 complex to the middle domains of the HSP90 dimer.

Substrate binding results in the dimerization of the NTDs and switch HSP90 into the 'closed-state 1'. This process is assisted by the co-chaperone AHA1 which binds the middle domain of HSP90 and stimulates its ATPase activity. Next, the NTDs contact the middle domains, which twist to an X-shape completing 'closed-state 2'. This state is stabilized by binding of p23 to NTDs, a co-chaperone reducing ATPase activity, thus stalling client release and promoting its maturation. The dimerization of NTDs and contact to MDs is crucial for ATP hydrolysis upon which HSP90 assumes the open V-shape conformation and the client protein is released in its active state [27]. Depending on the need of the client protein a different set of co-chaperones can interact with HSP90 to promote folding, activation, complex assembly or ligand binding of the respective substrate. Additionally, co-chaperones like CHIP can link HSP90 to downstream processing machineries, for instance the 26S proteasome, to degrade the client protein in case of unsuccessful folding. Due to its large conformational flexibility and cooperation with diverse co-chaperones, HSP90 can access different substrates from diverse cellular pathways [27]. As mentioned before, HSP90 can activate its client and it has been reported to be a major activator of human kinases.

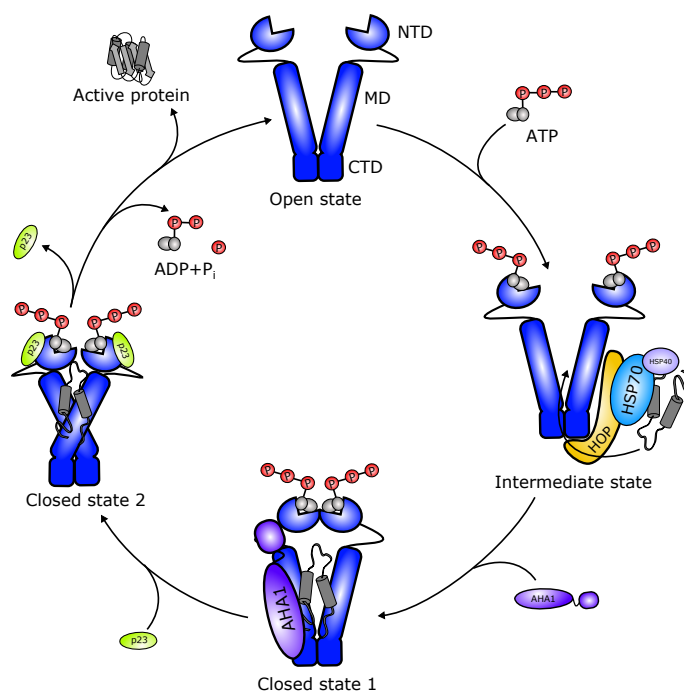


Figure 3. The HSP90 cycle. HSP90 is a homodimer, with each protomer consisting of the amino-terminal domain (NTD) linked via a flexible linker to the middle domain (MD). The dimer interface is provided by the carboxy-terminal domain (CTD), harbouring the MEEVD recognition motive. HSP90 assumes an open conformation and transitions to an intermediate state upon ATP binding. Various co-chaperones act on HSP90 to promote or inhibit cycle progression. The co-chaperone HOP stabilizes the open conformation, in order to deliver HSP90 substrates by binding the C-terminal recognition motives and tethering HSP70 to HSP90. Activator of HSP90 ATPase homologue 1 (AHA1) promotes lid closure and cycle progression by NTD dimerisation (closed state 1). Subsequent twisting of the HSP90 monomers leads to closed state 2 which is stabilized by co-chaperone p23. Reduction of ATPase activity by p23 stalls substrates in the closed conformation. Upon p23 dissociation and ATP hydrolysis HSP90 monomers assume open conformation, releasing the client protein.

Indeed, recent studies suggest that approximately 60 % of the human kinome associates with HSP90 [42]. Furthermore, predictions of possible interaction partners of HSP90 revealed its importance in DNA repair, development, the immune response, neuronal signalling, protein secretion and heat shock response [3][43].

Owing to its central function in protein folding it is not surprising that HSP90 levels are elevated in various cancer types and are linked to a negative prognosis in breast cancer [44]. More specifically it was found that during malignant transformation, the multi-chaperone HSP90:HSP70 complex is stabilized in over 50 % of tumours, presenting a platform to rewire the chaperone network for tumor cell survival [45]. Moreover, HSP90 activity has been associated with a number of neurodegenerative diseases including Alzheimer's disease and Parkinson's disease. The two diseases are characterised by protein aggregation of either plaque-forming protein amyloid- β ($A\beta$) or α -synuclein, respectively, both being clients of HSP90. Thus, upregulation of HSP90 activity could result in the stabilization of these targets reducing the aggregation-induced loss of neuronal function. However, scientists are only beginning to grasp the effects of HSP90 on neurodegenerative diseases and how it might be targeted for therapeutic approaches [27].

1.3 The ubiquitin-proteasome-system

1.3.1 Ubiquitin

Ubiquitin is a 76 amino acid small protein that is unique to eukaryotes and is attached to substrate proteins acting as a signalling moiety to alter the fate of its client. Interestingly, NMR analysis revealed significant structural homology to the sulphur carrier protein ThiS and MoaD from *Escherichia coli*. They display a conserved motif called the "ubiquitin fold" and utilise similar sulphur chemistry, even though sharing only 14 % sequence homology with ubiquitin. This indicates to common ancestry for both proteins [46]. The sequence of ubiquitin is strongly conserved in eukaryotes which is exemplified by only three residues being different between yeast and human ubiquitin, reflecting its importance in essential biological processes [47].

Ubiquitin is attached to a substrate protein via an isopeptide bond between the C-terminal glycine of ubiquitin and a lysine residue of the recipient protein or another ubiquitin. There are versatile types of ubiquitylation that induce a different downstream processing of the substrate. Ubiquitin can be linked as a monomer (monoubiquitination), as multiple monomers on one substrate (multiubiquitination) or as isopeptide-linked polymers (polyubiquitination). The polymer ubiquitin can be conjugated through one of its seven lysine residues (Lys6, Lys11, Lys27, Lys29, Lys33, Lys48, Lys63), either through homotypic or heterotypic linkage, offering countless possibilities of polyubiquitin chain versatility [48].

The canonical K48 ubiquitin chains target the substrate to proteasomal degradation [11] while K63-linked chains are involved in DNA damage tolerance, protein kinase activation and autophagy [47][49]. Recent research has also shed light on the biological relevance of atypical chain linkages like K27, K29 and K33. The discovery of their participation in diverse pathways, like DNA damage response, Wnt signalling and anterograde protein trafficking, increases the understanding of the complexity of ubiquitin signalling [48].

In the turnover of membrane proteins, monoubiquitylation initiates internalization and further modulation of the ubiquitin code probably governs the protein's fate throughout the endocytic pathway, concluding in lysosomal degradation or recycling to the plasma membrane. In contrast to the cytosolic protein quality control, formation K63-linked polyubiquitin chains at the plasma membrane target the substrate to protein degradation by the proteasome and/or lysosome in possibly interconnected pathways, further increasing the diversity and complexity of ubiquitin signalling [50].

Moreover, polyubiquitin chains can be subjected to post-translational modifications like phosphorylation and acetylation as well as shortening and linkage-alteration by deubiquitylating enzymes (DUB). In addition to ubiquitin, there are other small proteins, like NEDD8 and SUMO, that are utilised as post-translational modifications of macro-

molecules. They display high structural similarity to ubiquitin and are conjugated via a similar enzymatic cascade. Thus, these proteins are referred to as ubiquitin-like (UBL) proteins. However, they compete with ubiquitin for identical Lys-residues on substrates and lead to different downstream processing of the substrate [51].

The conjugation of ubiquitin and UBL proteins to a substrate is catalysed by the sequential interaction of three enzymes: E1 (ubiquitin-activating enzyme), E2 (ubiquitin-conjugating enzyme) and E3 (ubiquitin ligase).

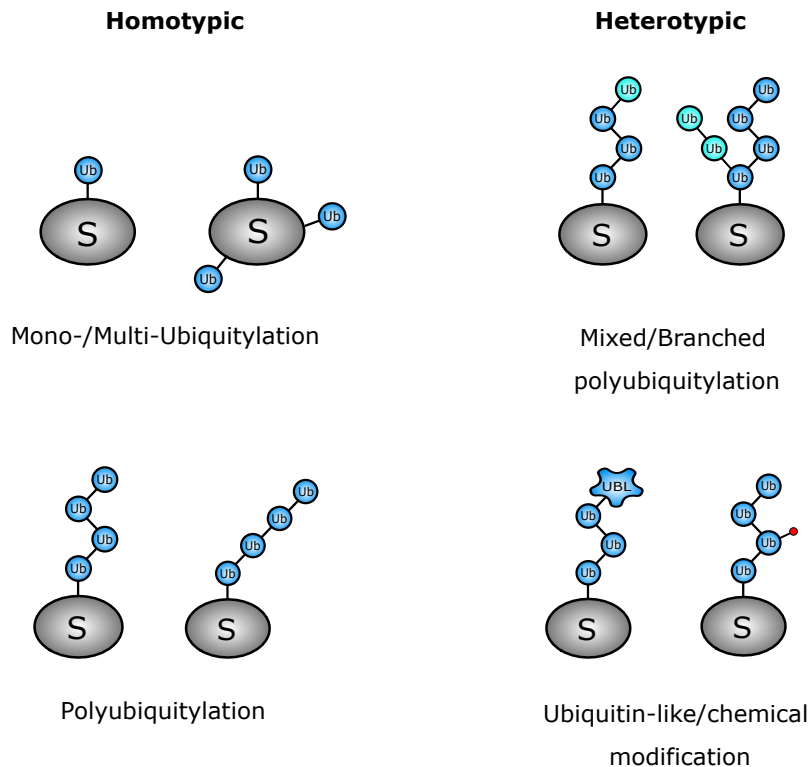


Figure 4. The ubiquitin chain diversity. Ubiquitin can be linked as a monomer (monoubiquitylation) or as multiple monomers on one substrate (multiubiquitylation), affecting protein interaction, localisation, trafficking and activity. Monoubiquitylation can be extended by conjugating additional ubiquitins through one of its seven lysine residues (Lys6, Lys11, Lys27, Lys29, Lys33, Lys48, Lys63), yielding polyubiquitin chains of different linkage types with distinct signalling properties [48]. Additional complexity is added by polyubiquitin chains of mixed linkage types like K11-K48 mixed chains, enhancing the proteolytic degradation signal of substrates [52]. Ubiquitin-like (UBL) proteins and chemical modifications can modify an existing polyubiquitin chain further modulating the clients fate [53][54].

1.3.2 Ubiquitylation cascade

At the start of the ubiquitylation cascade an E1 enzyme primed with ATP-Mg²⁺ catalyses a C-terminal adenylation of ubiquitin, followed by a nucleophilic attack of the active site cysteine, formation of the E1-Ub thioester and release of AMP+PP_i [47]. With respect to the evolutionary development of ubiquitin and its conjugation cascade, the initial adenylation is the most ancient part. The crystal structure of MoeB, the E1 equivalent in *E.coli*, which binds the ubiquitin-like protein Moad, revealed that the catalytic amino acids are conserved from *E.coli* to humans. However, the following thioester formation in eukaryotes is absent in *E.coli*. This is likely due to the lesser complexity of the MoeB binding pocket, lacking the ability to stabilize the oxyanion intermediate [55].

All known E1 enzymes display a complex architecture, forming a heterodimeric complex derived from two polypeptides. Key features are an active and an inactive adenylation domain (AAD/IAD), a four helix bundle (4HB), a domain harbouring the active site cysteine and a C-terminal ubiquitin-fold domain (UFD) [56]. The UFD is poorly conserved among eukaryotic E1s and is thought to be involved in discrimination of ubiquitin and the structurally very similar UBL proteins. The provided specificity is necessary for downstream processes, as following enzymes lack the capability to distinguish different UBL proteins [47]. There are two E1 enzymes mediating ubiquitylation in humans, UBA1 and UBA6. They are capable of simultaneously binding two ubiquitin molecules. One ubiquitin is non-covalently attached to the AAD after the initial ubiquitin formed the thioester with the active-centre cysteine [56]. In the subsequent step of the cascade this E1-Ub₂ ternary complex is engaged by a ubiquitin-specific E2 enzyme.

In *Saccharomyces cerevisiae*, eleven ubiquitin-conjugating E2s have been found while the human genome encodes for more than 40 E2s [57]. All active E2s, whether dedicated to ubiquitin or other UBL modifiers, share a conserved globular domain, termed the ubiquitin-conjugation (UBC) domain, where the active site cysteine is located in a shallow cleft. The first step of the E2 catalysis is the differentiation of E1-Ub₂ complexes from E1 bound to other UBL proteins. This selectivity is guaranteed by conformational changes in the UFD of E1, exposing cryptic binding sites, recognized only by the UBC domain of the proper E2. However, other regions of E2 enzymes can also contribute to E1 binding specificity. For example the NEDD8-conjugating E2 (UBE2M) bears a N-terminal extension that stabilizes the interaction with the respective E1 and simultaneously reduces its affinity for the E1 harbouring ubiquitin. Many E2 enzymes have similar N-terminal extensions, suggesting it to be a general recognition feature [58].

The second step is the transthioylation of the bound ubiquitin or UBL protein to the active-site cysteine of the E2. Despite many trials, the elucidation of the molecular mechanism underlying the thioester transfer remains largely elusive. Recently, a crystal structure of an ubiquitin binding E1:E2(UBC4):Ub:ATP complex was published that gave a first

glance on the interaction interface of E1 and E2 during thioester transfer [59]. The authors identified several contact sites as well as a 25 degree rotation of the UFD to be obligatory to bring both active site cysteines in close proximity .

After the thioester transfer, the E2 enzyme exposes binding sites in its UBC domain which can be recognized by several E3 ligases that deliver the final protein target for ubiquitylation. The E2~Ub thioester is subjected to a nucleophilic attack of the presented substrate lysine residue. Depending on the type of E3 ligase involved, the lysine originates either from the substrate (RING ligase) or from the E3 ligase itself (HECT/RBR ligases). Continuous cycling of these steps with addition of various E3 and E2 enzymes leads to the already mentioned diversity of ubiquitin chains (Fig.5).

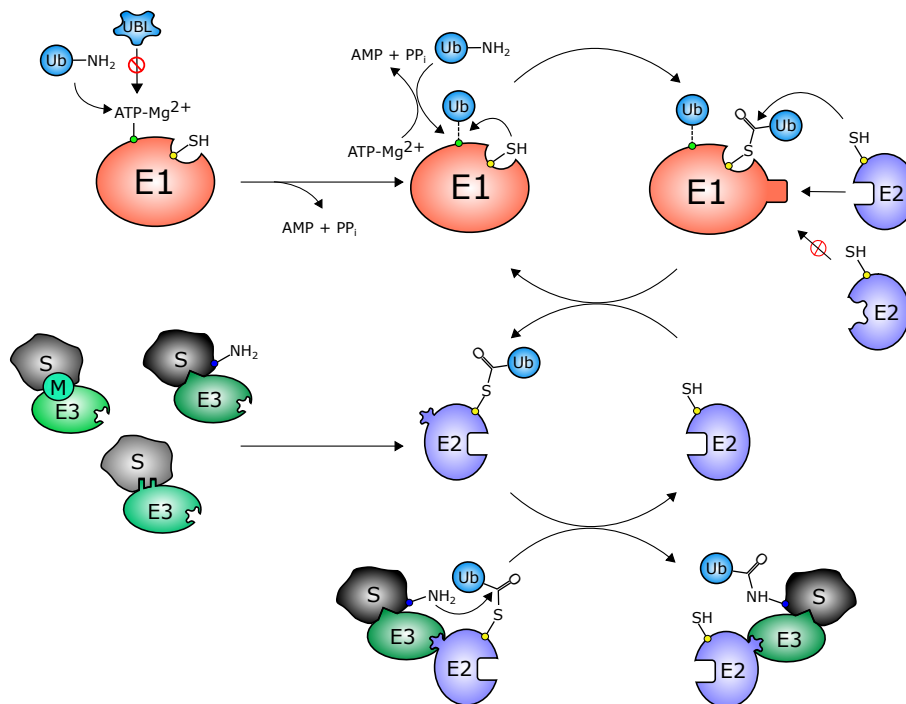


Figure 5. The ubiquitylation cascade. The ubiquitin-activating enzyme (E1) is specific for ubiquitin (Ub) or one of the UBL proteins (UBL), which are bound similarly through formation of a thioester bond consuming ATP. E1 can occupy two ubiquitin molecules simultaneously. Ubiquitin binding exposes E1 motifs that are recognized by a specific ubiquitin-conjugating enzyme (E2) to which the ubiquitin thioester is transferred. In turn, the E2 exposes residues recognized by the substrate delivering E3 ubiquitin ligase. Ubiquitin ligases provide the substrate specificity either through intrinsic motifs or mediator proteins (M). Depending on the nature of the E3 the conjugation of ubiquitin to the substrate is realized by a nucleophilic attack of either a substrate lysine (as shown) or an E3 lysine residue from which ubiquitin is transferred in an additional step to the substrate.

1.3.3 E3 ligases

The human genome encodes more than 600 E3 ligases which are classified on the basis of their E2~Ub-binding domain and ubiquitin transfer mechanism into RING (really interesting new gene), HECT (homologous to E6AP carboxyl terminus) and RING-between-RINGS (RBR) E3s. They provide substrate specificity for the ubiquitylation cascade, binding substrates either through one or several protein-protein interactions or indirect through an intermediate binding partner, whereas the E2 determines the specificity for the recipient lysine in the formation of polyubiquitin chains (Fig.5) [47]. With 300 members, RING-type ligases constitute the largest class [60]. They share a common architecture, consisting of the eponymous RING domain linked to a substrate-binding domain (SBD). The RING domain complexes two zinc ions that are essential for proper folding and RING-E2~Ub interaction. RING-type ligases do not catalyse the direct transfer of Ub to the substrate lysine. Instead, the RING domain induces allosteric changes in the E2~Ub complex, priming the thioester and orientating the substrate lysine for optimal formation of the isopeptide bond [61]. NMR analysis of UBC13~Ub and UBCH5c~Ub displayed a very dynamic conformation of bound ubiquitin in the absence of a RING-E3, opposing ubiquitin transfer. Upon RING E3 binding, ubiquitin is fixed in a closed conformation proximal to the RING domain, activating the thioester for the isopeptide bond formation [62]. The structural requirements for transfer to the substrate lysine were elucidated for substrate sumolation by human UBC9 [63]. The residues Asn85, Tyr87 and Asp127, located in a pocket of the UBC domain and surrounding the active-site cysteine, cooperatively orientate and deprotonate the substrate lysine, activating it for the nucleophilic attack. The high conservation of the UBC domain suggests that this model is broadly applicable (Fig.6A) .

U-box proteins resemble RING E3s in structure and ubiquitylation mechanism and are therefore included in the RING category. Unlike the RING domain, the about 70 amino acid U-box domain lacks the residues necessary for complexing zinc ions but is instead stabilized by a network of hydrogen bonds [61]. The initially identified U-box-containing UFD2 in yeast mediates the E2-target interaction and is required for polyubiquitin chain assembly in concert with E1, E2 and another E3. In contrast to UFD2, the eight human U-box homologs serve as E3 ligases, mediating ubiquitylation of themselves and of heterologous substrates without the requirement of additional E3 ligases. The U-box domain is essential for this E3 activity, as deletions and point mutations in conserved residues abrogate any ubiquitylation activity [64]. Given the number of RING E3s and their central role in controlling cellular homeostasis, it is not surprising that dysfunction of RING ligases like RNF11, MDM2 and BRCA1 have been found to be key factors in the onset and progression of various cancer types [65][66].

The family of HECT ligases comprises 28 members in humans and is characterised by a N-terminal substrate-binding domain and a C-terminal HECT domain of approximately 350 amino acids containing the catalytic components for ubiquitin conjugation and transfer [67]. The HECT family is further divided into three sub-families based on the structural composition of their N-terminal protein–protein interaction domains: The NEDD4 family, which contains a WW-domain; the HERC family, which contains a regulator of chromosome condensation 1-like domain and the HECT family with other protein–protein interaction domains [61].

The ubiquitin transfer mechanism was elucidated by extensive structural studies, primarily of NEDD4 family members [68]. In contrast to RING ligases, the HECT domain directly participates in the transfer of ubiquitin. It is composed of a N-terminal lobe which binds the E2~Ub complex and a C-terminal lobe containing the catalytic cysteine. They are connected by a flexible joint that enables the C-lobe to act as a switch between transthiolation of the E2~Ub complex and transfer of ubiquitin to the recipient substrate [61]. The transthiolation is facilitated by hydrophobic interactions of the C-lobe with the C-terminus of ubiquitin, constraining the flexibility of the thioester similarly as in RING ligases. However, since the C-lobe shows low conservation between the HECT subfamilies, this mechanism is only confirmed for NEDD4 family members [69].

After transfer of the thioester, the C-lobe rotates about the flexible joint to juxtapose with a substrate lysine. This conformation is then stabilized by C-lobe contacts with parts of the N-lobe, further exposing the thioester for the substrate lysine (Fig.6B) [70]. Well-known members of the HECT family, like NEDD4 which targets epithelial Na⁺ channel subunits and E6-AP, which targets p53 for ubiquitination, have been reported to contribute to the onset of several human diseases like the Liddle's syndrome, retroviral budding and the development of cervical cancer [64] [65].

Members of the RING-between-RINGS (RBR) class of E3 ligases all possess the RING1-IBR(In Between RING fingers)-RING2 domain architecture and are considered as hybrids between HECT and RING ligases. In humans, fourteen RBR E3s have been identified. Amongst them PARKIN, HHARI and HOIP are the best studied members. They still lack a detailed elucidation of the ubiquitin transfer mechanism. The RING1 domain displays significant structural similarity with the canonical RING domain but differs in its functional capabilities. HOIP crystal structure revealed that the RING1 domain lacks the arginine that promotes the closed conformation to activate the ubiquitin thioester for transthiolation present in RING domains. Instead, the thioester is primed by multiple interactions between RING1, RING2, IBR regions and ubiquitin is subsequently transferred to the catalytic cysteine present in the RING2 domain, resembling the functionality of the N-lobe in HECT ligases [61]. Finally ubiquitin is transferred to a lysine residue of the recipient substrate at the RING2 domain (Fig.6C).

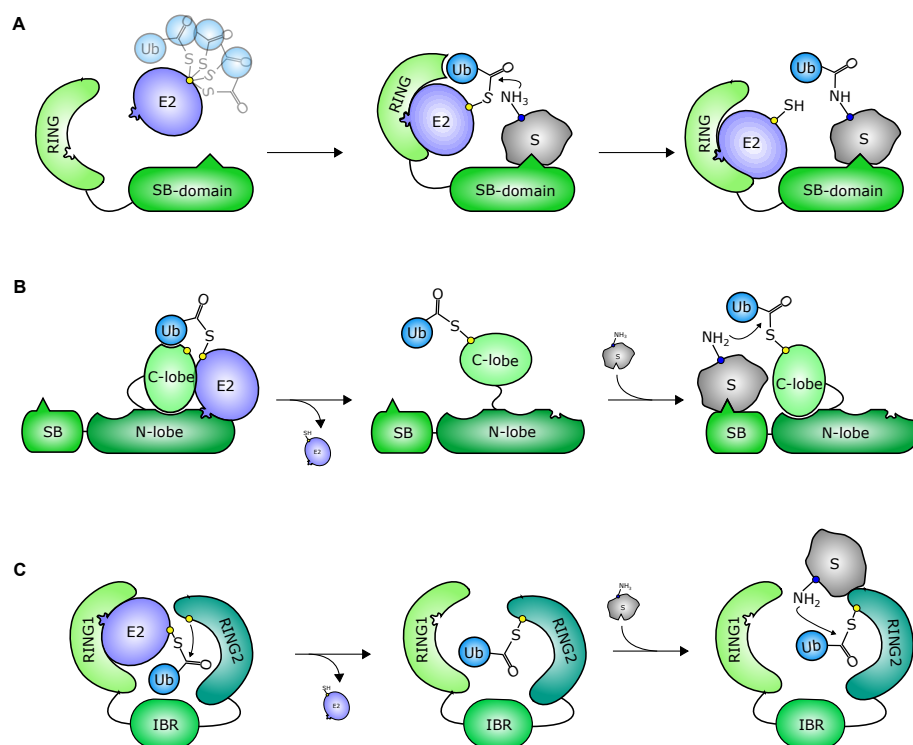


Figure 6. Structures and mechanisms of E3 ligases. (A) RING E3s are the most abundant type, consisting of a RING and a substrate binding (SB) domain. The RING domain restrains the conformational flexibility of the E2~Ub thioester to facilitate the nucleophilic attack of a lysine residue from the SB domain bound substrate. (B) HECT ligases directly participate in the ubiquitin transfer. Their structure encompasses a substrate binding (SB) domain connected to a N-lobe and a C-lobe. The E2~Ub complex binds the N-lobe and is positioned in cooperation with the C-lobe to enable transthiolation of ubiquitin to the active site cysteine of the C-lobe. Subsequently, the C-lobe switches to a contact site on the N-lobe to position the Ub thioester next to the substrate bound to the SB domain, enabling transfer of ubiquitin to the substrate. (C) RING-between-RINGS (RBR) ligases consist of two RING domains (RING1, RING2) and a connecting in-between RING (IBR) domain. RING1 primes the E2~Ub thioester for transthiolation to the catalytic cysteine of RING2. From there, it is transferred to the substrate bound to the RING2 domain, resembling the mechanism of HECT ligases.

1.4 The E3 ligase CHIP

1.4.1 Canonical and non-canonical activity of CHIP

CHIP (C-terminal HSC70-interacting protein) is a 35 kDa dimeric E3 ubiquitin ligase which is ubiquitously expressed in most mammalian tissues and cultured cell lines, with exception of cells of hematopoietic origin and undifferentiated neuronal cells [33]. It was found to be a primarily cytosolic protein, though a fraction of CHIP can be found in the nucleus, indicating the possibility of intracellular trafficking [71]. CHIP plays a crucial role in the protein quality control system. As part of the protein triage it provides the central link between chaperone mediated protein-folding and various degradation pathways. Moreover, CHIP has been reported to influence the regulation of various cellular pathways, like autophagy, signalling, ageing, organism development and apoptosis [72]. In a pioneering work by Ballinger et al., CHIP was discovered in a yeast two-hybrid

screen for tetratricopeptide repeat (TPR) containing proteins and was found to be a cytosolic interactor of HSP/HSC70. Antagonizing other co-chaperones, like HSP40, which promotes the substrate re-/folding cycle, CHIP negatively regulates HSP/HSC70 ATPase activity and cycle progression [33]. Another major chaperone that interacts with CHIP via the TPR domain is HSP90. In this interaction, CHIP again competes with other co-chaperones, like p23, preventing progression towards an active HSP90 client [73]. Later it was shown that CHIP contains a C-terminal U-box domain, classifying it as a U-box E3 ligase. Experimental studies revealed CHIP as a central link between chaperones and the degradation system, as a significant increase in degradation of HSP70/HSP90 clients, like the cystic fibrosis transmembrane conductance regulator (CFTR) and glucocorticoid receptor (GR), respectively, were observed in the presence of excessive CHIP *in vivo* [74]. Ubiquitylation of the disease-related, conformationally defective CFTR Δ F508 mutant by CHIP could be confirmed at the plasma membrane in an HSC70-dependent manner [75]. Further evidence of CHIP directly participating in protein degradation of misfolded chaperone clients was provided when the E3 was shown to selectively ubiquitylate thermally-denatured but not native luciferase in concert with HSC70 and HSP90 *in vitro* [76].

Downstream of the ubiquitylation pathway, CHIP has been implied to participate in the transport of ubiquitylated substrates to the proteasome due to co-precipitation and co-localisation with proteasome subunits, further consolidating its importance in linking chaperone processes to the degradation machineries (Fig.7A) [74].

CHIP associates with HSP70 and HSP90 through their disordered and highly dynamic C-termini which bind to the TPR domain of CHIP. In the TPR binding groove polar contacts dominate, where Lys30 and Lys95 of CHIP form a dicarboxylate clamp around the C-terminal Asp of HSP70/90 [77]. In contrast to HOP, which utilizes different TPR domains to bridge HSP70 and HSP90 simultaneously, CHIP can only bind one of the chaperones at a time. In an NMR based study the C-terminal EEVD motif of HSC70 was found to be both necessary and sufficient for CHIP association [78]. Additionally, the authors claimed that no further specific interactions with domains of HSC70 contribute to the binding, keeping CHIP loosely tethered to the disordered C-terminus of interacting chaperones. However, a later study argued that the TPR domain of CHIP also engages a part of the HSP70/HSC70 lid domain, docking and undocking during processing of the chaperone client [79]. This CHIP-TPR:lid domain interaction was required for efficient ubiquitylation of HSP70/HSC70 clients and offered an additional surface for the regulation of CHIP mediated ubiquitylation through posttranslational modification of the HSP70/HSC70 lid domain. Whether CHIP association to HSP90 is also facilitated by additional contact sites remained unclear [79]. The hypothesis of several contact site of CHIP on HSC/HSP70 was supported by findings on CFTR ubiquitylation by CHIP in a rabbit reticulocyte lysate [80]. The authors suggested an interplay of multiple domains of both proteins and potentially CHIP oligomerization to regulate TPR affinity towards the

HSC70 C-terminal EEVD motif. Additionally, they proposed that substrate properties, for example, stress-induced modifications, actively influence which type of co-chaperone is recruited to HSC/HSP70 and hence determine the fate of the ternary complex.

The ubiquitylation activity of CHIP is not restricted to HSP70/HSC70 clients but also acts on the client-free chaperones themselves. This is a necessity in stress recovery as the elevated levels of stress-induced HSP70 need to be degraded when the stress subsides. Indeed it was shown that CHIP is capable to distinguish between the highly homologous HSP70 and HSC70 (>86 % sequence identity and 93 % sequence conservation), suggesting the existence of CHIP-HSC70 contact sites apart from the disordered C-terminus. Even though both chaperones are ubiquitylated only on a limited number of available lysines, the inducible (HSP70), but not the constitutive form, is efficiently degraded. This can be due to the distribution of ubiquitin linkage types attached to HSP70 and HSC70. While HSC70 is primarily modified with an even distribution of K6, K11 and K48 chains, the dominant chain type in HSP70 is K48, which is required for recognition by the 19S subunit of the proteasome. This example highlights the importance of how subtle differences in substrates can be recognized by CHIP, leading to distinct downstream processing of CHIP client proteins [81].

In addition to the canonical function of CHIP as co-chaperone which depends on substrate delivery by HSP70 and HSP90, there have been studies claiming a direct interaction of CHIP with native substrates. CHIP-mediated ubiquitylation regulated their turnover, localization and/or activity during normal growth conditions and cellular stress.

The transcription factor RUNX1, whose stability and mutagenesis has been frequently implied in human leukemia, was found to be negatively regulated by CHIP-mediated ubiquitylation in a chaperone-independent manner [82]. However, there is an ongoing discussion about CHIP activity on RUNX1, as a study from 2017 using the same CHIP-K30A mutant, which is unable to bind molecular chaperones, found reduced affinity and ubiquitylation activity on RUNX1 and suggested instead a CHIP:HSP90 complex to be responsible for RUNX1 stability [83].

Another example is the turnover of the insulin receptor (INSR), suggesting a competitive role between chaperone-free CHIP maintaining steady-state levels of INSR and stress-induced channelling of CHIP to a chaperone-associated state, leading to an accumulation and a detrimental hyperactivity of INSR signalling (Fig.7B; Fig.10) [84].

In 2011 Wang et. al reported chaperone independent ubiquitylation of SMAD1 by CHIP [85]. SMAD1 is one of three receptor-regulated SMAD proteins (R-SMADs: SMAD1/5/8) that modulate TGF-bone morphogenetic protein pathway (BMP), together with other members of the SMAD protein family. TGF-BMP signalling is vital in cell proliferation and specification of developmental fate, implying a role of CHIP in embryonic development. Through ubiquitylation and subsequent degradation of SMAD1, CHIP inhibits the signalling activities of R-SMAD1/5/8. Heat shock proteins are not necessary

for CHIP-mediated ubiquitylation of SMAD1, as co-crystallisation of SMAD1 C-terminal peptide, which is essential for direct association of SMAD1 with the CHIP TPR domain, occupies the same binding cavity as heat shock proteins. In fact, HSP70 and HSP90 compete with SMAD1 for TPR binding, antagonizing CHIP:SMAD1 complex formation and suppressing subsequent ubiquitylation by CHIP (Fig7B).

Advancing this idea, a recent study proposed that the TPR domain mediates allosteric effects on CHIP's dynamic conformation and E3 ligase activity [86]. It was shown that depending on the nature of the substrate, HSP70 (C-terminal peptide) binding to CHIP can either facilitate or inhibit substrate ubiquitylation. While addition of HSP70/40 to CHIP stimulated ubiquitylation of BAG-1, it suppressed activity on p53 and interferon regulatory factor 1 (IRF-1). The authors reasoned that p53 and IRF-1 are engaged by the TPR domain of CHIP and compete with HSP70 for this binding site. In this context, HSP70 is not simply acting as a targeting moiety for CHIP in the canonical protein quality control pathways but would rather function as a negative regulator of IRF-1 and p53 ubiquitylation. Additionally, structural characterisation of the CHIP TPR domain in different binding modes revealed that HSP binding as well as mutation of Lys30 to alanine, reduced TPR flexibility and increased the amount of 'ordered' structures. This solidification of TPR was allosterically connected to structural changes in the U-box domains of the CHIP homodimer, reducing its affinity for the E2 UBCH5A. Thus, the TPR domain can provide the necessary flexibility to engage client proteins but also acts as an allosteric switch that can negatively regulate CHIP E3 activity.

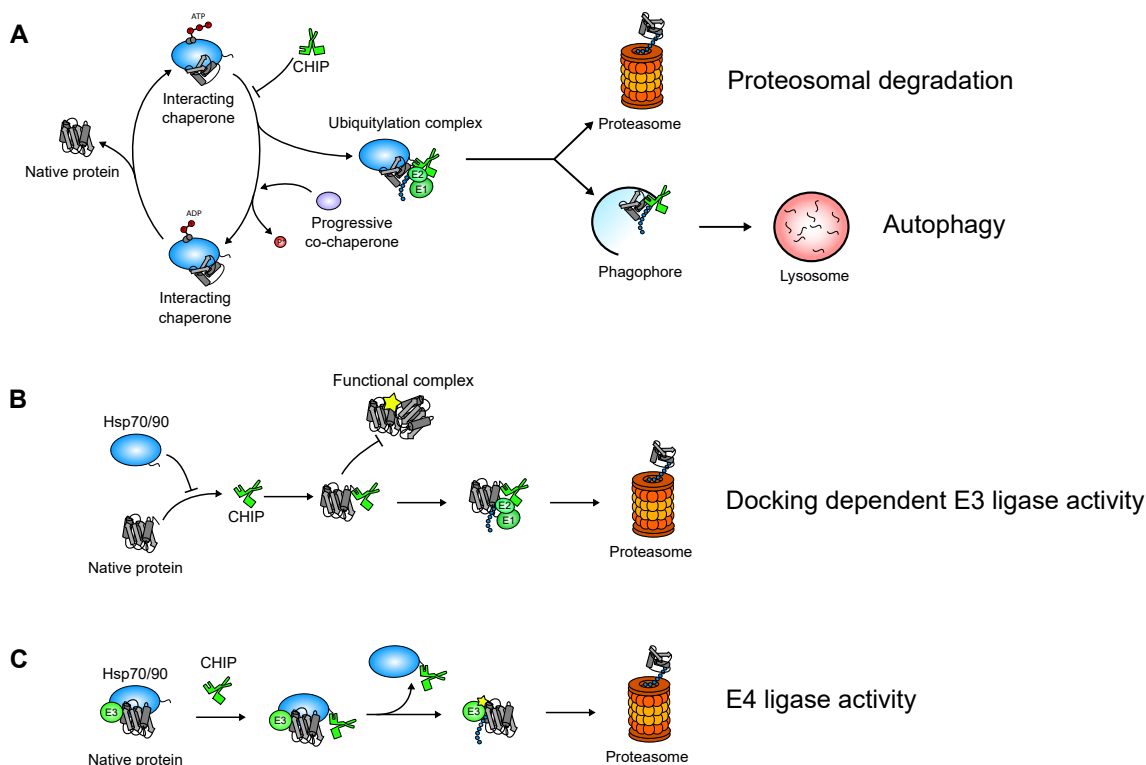


Figure 7. Chaperones and CHIP mutually influence their activity. (A) In the canonical pathways, CHIP interferes with the progression of the chaperone active cycle by competing with co-chaperones for chaperone binding and recruiting E2s to ubiquitylate the substrate, channelling it to degradation machineries. (B) The docking-dependent E3 ligase activity of CHIP entails binding of native substrates. Interacting chaperones inhibit this function by occupying the same binding moiety in the CHIP TPR domain, blocking substrate access. (C) E4 ligase activity of CHIP has only been reported for one interaction so far and activates another E3 ligase (PARKIN) by binding and dissociating HSC70 [87].

1.4.2 CHIP structure

The amino acid sequence of CHIP displays remarkable phylogenetic conservation in higher eukaryotes as shown by the comparison of human, *Mus musculus* (mouse), *Galus gallus* (chicken), *Danio rerio* (zebra fish), *Drosophila melanogaster* (fruit fly) and *Arabidopsis thaliana* (plant), with the C-terminal U-Box segment displaying the least variance among these species [71]. In mammals, CHIP is located within chromosome 16 and there are several splicing variants predicted for CHIP which lacks experimental confirmation to date. There has been no report of a CHIP homologue in any fungi or bacteria [71]. The crystal structure of murine CHIP (PDB: 2C2L), which differs from human CHIP by only one residue at the N-terminus, was solved in complex with human HSP90 C-terminal decapeptide (DDTSRMEEVD) [77]. It revealed that CHIP forms a homodimer, in which each protomer assumes a significantly different conformation. It is thus one among only 5 % of all known homodimeric proteins with extensive asymmetry [88].

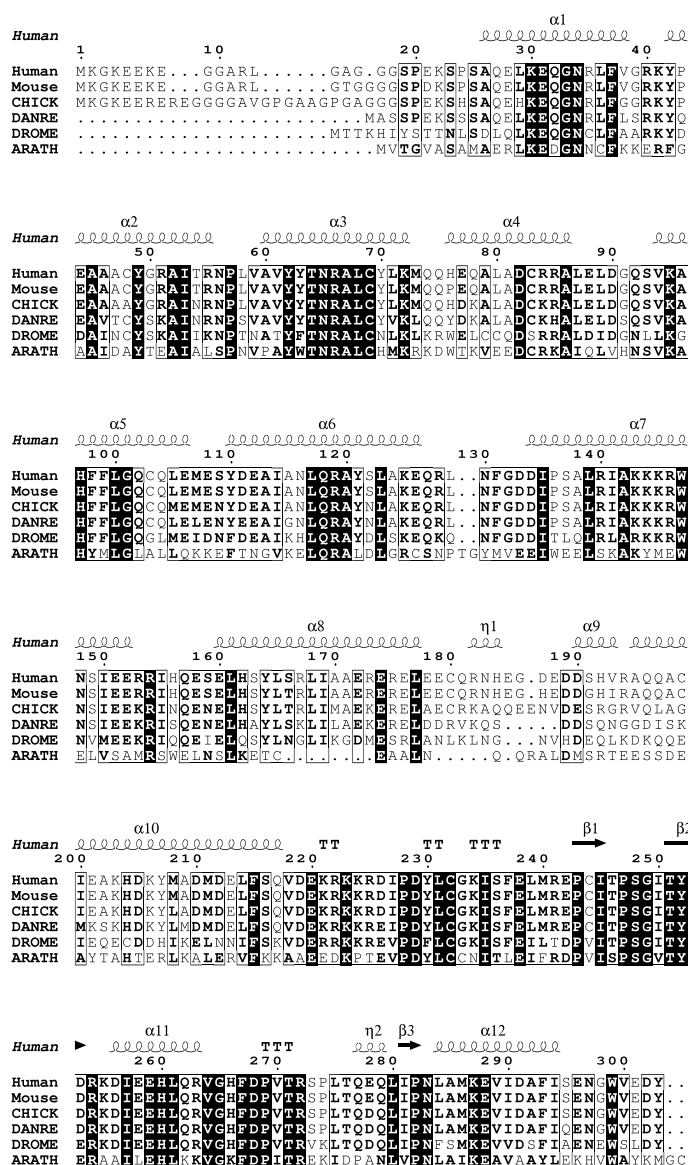


Figure 8. CHIP sequence alignment. Sequence alignment of amino acid sequence of CHIP from human, *Mus musculus* (mouse), *Gallus gallus* (chicken), *Danio rerio* (zebra fish), *Drosophila melanogaster* (fruit fly) and *Arabidopsis thaliana* (plant), with secondary structure indicated for human CHIP. Conserved residues are framed, identical residues underlaid black. This figure was produced by using ESPrpt 3.0 (<http://esprpt.ibcp.fr/ESPrpt/ESPrpt/>).

Each protomer comprises a C-terminal U-box domain and a N-terminal TPR domain, connected via an α -helical coiled-coil (CC) domain. The TPR domain is formed by three pairs of anti-parallel helices ($\alpha 1$ - $\alpha 6$), with $\alpha 1$ and $\alpha 2$ displaying high degrees of flexibility in deuterium exchange experiments [89]. Similarly, the 70 N-terminal amino acids of CHIP exchanged 100 % of hydrogen atoms to deuterium within 10 sec of exposure, indicating an intrinsically disordered patch. The third helix pair of the TPR domain is closely packed against the first helix of the CC-domain ($\alpha 7$), which forms an anti-parallel hairpin with the second helix of the CC-domain ($\alpha 8$).

In one protomer the CC-domain assumes a straight conformation, while in the other protomer $\alpha 7$ is split into two separate helices (Asp134 to Arg155 and Glu161 to Arg183),

connected by an extended patch from residue Ile156 to Ser160. The $\alpha 8$ helix displays less α -helical content in the "broken" protomer and connects the CC-domain, with a respectively longer extended coil region, to the C-terminal U-box. The orientation of the extended coil differs between the two protomers. In the "broken" protomer it is closely packed against the second half of $\alpha 7$ (Glu161 to Arg183), while assuming a distal position in the "straight" protomer.

The C-terminal U-box consists of a pair of β -hairpins ($\beta 1$, $\beta 2$), connected to a short α -helical patch ($\eta 2$), followed by a third hairpin ($\beta 3$) and leading to a C-terminal α -helix ($\alpha 10$). U-box domains display no asymmetry and are juxtaposed in the dimer [77].

The dimerization of CHIP involves two separate segments in the U-box domain and the distal segment of the CC-domain hairpins and is essential for its ubiquitylation activity [90]. All residues involved in both dimerization interfaces are strongly conserved even though the length of the hairpins can vary between species.

One dimerization interface is a hydrophobic patch located in the CC-domain, comprising Leu162, Tyr165, Leu166, Leu169, Ile170 from $\alpha 7$ and Tyr208, Met212, Leu215, Phe216, and Val219 from $\alpha 8$. They form a four-helix bundle with their equivalents in the other protomer.

The second dimerization interface is embedded in the U-box which forms a parallel dimer through highly conserved clusters in each protomer, packing against each other. It has been shown that isolated U-boxes form dimers of low stability in solution but have the potential to bind two E2 enzymes at a time [77][91]. This binding however, is precluded in full length CHIP due to the asymmetry generated by the broken hairpin and the U-box dimerization.

The TPR domains of each protomer acquire different positions with respect to their U-box. While the TPR of the "straight" protomer assumes a distal position, another TPR domain contacts its U-box domain presenting an obstacle for successful E2 binding. The result of this asymmetry induced conformation is the blockade of the E2 binding site, rendering this U-box inactive. Thus, CHIP displays a "half-of-sites" activity and effectively couples the formation of a monotonic polyubiquitin chain to a dimeric protein [77].

The exclusive occurrence of the asymmetric dimer is however subject to discussion, as a crystal structure of zebra fish CHIP showed a symmetric dimer, with both CC-domains assuming a straight conformation. However, a deletion of the TPR domain was necessary to acquire this structure, suggesting some influence of the TPR domain on the dimer conformation of CHIP. Arguing against the natural appearance of the symmetric dimer, which would be able to form a 2:2 complex with E2s, a 2:1 complex was observed by isothermal titration calorimetry for mouse CHIP. The authors of the zebra fish structure suggest that CHIP might morph between conformations of differing symmetry, depending on the nature of its interaction partners [92].

Recent molecular simulations suggested a mechanism combining features of both structures [93]. The model proposes a chimeric inactive monomer of CHIP which is more stable than either the straight or the broken protomer in the mouse CHIP crystal structure. Those monomers initially form a symmetric dimer through hydrophobic interfaces in their respective helical domains. The close proximity of U-box domains in this conformation triggers U-box dimerization which, in turn, moves positively charged residues in opposing positions. The resulting repulsion is compensated by the breaking of a middle domain helix in one of the protomers, forcing the formation of the active asymmetric dimer. Thus claiming the formation of asymmetry as a mechanism of activation.

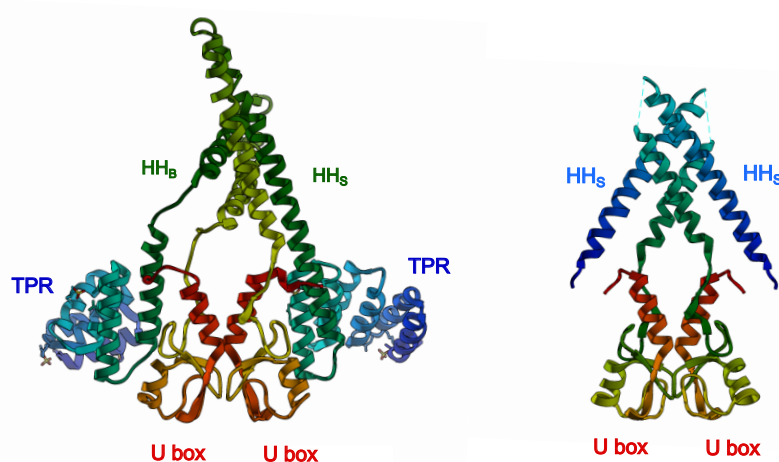


Figure 9. Crystal structures of the symmetric and asymmetric CHIP dimer. (A) Crystal structure of the asymmetric homodimer of murine CHIP bound to HSP90 decapeptide (PDB: 2C2L). Each protomer consists of a TPR domain (blue), a U-box domain (orange-red) and a connecting α -helical domain (green). Dimerization interfaces are located in the U-box domain and the middle domain which assumes a straight (HH_S) and a broken (HH_B) conformation. (B) Crystal structure of the symmetric CHIP homodimer from *Danio rerio* (zebra fish) (PDB: 2F42). Both α -helical domains (blue) assume a straight conformation (HH_S) while displaying both dimerization interfaces (U-box domain and middle domain). The TPR domain was removed by genetic modification.

As an E3 ligase of the U-box family, CHIP interacts with E2 proteins from the ubiquitylation cascade and facilitates the transfer of ubiquitin from the E2~Ub complex to the substrate. Initially, CHIP was discovered to interact with the stress associated UBCH5 family of E2s, attaching K48-linked polyubiquitin chains to substrate proteins and targeting them for proteosomal degradation [71].

The structural determinants for CHIP interaction with an E2 are two hairpin turns (234 to 239 and 269 to 274) and a short helix (η 2) in the U-box domain, forming a hydrophobic groove. The equivalent interface on the interacting E2 inserts into this groove when binding to CHIP. For the specific interaction of CHIP with certain E2s a serine-proline-alanine motif (S-P-A) in the inserting interface of the E2 is necessary. CHIP-interacting E2s from the UBCH5 family contain this motif as well as E2s from the UBC4 family and UBE2E1-3 [92]. Additionally, an association of CHIP with the UBC13-UEV1A heterocomplex was reported, with S-P-A motif present in UBC13. The heterodimeric E2

produces K63-linked polyubiquitin chains instead of K48, which have been implied to have regulatory functions [94]. In contrast to the interaction with UBCH5A, CHIP does not undergo autoubiquitylation in complex with UBC13-UEV1A, suggesting a synthesis of unanchored ubiquitin chains [95]. The auto-ubiquitylation of CHIP could not be linked to its degradation but might serve as a regulatory element or a localisation signal [96].

1.4.3 CHIP regulation

Only a limited number of studies is available on the transcriptional regulation of CHIP in different physiological and pathological contexts. An upregulation of CHIP and HSP70 mRNA levels was observed under various stress conditions, like heat shock and oxidative damage. In several human malignancies, both protein and mRNA levels were shown to be lower than in corresponding normal tissues and were linked to clinical prognosis. Similar few examples are known of posttranscriptional regulation of CHIP mRNA. It has been found that during differentiation of osteoblasts, CHIP is downregulated through inhibition of translation by microRNA (miR-764-5p) which binds the 3'-UTR of CHIP mRNA [97]. Most post-translational modifications of CHIP are realised by interaction with other proteins, even though N- and C-terminal regions of CHIP have been predicted to contain functional phosphorylation sites. In this regard, the reported interaction with kinases such as ERK5 and LIM kinase 1 (LIMK1), which increase CHIP ubiquitin ligase activity, seem to offer an interesting possibility for a phosphorylation-dependent regulation.

Another possibility of direct modification on CHIP is its ubiquitylation status. CHIP is capable of auto-ubiquitylation with yet unknown functional consequences. One could however speculate that a modulation of CHIP ubiquitylation offers a possibility for deubiquitylation enzymes (DUB) to act on CHIP's activity. The validity of this assumption has been confirmed for the DUB ATAXIN-3, which limits the ubiquitin chain length attached to substrates by CHIP~UBE2W through deubiquitylation of CHIP [98].

Another mechanism for the regulation of CHIP activity is the competition for binding sites and inhibition of CHIP-chaperone complex formation. Recent studies have shown that proteins of the S100 family (S100A2 and S100P) associate with the TPR domain of CHIP and other TPR-containing proteins in a calcium dependent manner, interfering with CHIP interaction towards HSP70 and HSP90 and subsequently suppressing complex dependant substrate ubiquitylation [99]. A similar regulation of CHIP activity was found for the ATPase OLA-1, which competes with CHIP for the HSP70 binding site, hence protecting HSP70 from CHIP mediated ubiquitylation and subsequent degradation [91]. Indirect modification of CHIP activity through other proteins is realised by modulation of CHIP:HSP70 complex formation. The Bcl-2-associated athanogen (BAG) proteins are a protein-family comprising six members (BAG1 to BAG6) which act on the NBD domain of HSC/HSP70 and can modulate activity in both, positive and negative, manners. BAG1

stimulates CHIP:HSP70 complex formation and enhances CHIP induced degradation by UPS, while BAG3 induces client degradation by autophagy. BAG2 inhibits CHIP E3 ligase activity by disrupting association with E2s. BAG5 has been reported to exhibit specialized function, enhancing activity of CHIP on α -synuclein [3].

1.4.4 CHIP in physiology and disease

Due to its central function in the PN and despite its redundancy in some cellular pathways, CHIP is involved in a wide array of cellular processes under resting conditions as well as in response to stress. CHIP is of particular importance in clearing misfolded HSP70/90 clients that are prone to aggregate. Many of such aggregate-forming proteins like α -synuclein, huntingtin, and tau-protein, are implicated in severe human pathologies of the neuronal system [100][101][102].

Due to its regulatory function on the abundance of proliferation-regulating proteins, CHIP has been identified as a critical factor in various types of cancer, influencing progression and malignancy of the disease. Pioneering work by Kajiro et al. identified CHIP as a suppressor of tumour growth and metastasis in breast cancer [103]. Later studies on CHIP mRNA levels confirmed the findings and linked high CHIP-expressing tumours to better overall patient survival [104]. In recent years, several onco-proteins from various cancer types have been reported to be negatively regulated by CHIP, supporting the role of CHIP as a tumour suppressor [91]. A possible explanation for the negative regulation by CHIP is that it shifts the chaperone cycle of HSP90, a highly expressed chaperone in many cancers, towards degradation instead of refolding, by out-competing the co-chaperone HOP [105].

On the other side, in a number of publications, high levels of CHIP were linked to poor patient prognosis in several cancer types. For example, it was shown that the tumour suppressor PTEN is a target of CHIP-mediated degradation in prostate cancer [106]. The controversial role of CHIP regarding its oncogenic or tumour suppressive potential underlines its versatile and complex role in cellular homeostasis. The opposing functions might originate from the relative interaction and abundance of HSP90 and HSP70 in different cancer cells and the competition with other diverse co-chaperones of which expression levels and identities are not completely understood at present time [91].

Exceeding its importance in various diseases, CHIP is also important for development and longevity of mammals. CHIP deficient mice (CHIP $-/-$), show increased lethality and sensitivity to thermal stress in embryonic stages [107]. Post-developmentally, knockout of CHIP in mice results in a significantly reduced life span [108]. Even though ageing has been linked to an accumulation of misfolded proteins and a collapse of the PN, the mice that display premature ageing show no general increase of CHIP substrate stability, suggesting that CHIP turnover of a specific target leads to accelerated ageing. A recent study

proposed a scheme by which the turnover of insulin receptor (INSR) by CHIP could be a major factor in understanding this phenotype and the role of CHIP in longevity. Under normal growth conditions, CHIP is regulating INSR levels by ubiquitylation and subsequent degradation in an HSP70/90-independent manner. Simultaneously, the pool of CHIP maintains cellular proteostasis in concert with chaperones. Under stress conditions and the elevation of proteotoxic stress during ageing, the available pool of CHIP is channelled towards proteostasis tasks, leading to accumulation of INSR and hyperactivity of its signalling [109].

Beyond the function as an E3 ligase, CHIP can act as an E4 ligase, potentiating the activity of other E3 ligases. Of particular interest regarding this function was a study that found CHIP to enhance PARKIN ubiquitylation towards unfolded PAEL receptor (PAEL-R) *in vitro* and *in vivo*. By promoting PAEL-R release from the HSC/HSP70 complex, CHIP facilitates PARKINs access on PAEL-R. Furthermore, CHIP enhances ubiquitylation activity of PARKIN *in vitro* in a HSP70-independent manner. If not degraded by PARKIN, PAEL-R accumulates at endoplasmic reticulum (ER) membranes of dopaminergic neurons, inducing neuronal death and hence fostering juvenile Parkinson's disease [87].

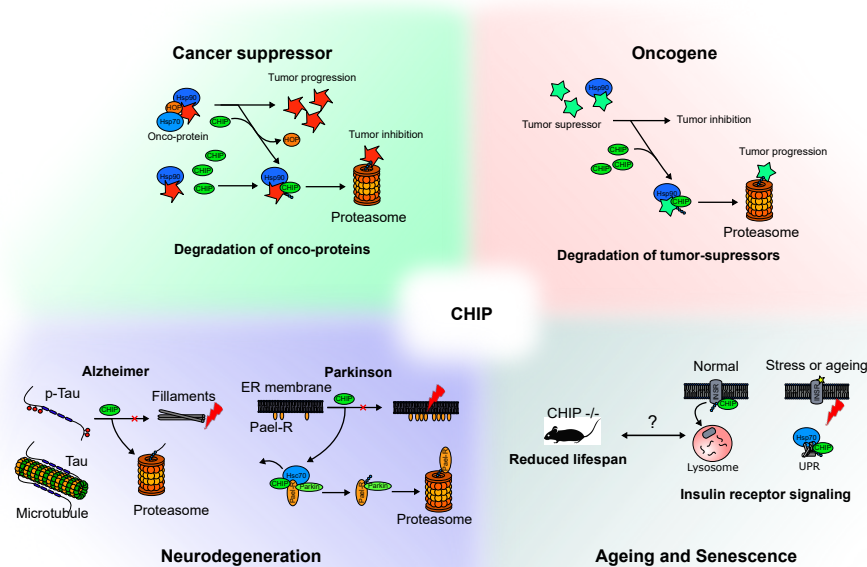


Figure 10. The impact of CHIP on various diseases. CHIP has a bivalent role in different types of cancer. It can act as a tumour suppressor through release of onco-proteins from the stabilizing chaperone complex and their proteasomal degradation. In other cancer types, tumour suppressors are subjected to CHIP-mediated degradation, thus fostering cancer progression. In the neurodegenerative Alzheimer's disease, CHIP has a protective function by mediating degradation of phospho-Tau which otherwise would accumulate to toxic filaments. In Parkinson's disease, it promotes activity of the E3 ligase PARKIN, indirectly preventing the detrimental accumulation of PAEL-R at the ER-membrane. CHIP importance in longevity has been shown by knock-out mice, which is possibly linked to the CHIP-governed turnover of insulin receptor (INSR).

1.5 Objectives of this thesis

The E3 ligase CHIP is a central node in the maintenance of an intact and functional proteome, a necessity for every living cell. It not only regulates chaperone-assisted folding of client proteins but simultaneously selects irreversibly misfolded proteins for degradation by the proteasome or initiates their disposal by autophagy. Exceeding its function in immediate proteostasis, CHIP has been implied in various cellular functions like signalling, ageing, development and apoptosis. The wide array of substrates, many of them connected to life-threatening diseases, makes CHIP a promising candidate for future therapeutic approaches.

Despite the significant progress in structural and functional understanding of this versatile E3 ligase, many questions surrounding its chaperone dependency and the bilateral regulation of chaperone and ligase, remain unclear. This becomes especially important when the capacity of the PN is challenged and chaperones are engaged with increasing amounts of unfolding proteins and aggregates, a situation occurring during ageing and in several human pathologies.

This thesis work was aimed to elucidate how CHIP participates in recognition of per-

turbed proteostasis during acute stress exposure and how this participation depends on molecular chaperones. The later question is of special interest as an increasing number of studies claimed a chaperone-independent function of CHIP, which partially contradicts the current view and needs further investigations. With respect to the spatial distribution of the protein quality control system, localisation of CHIP was investigated during stress exposure and how it might impact cellular architecture. It has been mentioned that little is known about the interconnection of PN components and the adjustment of cellular structures upon stress. As a key protein in protein folding and degradation, CHIP was an obvious choice to investigate possible connections, especially due to the unique variety of CHIP substrates in diverse cellular pathways. The study of CHIP offers the possibility to convey discovered principles to regulatory loops involving other TPR-containing proteins.

Material and Methods

2.1 Materials

2.1.1 Chemicals

Table 1. Reagents

Specification	Cat. Nr.	Company
DAPI dihydrochloride	D9542	Sigma Aldrich, St. Louis, MO
6-Carboxyfluorescein	21877	Sigma Aldrich, St. Louis, MO
7-Aminoactinomycin	BML-AP400-0001	Enzo Life Sciences, Germany
ANS	A1028	Sigma Aldrich, St. Louis, MO
Acetic acid	6755.1	Carl Roth GmbH, Germany
Adenosine triphosphate	A1852-1VL	Sigma Aldrich, St. Louis, MO
Ammonium acetate	7869.2	Carl Roth GmbH, Germany
Ampicilin	10835242001	Sigma Aldrich, St. Louis, MO
Arsenite	S7400-100G	Sigma Aldrich, St. Louis, MO
Bovine serum albumin, FA free	A7030	Sigma Aldrich, St. Louis, MO
Bovine serum albumin, FA free	10775835001	Roche, Switzerland
Bradford Reagent	B6916-500ML	Sigma Aldrich, St. Louis, MO
Bromphenol Blue	T116.1	Carl Roth GmbH, Germany
Calcium chloride	CN93.4	Carl Roth GmbH, Germany
Chloramphenicol	C0378-5G	Sigma Aldrich, St. Louis, MO
Chloroform	1024451000	Merck KGaA, Germany
Di-potassium phosphate	P749.2	Carl Roth GmbH, Germany
Dithiothreitol (DTT)	D9779	Sigma Aldrich, St. Louis, MO
EDTA	03677	Sigma Aldrich, St. Louis, MO
EGTA	E3889	Sigma Aldrich, St. Louis, MO
Ethanol	1.00974	Sigma Aldrich, St. Louis, MO
Ethanol 99.9 %	P076.1	Carl Roth GmbH, Germany

CHAPTER 2. MATERIAL AND METHODS

Glutaraldehyde	G6257	Sigma Aldrich, St. Louis, MO
Glycerol	3783.5	Carl Roth GmbH, Germany
Glycine	3187.4	Carl Roth GmbH, Germany
HEPES	9105.4	Carl Roth GmbH, Germany
Hydrochloric acid	H1758	Sigma Aldrich, St. Louis, MO
IGEPAL [®]	I8896	Sigma Aldrich, St. Louis, MO
Isopropanol	I9516	Sigma Aldrich, St. Louis, MO
IPTG	10724815001	Sigma Aldrich, St. Louis, MO
Kanamycin	60615	Sigma Aldrich, St. Louis, MO
Magnesium chloride	KK36.2	Carl Roth GmbH, Germany
Magnesium sulphate	0261.1	Carl Roth GmbH, Germany
Methanol	8388.1	Carl Roth GmbH, Germany
Paraformaldehyde	158127	Sigma Aldrich, St. Louis, MO
Potassium chloride	5346.2	Carl Roth GmbH, Germany
Potassium diphosphate	3904.1	Carl Roth GmbH, Germany
Potassium hydrochloride	6781.1	Carl Roth GmbH, Germany
Sodium chloride	9265.2	Carl Roth GmbH, Germany
Sodium citrate	3580.3	Carl Roth GmbH, Germany
Sodium dodecyl sulphate	0183.2	Carl Roth GmbH, Germany
Sodium hydroxide	221465	Sigma Aldrich, St. Louis, MO
Sodium molybdate	243655	Sigma Aldrich, St. Louis, MO
Staurosporine	S5921	Sigma Aldrich, St. Louis, MO
Sucrose	4621.3	Carl Roth GmbH, Germany
Terbium(III)-chloride	451304	Sigma Aldrich, St. Louis, MO
Tergitol NP-40	NP40S	Sigma Aldrich, St. Louis, MO
TRIZMA [®] base	T1503	Sigma Aldrich, St. Louis, MO
Tween-20	9127.1	Carl Roth GmbH, Germany
PreScission protease	27084301	GE Healthcare, UK
Polyethylenimine	#23966-2	Polysciences Inc., Warrington, PA
XTT sodium salt	X4626	Sigma Aldrich, St. Louis, MO
Phenazine methosulfate	P9625	Sigma Aldrich, St. Louis, MO

2.1.2 Equipment

Table 2. Laboratory equipment

Specification	Model	Company
Tabletop centrifuge	MIKRO 200R	Hettich GmbH, Germany
Tabletop centrifuge	accuSpin Micro 17R	Thermo Fischer, Waltham, MA
Swing-Bucket centrifuge	MEGAFUGE 16R	Thermo Fischer, Waltham, MA
Swing-Bucket centrifuge	Allegra X-15R	Beckman Coulter, Brea, CA
Fixed-Bucket centrifuge	Avanti J-26	Beckman Coulter, Brea, CA
Ultracentrifuge	TL-100	Beckman Coulter, Brea, CA
Thermomixer	comfort	Eppendorf, Germany
Thermomixer	TS1	Biometra GmbH, Germany
Block heater	SBH1300	Stuart Equipment, UK
Roller board	TRM 50	IDL GmbH, Germany
Platform shaker	Rotamax 120	Heidolph Instruments GmbH, Germany
Magnetic stirrer	MR Hei-Mix S	Heidolph Instruments GmbH, Germany
Spectrometer	BioSpectrometer basic	Eppendorf, Germany
Incubator	Ecotron	INFORS HT, Switzerland
Vacuum Concentrator	RVC 2-18 CO	Christ GmbH, Germany
pH meter	PB-11	Sartorius AG, Germany
Balance	PCB	KERN GmbH, Germany
Balance	S-234	Denver Instruments, Bohemia, NY
PCR cycler	peqSTAR 2xGradient	PEQLAB Biotechnologie GmbH, Bohemia, NY
Sonicator	SONOPULS	BANDELIN, Germany
Imaging system	ChemiDOC™MP	Bio-Rad, Hercules, CA
CO ₂ Incubator	HERAcell 150i	Thermo Fischer, Waltham, MA
Sterile workbench	MAXISAFE 2020	Thermo Fischer, Waltham, MA
Electroporation system	GenePulser Xcell	Bio-Rad, Hercules, CA
Inverted confocal microscope	LSM780	Carl Zeiss, Germany
Inverted microscope	Observer Z1	Carl Zeiss, Germany
Stereo microscope	Motic SMZ-168	Carl Zeiss, Germany
SIM/PALM microscope	ELYRA PS.1	Carl Zeiss, Germany

Electrophoresis	Mini-PROTEAN Tetra Cell	Bio-Rad, Hercules, CA
Western blot transfer	Criterion Blotter	Bio-Rad, Hercules, CA
Protein purification	ÄKTApurifier	GE Healthcare, UK
Extruder	LiposoFast-Basic	AVESTIN Inc., Canada, ON
NanoSight	LM10-HS	Malvern Instruments, UK
Tecan plate reader	infinite M200	Tecan, Switzerland
Spectropolarimeter	J-810	Jasco, Easton, MD
Isothermal calorimeter	Nano ITC	TA instruments, New Castle, DE
Thermal cycler	C1000	Bio-Rad, Hercules, CA

2.1.3 Kits

Table 3. Preparation and assay kits

Specification	Company
PCR Mycoplasma test kit II	Applichem, Germany
GenElute HP Endotoxin-free Plasmid Maxiprep Kit	Sigma Aldrich, St. Louis, MO
GenJET Plasmid Miniprep Kit	Sigma Aldrich, St. Louis, MO
NovaBright SEAP Detection System 2.0	Thermo Fischer, Waltham, MA
Luciferase Assay System	Promega, Madison, WI

2.1.4 Plasmids and primer

Table 4. Plasmids

Specification	Application	Reference
EGFP-N1	Control	1-18
EGFP-C2	Cloning	1-19
L-EGFP	Monomeric EGFP	1-388
EGFP-F	Membranous EGFP	1-68
EGFP-CHIP	Microscopy /MS	1-800
EGFP-CHIP-m2 Δ	Microscopy	1-802
EGFP-CHIP-K30A	Microscopy/MS	1-828
EGFP-CHIP-K30A-m1 Δ	Microscopy	1-829
EGFP-CHIP-K30A-m2 Δ	Microscopy	1-830
Beta-1,4-galactosyltransferase1-EGFP	Microscopy	1-410
pcDNA3	Control/Cloning	1-10
pCMV10-CHIP	Mammalian expression	1-813

pCMV10-K30A	Mammalian expression	1-814
pcDNA3.1-HSP70	Mammalian expression	1-879
pcDNA3.1-HSP70ΔD	Mammalian expression	1-937
pcDNA/V5-DEST-HSC70	Mammalian expression	1-716
pcDNA-HSC70	Mammalian expression	1-938
pEF-SEAP	SEAP secretion assay	1-558
6xNF-kB-Luciferase	NF-kB induction assay	1-73
Flag-TRAF6	NF-kB induction assay	1-97
pEF-luci	Luciferase assay	1-37
pGEX-CHIP	Protein purification	2-82
pETDuet-I-His-CHIP	Protein purification	2-186
pGEX-extTPR	Protein purification	2-215
pET15-UbE2W	Protein purification	2-227
pET17b-αsynuclein	Protein purification	2-228
pET17b-βsynuclein	Protein purification	2-229
pET17b-γsynuclein	Protein purification	2-230
pGEX-CHIP-24aa	Protein purification	2-253
pGEX-CHIP-ΔTPR	Protein purification	2-177
pGEX-CHIP-m2Δ	Protein purification	2-217

Table 5. Primer

Template	Application	Sequence 5'-3'
pGEX-CHIP	Deletion N-terminal 24aa	FW: CAGGGGCCCTGGGATCCCC- GAGCGCGCAGGAGCTC REV: GCGGCCGCTCGAGCTAG- TAGTCCTCCACCCAG
pcDNA/V5- DEST-HSC70	Deletion of V5 region	FW: GAGGTTGATTAGGACCCAGC REV: GCTGGGTCCTAATCAACCTC
pcDNA3- HSP70	Deletion C-terminal D	FW: GAGGAGGTATAGTAGGGGC- CTTTCC REV: GGAAAGGCCCTACTATAC- CTCCTC

2.1.5 Cell lines and bacteria strains

Table 6. Mammalian cell lines and bacteria strains

Specification	Species	Source
Murine embryonic fibroblasts	Mouse	Dr. A. Reichert
Hek293T	Human	ATCC, CRL-3216
DH5 α	<i>Escherichia coli</i>	Thermo Fischer, 18265017
BL21	<i>Escherichia coli</i>	Thermo Fischer, C6000-03

2.1.6 Inhibitors

Table 7. Inhibitors

Specification	Target	Cat. Nr.	Company
VER-155008	HSP70	SML0271	Sigma Aldrich, St. Louis, MO
Geldanamycin	HSP90	G3381	Sigma Aldrich, St. Louis, MO
VU0155069	PLD1	13206	Cayman Chemical, Ann Arbor, MI
Wortmannin	PI3K/PI4K	W1628	Sigma Aldrich, St. Louis, MO
CAY10594	PLD2	13207	Cayman Chemical, Ann Arbor, MI
FIPI	PLD1/2	13563	Cayman Chemical, Ann Arbor, MI
IN-10	PI4KIII- β	HY-100198	MedChemExpress Europe, Sewden
Protease inhibitors	Proteases	S8820	Sigma Aldrich, St. Louis, MO

2.1.7 Lipids

Table 8. Lipids

Specification	Cat. Nr.	Company
1,2-dioleoyl-sn-glycero-3-phosphocholine	850375	Avanti Polar Lipids, Alabaster, AL
1,2-dipalmitoyl-sn-glycero-3-phosphate	830855	Avanti Polar Lipids, Alabaster, AL
1,2-dipalmitoyl-phosphatidylinositol-4-phosphate	P-4016	Echelon Bioscience, Salt Lake City, UT

2.1.8 Media, buffers and solutions

Table 9. Media and ready-to-use solutions

Specification	Cat. Nr.	Company
Dulbecco's modified Eagle's medium	D5671	Sigma Aldrich, St. Louis, MO
Fetal bovine serum	F0804	Sigma Aldrich, St. Louis, MO
L-glutamine solution	250030	Sigma Aldrich, St. Louis, MO
Streptomycin sulphate	P4333	Thermo Fischer, Waltham, MA
Non-essential amino acids solution	11140	Thermo Fischer, Waltham, MA
Reduced Serum Medium	31985062	Thermo Fischer, Waltham, MA
OPTI-MEM I		
Hank's Balanced Salt Solution	H4641	Sigma Aldrich, St. Louis, MO
Phosphate buffered saline solution	10010023	Thermo Fischer, Waltham, MA
Trypsin-EDTA solution	T4049	Thermo Fischer, Waltham, MA
LB-medium	X964.3	Carl Roth GmbH, Germany
Glyoxal solution(40 %)	128465	Sigma Aldrich, St. Louis, MO
SuperSignal™West Pico PLUS	34577	Thermo Fischer, Waltham, MA
SYPRO Orange	S5692	Sigma Aldrich, St. Louis, MO
Trypsin/Lys-C Mix	5071	Promega, Madison, WI

Table 10. Established Buffers

Name	Application	Composition
Electroporation buffer	Cell culture	135 mM KCl 0.2 mM CaCl ₂ 2 mM MgCl ₂ 5 mM EGTA 10 mM HEPES-KOH pH 7.5
Sample buffer	SDS-PAGE	0.5 M TRIS-HCl pH 6.8 10 % (v/v) SDS 50 % (v/v) glycerol 0.01 % (w/v) bromphenol blue
Running buffer	SDS-PAGE	3g/l TRIZMA® base 14.4g/l glycine 1g/l SDS
Transfer buffer	Western Blot	3g/l TRIZMA® base 14.4g/l glycine 20 % (v/v) methanol

CHAPTER 2. MATERIAL AND METHODS

TBS	Western Blot	50 mM TRIS-HCl pH 7.6 150 mM NaCl
CHIP lysis buffer	Purification	25 mM HEPES-KOH pH 7.5 150 mM KCl 5 mM MgCl ₂ 10 % (v/v) glycerol 1 mM DTT 0.1 % (v/v) IGEPAL 1x protease inhibitors
HSP70 buffer	Purification	25 mM HEPES-KOH pH 7.5 150 mM KCl 5 mM MgCl ₂ 10 % (v/v) glycerol 1 mM DTT
Osmotic shock buffer	Purification	30 mM TRIS-HCl 7.2 2 mM EDTA 40 % (v/v) sucrose
Subcellular fractionation buffer	Cell fractionation	20 mM HEPES-KOH pH 7.5 10 mM KCl 250 mM sucrose 1.5 mM MgCl ₂ 1 mM EDTA 1 mM EGTA 1 mM DTT 1x protease inhibitors
Reconstitution buffer	Liposomes	25 mM HEPES-KOH pH 7.5 50 mM NaCl
Tb-encapsulation buffer	Liposomes	20 mM HEPES-NaOH pH 7.5 100 mM NaCl 100 mM Na ₃ (C ₆ H ₅ O ₇) 15 mM TbCl ₃
CF-encapsulation buffer	Liposomes	20 mM HEPES-NaOH pH 7.5 150 mM NaCl 10 mM CF
Leakage assay buffer	Liposomes	20 mM HEPES-NaOH pH 7.5 150 mM NaCl 1 mM EDTA, only for Tb(DPA)
Ubiquitylation buffer	Ub-assay	50 mM TRIS-HCl pH 7.5

		50 mM NaCl 10 mM MgCl ₂ 2 mM DTT 2 mM ATP
Lysis buffer MS-Interactome	MS	10 mM TRIS-HCl pH 7.4 150 mM NaCl 10 mM Na ₂ MoO ₄ 0.5 mM EDTA 0.5 % (v/v) NP-40
Dilution buffer interactome	MS	10 mM TRIS-HCl pH 7.4 150 mM NaCl 10 mM Na ₂ MoO ₄ 0.5 mM EDTA
MS wash buffer	MS	20 mM TRIS-HCl pH 7.5 150 mM NaCl
Lysis buffer proteome	MS	100 mM HEPES-NaOH pH 7.6 150 mM NaCl 10 % (v/v) SDS

2.1.9 Special consumables

Table 11. Resins and Columns

Specification	Cat. Nr.	Company
PD-10 Desalting column	GE17-0851-01	GE Healthcare, UK
HisTrap High Performance	GE29-0510-21	GE Healthcare, UK
HiLoad Superdex 200	GE28-9893-35	GE Healthcare, UK
HighPrep Q FF	28936543	GE Healthcare, UK
VIVASPIN 15R 3,000 MWCO	VS15RH11	Sartorius, Germany
VIVASPIN 15R 10,000 MWCO	VS15RH22	Sartorius, Germany
Glutathion Sepharose 4B	17075605	GE Healthcare, UK
EGFP-Trap-M magnetic beads	gtm-20	Chromotek, Germany

Table 12. Membranes and Tools

Specification	Cat. Nr.	Company
Supported nitrocellulose membrane	10600098	GE Healthcare, UK
Amersham nitrocellulose membrane	10600012	GE Healthcare, UK
Amersham PVDF membrane	10600029	GE Healthcare, UK
Glass capillary 2 μ l	552-0042	VWR, Randor, PA
0.4cm GenePulser cuvettes	552-0042	Bio-Rad, Hercules, CA

2.1.10 Antibodies

Table 13. Primary and secondary antibodies

Specification	Dilution	Company/Reference
C-terminal CHIP (rabbit)	1:1,000	Sigma Aldrich, C9243
N-terminal CHIP (rabbit)	1:1,000	Sigma Aldrich, C9118
C-terminal NQO1 (rabbit)	1:1,000	Sigma Aldrich, N5288
HSP70 (mouse)	1:500	Enzo Life Sciences, C92F3A-5
HSC70 (mouse)	1:500	Enzo Life Sciences, N27F3-40
GAPDH (rabbit)	1:1,000	Cell Signaling, 2118
α -synuclein (rabbit)	1:1,000	Santa Cruz, sc-7011-R
Ubiquitin (mouse)	1:1,000	Santa Cruz, sc-8017
eIFA4 (rabbit)	1:1,000	Cell Signaling, 9742S
anti-rabbit IgG	1:3,000	Sigma Aldrich, A9169
anti-rabbit Alexa Fluor 647	1:3,000	Cell Signaling, #4414
anti-mouse IGg	1:3,000	Sigma Aldrich, A4416

2.2 Methods

2.2.1 Cloning

Amplification of DNA was performed with a peqSTAR 2xGradient PCR cycler, using Phusion DNA Polymerase, respective buffer, dNTP-mix and DMSO from New England Biolabs (Ipswich, MA). A standard cycling program for Phusion DNA-Polymerase from New England Biolabs was used with 18-25 cycles and annealing temperatures adjusted to fit the respective primers. Restriction enzymes were purchased from New England Biolabs and digestion mixes were assembled according to enclosed protocols. For the mammalian expression of EGFP, the expression vector EGFP-N1 (Dr. Vabulas) was used. N-terminal fusion of EGFP to CHIP and CHIP mutants was constructed by cloning human CHIP coding sequence in pEGFP-C2 vector using HindIII and BamHI restriction sites. Untagged human CHIP and CHIP-K30A were constructed by deletion of 3xFLAG-tag from pCMV10-3xFLAG-CHIP expression vector (Dr. Schuster). EGFP fusions of the farnesylation signal of C-HA-Ras (Dr. Vabulas) and β -1,4-galactosyltransferase1 (Dr. Pohl) were used as markers for the plasma membrane and the Golgi apparatus respectively. HSP70 was amplified from human cDNA and cloned without a tag into pCMV10 expression vector. HSP70 Δ D, lacking the C-terminal aspartic acid, was prepared by shifting the stop codon with site directed mutagenesis. HSC70 without tag was constructed by site directed mutagenesis from pcDNA/V5-DEST-HSC70 (Dr. Vabulas) shifting the stop codon to delete the C-terminal V5 region. For bacterial expression of GST-tagged CHIP and CHIP mutants, respective coding sequences were cloned into pGEX-6P1 expression vector using BamHI and XhoI restriction sites. Deletion of the N-terminal 24 amino acids of CHIP in bacterial expression vector was prepared using the fast cloning method [110].

2.2.2 Cell culture and transfection

Immortalized murine embryonic fibroblasts (MEF) were a gift from Dr. A. Reichert (Düsseldorf University). The identity of the cells was confirmed by highly polymorphic short tandem repeat loci (Microsynth, Switzerland). Human embryonic kidney cells transformed with large T antigen (HEK293T) were from ATCC. Cell lines were free of mycoplasma contamination, confirmed by Mr. H. Wang, using the PCR Mycoplasma test kit II (Applichem, Germany). Unless stated otherwise all cell lines were cultured in Dulbecco's modified Eagle's medium -high glucose- (DMEM), supplemented with 10 % fetal bovine serum (FBS), 2 mM L-glutamine solution (200 mM), 100 IU/ml penicillin G, 100 μ g/ml streptomycin sulphate and non-essential amino acids at 37°C and 5 % CO₂ in a humidified incubator. MEF clones lacking CHIP (MEF K.O.) were engineered by Mr. Wei-Han Lang, using CRISPR/Cas9 system according to the protocol described in Ran

et al. 2013 [111]. pSpCasn(BB)-2A-GFP (PX461) and pSpCas9n(BB)-2A-Puro (PX462) plasmids were a gift from Feng Zhang (Addgene # 48140 and # 48141). Mammalian cells were transfected with DNA, acquired from GenElute HP Endotoxin-free Plasmid Maxiprep Kit, using either electroporation or polyethylenimine (PEI, 25kDa, linear).

PEI transfection

For transfection with polyethylenimine (PEI), DNA was mixed with OPTI-MEM I Reduced Serum Medium. The volume of OPTI-MEM was equal to 10 % of the final culture vessel's volume. PEI was added from a sterile stock solution (1 mg/ml H₂O) in indicated amounts and the suspension was briefly vortexed. After incubation at RT for 10 min, the transfection mix was added dropwise to a ~70 % confluent culture. Cells were processed 24 h to 48 h after transfection.

For live cell imaging during heat stress, 0.1×10^6 wild-type MEF cells were seeded per well in a 24-well Cell Imaging Plate with clear film bottom (Eppendorf, Germany). Cells were transfected ~12 h after seeding, with 1 μ g of EGFP-CHIP or EGFP as control, using PEI transfection in a 9:1 PEI to DNA ratio. Transfected cells were incubated for 24 h before transfer to the microscope incubator at 37°C and 5 % CO₂. Distinct positions were imaged during quiescent conditions, followed by their observation during heat shock at 43°C and 5 % CO₂ for 120 min. Similar processing was applied for co-transfection of EGFP-CHIP with HSC70 and subsequent heat exposure. Transfection was carried out with 0.5 μ g EGFP-CHIP and 0.5 μ g HSC70 (9:1 PEI:DNA).

For the treatment with wortmannin and IN-10 inhibitors, 0.05×10^6 wild-type MEF cells were seeded per well in 24-well Cell Imaging Plate with clear film bottom and transfected with 0.5 μ g EGFP-CHIP-K30A or EGFP-F respectively (9:1 PEI:DNA ratio). 24 h after transfection distinct positions were imaged at the microscope incubator at 37°C and 5 % CO₂. Following, serum-free medium containing either 0.1 μ M, 10 μ M wortmannin or 10 μ M IN-10 was added. Treated cells were imaged at distinct positions after 10 min and 20 min for wortmannin and after 20 min for IN-10. For CHIP localisation under arsenite stress and visualisation of stress granules, cells were seeded and transfected under similar conditions. Medium was exchanged containing 0.5 mM arsenite and incubated at the microscope incubator for 30 min at 37°C and 5 % CO₂ before imaging or processing for immunofluorescence.

For the analysis of cellular localisation of EGFP-CHIP, EGFP-CHIP-K30A, EGFP-CHIP-K30A-m1 Δ and EGFP-CHIP-K30A-m2 Δ , 0.2×10^6 wild-type MEF cells were seeded per well on poly-lysine coated cover slides in a 12-well plate. Transfection was carried out ~12 h after seeding with 1 μ g DNA respectively (9:1 PEI:DNA ratio) and cells were mounted for microscopy 24 h after transfection. For the analysis of CHIP mobilisation to the plasma membrane upon HSP70/90 inhibition, cells were transfected similarly, with 1 μ g of EGFP-CHIP or EGFP as control. 20 μ M VER-155008, 20 μ M 17-AAG or DMSO

as control, were added in serum-free medium 24 h after transfection and incubated for 4 h before mounting. For the microscopic analysis of EGFP-CHIP-K30A localisation upon PLD inhibitor treatment, cells were transfected as described with 1 μ g EGFP-CHIP-K30A or EGFP-F respectively. PLD inhibitors or DMSO as control were added in serum-free medium at a concentration of 1 μ M FIPI, 500 nM VU0155069 (PLD1) or 500 nM CAY10594 (PLD2) for 12-16 h before mounting.

For microscopy of staurosporine treated cells, 0.5×10^6 MEF K.O. were transfected by means of PEI with 1 μ g EGFP-CHIP or EGFP as control (6:1 PEI:DNA ratio). 24 h after transfection medium was exchanged to serum-free medium containing 2 μ M staurosporine from *Streptomyces sp* or an equivalent volume of DMSO as control and incubated for 12 h before mounting.

For microscopy of Golgi apparatus morphology upon CHIP or CHIP-m2 Δ overexpression, 0.2×10^6 MEF K.O. cells were seeded per well on poly-Lys coated cover slides in a 12-well plate. At 70 % confluence and \sim 12 h past seeding, medium was refreshed and cells were transfected with a 200 ng β -1,4-galactosyltransferase1-EGFP and 800 ng CHIP or CHIP-m2 Δ (9:1 PEI:DNA ratio). For the influence of HSP70 and CHIP co-expression on Golgi morphology, transfection was performed as described with 0.4 μ g β -1,4-galactosyltransferase1-EGFP, 1 μ g CHIP and 1 μ g HSP70 or HSP70 Δ D respectively. At least 24 h after transfection cells were processed for confocal microscopy. For the morphology of Golgi apparatus under heat stress conditions, 0.1×10^6 MEF K.O. and wild-type MEF cells were seeded per well on poly-Lys coated cover slides in a 12-well plate. Transfection was performed \sim 12 h after seeding with 1 μ g β -1,4-galactosyltransferase1-EGFP using a 9:1 PEI to DNA ratio. At least 24 h after transfection cells were subjected to 43°C heat for 30 min, followed by fixation and DAPI staining.

For the MS interactome analysis of chaperone-free CHIP 4×10^6 MEF K.O. cells were seeded on 10 cm dishes. Transfection was carried out 12 h after seeding by means of PEI (6:1 PEI to DNA ratio) with 10 μ g EGFP-CHIP-K30A or empty vector. Medium was exchanged 24 h after transfection to serum -free DMEM, supplemented with 500 nM PLD1 inhibitor (VU0155069) or DMSO. After 12 h treatment cells were washed with PBS and harvested with a cell scraper for MS processing.

Electroporation

For electroporation cells were trypsinized and washed once with 10 ml PBS. Following, the cells were resuspended in cold electroporation buffer, supplemented with 25 % FBS and transferred together with DNA to cold 0.4 cm GenePulser cuvettes. Murine embryonic fibroblasts (MEF) were transfected with 350 V, 950 μ F and human embryonic kidney cells transformed with large T antigen (HEK293T) were transfected with a 240 V, 950 μ F using a GenePulser Xcell. Avoiding the transfer of cellular debris, transfected cells were washed once with DMEM before seeding in the respective culture dishes.

For analysis of EGFP-CHIP-m2 Δ localisation, 5×10^6 wild-type MEF cells were transfected by means of electroporation with 10 μ g DNA and seeded on poly-lysine coated cover slides in a 12-well plate. About 24 h after transfection, cells were mounted in PBS. For the localisation of EGFP-CHIP and EGFP under nutrient starvation, wild-type MEF cells were transfected similarly. 24 h after transfection cells were rinsed with PBS and incubated in Hank's Balanced Salt Solution at 37°C and 5 % CO₂ for 6 h before mounting. For visualisation and FACS analysis of CHIP and CHIP-K30A overexpression on Hek293T viability, 3×10^6 cells were continuously split for seven days in a 1:2 dilution before using for experiments. Cells were transfected by means of electroporation with 3 μ g L-EGFP and 10 μ g CHIP or CHIP-K30A respectively.

Ex vivo subcellular fractionation of transiently transfected CHIP and CHIP-K30A was performed with 10×10^6 MEF K.O. cells, electroporated with 20 μ g DNA respectively and seeded on 10 cm culture dishes. 24 h after transfection cells were processed for subcellular fractionation.

For secreted placental alkaline phosphatase (SEAP) assay 6×10^6 MEF K.O. cells were transfected by means of electroporation with 10 μ g SEAP, 5 μ g luciferase and 30 μ g CHIP. Controls were transfected with equivalent amounts of empty plasmid and seeded in triplicates on a 12-well plate.

Membrane distribution of EGFP-CHIP-K30A was analysed in wild-type MEF cells (4×10^6) transfected with 10 μ g of EGFP-CHIP, EGFP-CHIP-K30A or EGFP respectively. Transfected cells were incubated O/N on a 10 cm dish before seeding on poly-Lys coated cover-slides. 12 h after seeding cells were processed for TIRF microscopy.

2.2.3 Confocal fluorescence microscopy

A Zeiss LSM780 inverted confocal microscope with a 63x oil immersion objective was used for fluorescence microscopy if not stated otherwise. For analysis of CHIP localisation cells were not fixed and the cover slides with the living cells were mounted in growth medium on glass slides with parafilm spacers. Cover slides were sealed with vaseline and immediately imaged at RT. For live cell imaging during heat stress and inhibition of lipid metabolism (PLD, wortmannin, IN-10) a black 24-well Cell Imaging plate was incubated at the microscope at 37°C and 5 % CO₂ or indicated temperatures and images were acquired at distinct positions on the slide before and after treatment. Photobleaching was avoided by low laser intensities and minimal acquisition time. ImageJ was used to quantify localisation phenomenons from an average number of cells noted at the respective figure and in the appendix (Tab.14).

For the analysis of Golgi morphology, cells were rinsed twice with PBS and fixed with 4 % (w/v) paraformaldehyde (PFA) for 20 min at RT, at least 24 h after transfection. Fixed cells were washed two times with PBS, followed by 1 μ g/ml DAPI staining for 3 min at RT

and three washing steps with PBS before mounting in PBS and sealing with nail polish. For quantification purposes the acquired image size was set to fit the maximal amount of cells and provide enough details to distinguish the respective phenotypes. ImageJ was used to quantify membrane localisation and Golgi morphology from an average number of cells noted at the respective figure and in the appendix (Tab.14).

2.2.4 Brightfield microscopy

For the analysis of heat stress on cell viability, 0.3×10^6 wild-type MEF and MEF K.O. were seeded per well in a 24-well plate. Each well was marked with a centred cross, ensuring imaging of the same cell population before and after treatment. Immediately after exposure to 43°C for 2 h in 1 ml medium containing 25 mM HEPES pH 7.5, cells were imaged with a 10x objective on a Zeiss Observer Z1 equipped with a AxioCam 503 mono camera, using brightfield illumination.

Analysis of Hek293T morphology after overexpression of CHIP and CHIP-K30A was performed at a magnification of 4.3x with a Motic SMZ-168 stereo zoom microscope, equipped with a Leica M165FC camera. The field of vision was centred to the middle of the a well, minimizing reflection effects.

2.2.5 TIRF microscopy

Cells were mounted alive in growth medium with parafilm spacers and sealed with vaseline. A SIM/PALM Zeiss ELYRA PS.1 microscope with a 63x oil immersion objective was used to acquire epifluorescent and total internal reflection fluorescence (TIRF) images on single, representative cells.

2.2.6 Immunofluorescence

For stress granules visualisation, arsenite treated cells were fixed 10 min at RT with 4 % (w/v) PFA after aspiration of growth medium and rinsing with PBS. Cells were permeabilized with acetone for 5 min at -20°C, followed by two times 5 min washing with PBS. Blocking with 1 % (w/v) BSA in PBS for 1 h was followed by addition of primary antibody anti-eIF4 in a 1:100 dilution in blocking buffer for 1 h at RT. Remaining primary antibody was removed by three wash steps with PBS for 5 min each and replaced with anti-rabbit Alexa Fluor(R) 647 at 1:1000 in blocking buffer for 1 h at RT. Aspiration of secondary antibody was followed by three wash steps with PBS and DAPI staining.

2.2.7 Fluorescence-activated cell sorting (FACS)

Hek293T cells co-transfected with CHIP or CHIP-K30A and EGFP-L were harvested 24 h after transfection in PBS with a cell scraper. To prepare cells for flow cytometry the suspension was filtered using 5 ml round-bottom tubes with cell-strainer cap and subsequently stained with 10 µg/ml 7-AAD for 30 min on ice. FACS analysis was run on a S3 cell sorter (Bio-Rad, Hercules, CA). Analysed cells were gated from a FCS/SSC dot plot to determine cell population and subsequently analysed for cells with simultaneous exhibition of green and red fluorescence. A total of 50,000 events was counted and analysed using FCSexpress 5 software (Fig.59).

For the selection of CHIP overexpressing cells for mass spectrometry, MEF K.O. cells were co-transfected with 3 µg EGFP and 30 µg CHIP expression vectors by electroporation. 24 h past transfection cells were trypsinized to yield a concentration of 10×10^6 cells/ml and processed as described for FACS sorting. Green fluorescence cells were sorted using a S3 Cell Sorter to a purity of 87-92 %. The sorted cells were centrifuged at 21,000 x g for 1 min at 4°C. The supernatant was discarded and the pellet was frozen at -80°C until processing for mass spectrometry.

2.2.8 SDS-PAGE and immunoblotting

Samples were boiled at 95°C for 5 min in 2x sample buffer supplemented with β-mercaptoethanol before separation with a self-cast 10 % polyacrylamide gel, if not stated otherwise, at 120-200 V in running buffer. Following transfer to 0.45 µm nitrocellulose or PVDF membranes was performed at 100 V for 35-40 min in a cooled Criterion Blotter filled with transfer buffer at 4°C. Membranes were blocked in 5 % (w/v) milk powder in TBS for 1 h at RT, before addition of primary antibody in indicated dilutions and incubation over night at 4°C. Membranes were washed trice with TBS followed by addition of secondary antibody in a 1:3,000 dilution in blocking buffer for 1 h at RT. Finally, membranes were washed trice with TBS + 0.1 % Tween-20. Chemiluminescence was developed with SuperSignal™West Pico PLUS and images were acquired with a ChemiDoc MP imaging system and quantified using Image Lab 5.0 software.

2.2.9 Recombinant protein purification

Human recombinant full length CHIP as well as mutants and truncated versions were purified from 2-4 l *Escherichia coli* BL21 cells inoculated at OD₆₀₀ of 0.1 in LB-medium and incubated at 37°C. Protein expression was induced with 0.5 mM IPTG at OD₆₀₀ 0.4-0.6 and incubation proceeded at 18°C over night. Bacterial cultures were harvested in a 1 l bucket centrifuge Avanti J-26 XP at 9000 x g and the resulting pellet was resuspended in CHIP lysis buffer. Bacteria were opened using French Press followed by probe

sonication MS72 at 90 % power in five cycles of 30 sec sonication plus 90 sec pause. Bacterial debris were removed by centrifugation at 45,000 x g for 30 min and supernatant was rotated with Glutathion Sepharose 4B for 2 h at 4°C. Sepharose-bound GST-tagged protein was subjected to overnight treatment with 500 µg PreScission protease yielding the released tag-free protein. Further purification was achieved by repeated size exclusion chromatography using a HiLoad Superdex 200 column on an ÄKTApurifier equipped with a UPC-900 detector, a P-900 flow system, a INV-907 injection module and a M-925 mixing unit. The volume of Glutathion Sepharose elution was reduced to 2-3 ml using VIVASPIN 15R 10,000 MWCO and injected onto the column at a flow rate of 1 ml/min. All CHIP variants were concentrated and stored in HSP70 buffer. Purifications of CHIP-ΔTPR and CHIP-m1Δ, following the described protocol were provided by Mr. Adrian Martínéz-Limon and Mr. Viktor Pfeifer.

Human his-tagged C-terminal, N-terminal and full-length HSP70 were purified from *Escherichia coli* BL21 cells as described but using 1 ml HisTrap column (GE Healthcare, UK) for affinity chromatography. Elution of bound protein was achieved by applying an imidazole gradient from 1 mM to 500 mM over 40 min. The respective fractions were subjected to repeated size exclusion chromatography using HiLoad Superdex 200 in HSP70 buffer until sufficient purity was achieved. Human his-tagged NQO1 wild-type and mutants, UBCH5A, UEV1A, UBC13 were purified equivalently by Mr. Adrian Martínéz-Limon and Dr. Martin Vabulas but using PBS supplemented with 1 mM DTT for size exclusion chromatography.

For human wild-type α -synuclein and A30P mutant purifications, *Escherichia coli* BL21 cells were cultivated and induced as described. Following harvest in PBS, cells were subjected for 10 min at RT to osmotic shock buffer and centrifuged at 9000 x g and 4°C for 20 min in a Avanti J-26 XP. The pellet was resuspended in ice-cold water supplemented with 2 mM MgCl₂ and incubated on ice for 3 min. The lysed periplasm was separated from cellular material by centrifugation at 9000 x g and 4°C for 20 min and loaded without concentration or dialysis onto a HiPrep Q FF anion exchange column at 2 ml/min with a 20 mM TRIS-HCl pH 8.0 running buffer. Protein was eluted by a 0-500 mM NaCl gradient over 140 min at 1 ml/min. Respective fractions were pooled and injected on a desalting column prior to a second HiPrep Q FF run. α -synuclein containing fractions were concentrated using VIVASPIN 15R 3000 MWCO and boiled at 95°C for 30 min, followed by centrifugation at 17.000 x g and 4°C for 30 min. The supernatant was injected on a HiLoad Superdex 200 column at 1 ml/min in PBS and final concentration of respective fractions. Purified α -synuclein A53T mutant was provided by Dr. Martin Vabulas.

Purity of all recombinant proteins was verified by coomassie-blue staining and concentration was determined by absorbance at 280 nm with a BioSpectrometer basic. Protein aliquots were snap frozen in liquid nitrogen and stored at -80°C.

2.2.10 Subcellular fractionation and chemical crosslinking

Wild-type MEF cells or transiently transfected MEF cells were cultured on a 10 cm dish to 80-90 % confluence and lysed in subcellular fractionation buffer to yield a 20×10^6 cell/ml suspension. Cells were disrupted by passing thirty times through a 26G needle. The suspension was cleared from nuclei by centrifugation at $720 \times g$ and 4°C for 5 min, followed by two centrifugation steps at $10,000 \times g$ for 5 min to clear mitochondria. The cytosolic fraction was acquired by ultracentrifugation of the supernatant at $100,000 \times g$, 1 h, 4°C in a TLA 120.1 fixed angle rotor. The transparent membrane pellet was washed once by addition of 400 μl subcellular fractionation buffer, followed by ultracentrifugation $100,000 \times g$, 45 min, 4°C . The washed pellet was resuspended in 80 μl CHIP-lysis buffer. 20 μl of total lysate, cytosolic fraction and membrane fraction were incubated with 800 μM HSP70 C-terminal octapeptide (GPTIEEVD) for 30 min at 37°C followed crosslinking with 0.025 % glutaraldehyde for 10 min at 30°C . Crosslinking reaction was quenched by addition of 100 mM TRIS-HCl pH 7.5 and analysed by western blotting with C-terminal reactive anti-CHIP antibody.

2.2.11 Liposome preparation

Liposomes were prepared by mixing 1,2-dioleoyl-sn-glycero-3-phosphocholine (DOPC) with either 5 %, 20 % (wt/wt) 1,2-dihexadecanoyl-sn-glycero-3-phosphate (DPPA) or 1 % (wt/wt) Phosphatidylinositol 4-phosphate diC16 (PI4P) in a 1.5 ml reaction tube. Lipid mixtures were dried under a nitrogen stream and kept for 1 h under vacuum to remove residual organic solvent. Liposomes were rehydrated in 1 ml reconstitution buffer to a concentration of 10 mM lipids. Liposomes were resuspended by shaking 1 h at 50°C 2000 rpm in a Thermomixer, followed by 1 h at 50°C in a sonication-waterbath. The liposome suspension was subjected to five freeze-thaw cycles in liquid nitrogen to promote unilamellar vesicle formation. Aliquots of 200 μl were pulse-sonicated for 8 sec at 45 % MS72 sonotrode to create a population of homogeneously sized liposomes. Sonicated liposomes were pooled, aliquoted, snap-frozen and stored at -80°C . For the analysis of size dependent binding, sonicated liposomes were subjected to twenty one times extrusion using a LiposoFast-Basic extruder with filter membranes of 100 nm, 50 nm and 30 nm pore size.

For the encapsulation of terbium citrate, 95 % (wt/wt) POPC and 5 % (wt/wt) DPPA were dried under a nitrogen stream and rehydrated in 20 mM HEPES-NaOH pH 7.5, 100 mM NaCl, 100 mM $\text{Na}_3(\text{C}_6\text{H}_5\text{O}_7)$, 15 mM TbCl_3 . For the encapsulation of $\text{Tb}(\text{DPA})_3^{3-}$ complexes the dried lipid were resuspended in 20 mM HEPES-NaOH pH 7.5, 100 mM NaCl, 50 mM $\text{Na}_3(\text{C}_6\text{H}_5\text{O}_7)$, 10 mM TbCl_3 , 50 mM DPA before processing as described to gain unilamellar vesicles. Additionally, liposomes were washed with a PD-10 Desalting column using a spin protocol with a liposome wash buffer (20 mM HEPES-NaOH pH

7.5, 100 mM NaCl) supplemented either with $\text{Na}_3(\text{C}_6\text{H}_5\text{O}_7)$ for Tb(citrate) encapsulating liposomes or EDTA for $\text{Tb}(\text{DPA})_3^{3-}$ complex encapsulating liposomes. Quality of liposomes after encapsulation and desalting was confirmed by Nanoparticle tracking analysis. Encapsulation of carboxyfluorescein (CF) based on the published protocol, rehydrating a lipid film of 80 % (wt/wt) POPC and 20 % (wt/wt) DPPA with 20 mM HEPES-NaOH pH 7.5, 150 mM NaCl, 10 mM CF [112]. Next, liposomes were processed to unilamellar vesicles as described and frozen at -80°C . Immediately before usage CF encapsulating liposomes were washed with PD-10 Desalting column using 20 mM HEPES-NaOH pH 7.5, 150 mM NaCl and 0.1 mM EDTA as wash buffer.

2.2.12 Nanoparticle tracking analysis

For nanoparticle analysis of liposome quality a LM10-HS instrument, equipped with sCMOS camera was used (NanoSight Ltd, Malvern, UK). Sonicated liposomes were diluted 1:1000 in filtered reconstitution buffer (25 mM HEPES-KOH pH 7.5, 50 mM NaCl) and injected into the instrument. A minimum of 6000 valid tracks were recorded at 25°C and analysed by Nanoparticle Tracking Analysis (NTA) using FTLA algorithm with a threshold set to 10 and a sample viscosity of 0.9 cP.

2.2.13 Liposome leakage assay

For CHIP induced leakage of $\text{Tb}(\text{DPA})_3^{3-}$ complex, POPC+5 %PA liposomes were mixed with assay buffer (20 mM HEPES-NaOH pH 7.5, 150 mM NaCl, 1 mM EDTA) and transferred to a black 96-well plate with half of the final assay volume. 10 μM CHIP was added in assay buffer to a separate well. Immediately before measurement of fluorescence at Tecan infinite M200 plate reader CHIP, or only buffer for controls, was mixed with liposomes to yield the final assay volume of 100 μl per well. Decrease of fluorescence was measured with 272 nm excitation and 490 nm emission with a gain of 160-220 over 30 min at 25°C . Finally, liposomes were lysed by the addition 0.1 % (v/v) triton X-100 to gain 100 % release of encapsulated $\text{Tb}(\text{DPA})_3^{3-}$ complexes [112]. The extent of released material (R_t) was calculated with the following equation.

$$R_t = 100 * \frac{I_0 - I_t}{I_0 - I_*}$$

Where I_t is the fluorescence at a time t , I_0 is the initial fluorescence intensity of the $\text{Tb}(\text{DPA})_3^{3-}$ encapsulating liposomes and I_* is the fluorescence intensity after lysis of the liposomes with triton X-100.

For leakage of carboxyfluorescein (CF) from POPC+20 %PA liposomes, 2.5 mM lipids were mixed with 10 μM CHIP in assay buffer (20 mM HEPES-NaOH pH 7.5, 150 mM NaCl) to a final volume of 200 μl , immediately before measurement at Tecan infinite

M200 plate reader. Fluorescence was measured with 490 nm excitation and 530 nm emission with a gain of 51 over 30 min at 25°C. Liposomes were lysed by the addition 0.1 % (v/v) triton X-100 to gain 100 % release of encapsulated CF [112]. The relative amount of released material (R_t) was calculated with the following equation.

$$R_t = 100 \times \frac{I_t - I_0}{I_* - I_0}$$

Where I_t is the fluorescence at a time t , I_0 is the initial fluorescence intensity of the CF encapsulating liposomes and I_* is the fluorescence intensity after lysis of the liposomes with triton X-100.

2.2.14 Lipid binding assay

Membrane-immobilized lipids were purchased from Echelon Research Laboratories. Each membrane was processed according to manufactures protocol and incubated with blocking buffer (3 % fatty acid free BSA, 0.1 % (v/v) Tween-20 in PBS pH 7.5) 1 h at RT. 0.5 $\mu\text{g/ml}$ (14 nM CHIP) of recombinant protein was added in blocking buffer and incubated 1 h at RT. For competition experiments on PIP-strips, ten times molar excess C-terminal HSP70 recombinant protein or 10 μM of C-terminal HSP70 octapeptide were added to CHIP in blocking buffer. Strips were washed trice with PBST and bound protein was detected by anti-C-CHIP or anti-N-CHIP antibody.

2.2.15 Preparation of lipid strips

Lipid strips were prepared from supported nitrocellulose membranes (GE Healthcare, UK) by cutting 1.5x8.5cm strips. The strips and the enclosed coversheet were put on a glass plate and spotted from DPPA in CHCl_3 or PI4P in 1:1 CHCl_3 :MeOH solutions on the membrane using a 2 μl glass capillary. Spotted strips were covered and dried at RT for at least 2 h before using or storing in a closed plastic bag at 4°C. Dried strips were blocked with blocking buffer for lipid strips (3 % fatty acid free BSA, 0.1 % (v/v) Tween-20 in PBS pH 7.5) 1 h at RT. 1 $\mu\text{g/ml}$ of recombinant protein was added in blocking buffer and incubated 1 h at RT. Strips were washed trice with PBST and bound protein was detected by anti-C-CHIP antibody.

2.2.16 Flotation assay

1 mM liposomes and 0.5 μM CHIP were incubated in 150 μl reconstitution buffer 30 min at 37°C. The suspension was adjusted to 30 % sucrose by adding 100 μl of a 75 % (w/v) sucrose solution in reconstitution buffer. The resulting high-sucrose solution was transferred to a 500 μl ultracentrifugation tube and overlaid with 200 μl of a 25 %

(w/v) sucrose solution and 50 μ l reconstitution buffer. The gradients were centrifuged at 240,000 \times g in a TLA 120.1 fixed angle rotor for 1 h at 25°C. The bottom (250 μ l), middle (150 μ l) and top (50 μ l) fractions were manually collected from bottom to top using a 100 μ l Hamilton syringe. Resulting fractions were analysed by western blotting using anti-C-CHIP after normalizing protein loading of respective fractions.

2.2.17 Co-sedimentation assay

2 mM of indicated liposomes were mixed with 2 μ M recombinant protein in 50 μ l reconstitution buffer. The suspension was incubated shaking at 450 rpm for 30 min at 37°C. Liposomes with bound protein were pelleted by ultracentrifugation at 100,000 \times g for 30 min at 25°C. The liposome pellet was washed with 50 μ l of reconstitution buffer and sedimented by ultracentrifugation at 100,000 \times g for 30 min at 25°C. The pellet was resuspended in 10 μ l reconstitution buffer, resolved by SDS-PAGE and analysed by overnight coomassie-blue staining. Controls were processed accordingly without addition of liposomes. For competition assays on liposomes indicated amounts of peptide or C-terminal HSP70 recombinant protein were incubated with 2 μ M CHIP for 30 min at 37°C prior to co-sedimentation. For the release of liposome-bound recombinant protein by increasing ionic strength, the washing buffer was supplemented with indicated amounts of NaCl. Images were acquired with ChemiDoc MP (Bio-Rad, Hercules, CA) and quantified with Image Lab 5.0 software.

2.2.18 Chemical crosslinking *in vitro*

5 μ M of recombinant CHIP were crosslinked with 0.025 % glutaraldehyde for 10 min at 30°C unless stated otherwise. Crosslinking reaction was quenched by addition of 100 mM TRIS-HCl pH 7.5. Crosslinking on 20 % (wt/wt) DPPA containing liposomes was performed after co-sedimentation on the resuspended pellet. Controls lacking liposomes were crosslinked with recombinant protein correlating to the determined binding capacity of the respective liposome. Samples were resolved by SDS-PAGE and analysed by overnight coomassie-blue staining. Images were acquired with ChemiDoc MP (Bio-Rad, Hercules, CA) and quantified with Image Lab 5.0 software.

2.2.19 *In vitro* ubiquitylation assay

In vitro ubiquitylation reactions were carried out in ubiquitylation buffer and contained 2.5 μ M substrate (NQO1-P187S), 100 nM UBE1, 1 μ M UBCH5A, 1 μ M UBC13, 1 μ M UEV1A respectively, 2.5 μ M CHIP for samples without liposomes and 100 nM ubiquitin from bovine erythrocytes. For liposome containing samples a co-sedimentation with 5 μ M CHIP and 2 mM of 20 % (wt/wt) DPPA containing liposomes was carried out and

the resulting pellet was resuspended in the ubiquitylation reaction mix. Reactions were incubated at 37°C for 1 h and eventually stopped by addition of reducing sample buffer and boiling at 95°C for 5 min. Analysis was done by western blotting using rabbit anti-C-CHIP, anti-C-NQO1 and mouse anti-ubiquitin antibodies.

2.2.20 CD spectroscopy

Far-UV CD spectra of 10 μ M CHIP with and without 2 mM 20 % (wt/wt) DPPA containing liposomes were recorded on a Jasco J-810 spectropolarimeter at 37°C in 10 mM KH_2PO_4 pH 7.5. Prior to measurement samples were incubated 30 min at 37°C. Compensating reconstitution buffer influences, on the spectra controls lacking liposomes, were supplemented with an equivalent amount of reconstitution buffer. Three repeated scans were obtained for each sample and subtracted from the buffer (10 mM KH_2PO_4) baseline. Data was collected in 1 mm path cell (Helma Analytics) from 250 nm to 200 nm in 0.2-1 nm steps at 50 nm/min if not indicated otherwise.

2.2.21 Protease sensitivity assay

2 μ M CHIP pelleted with 20 % (wt/wt) DPPA containing liposomes was subjected to 0.5 ng/ μ l trypsin treatment at 37°C. The reaction was eventually stopped by addition of reducing sample buffer and boiling at 95°C for 5 min. Controls lacking liposomes were incubated with recombinant protein correlating to the determined binding capacity of the respective liposome. Samples were resolved by SDS-PAGE and analysed by overnight coomassie-blue staining. Images were acquired with ChemiDoc MP and quantified with Image Lab 5.0 software.

2.2.22 Isothermal titration calorimetry

ITC was carried out using a Nano ITC. The calorimetric cell was filled with 10 μ M recombinant CHIP or CHIP-K30A protein in HSP70 buffer at a temperature of 37°C. HSP70 octapeptide (GPTIEEVD) was titrated from a 500 μ l syringe at 350 rpm stirring speed in 25 injections of 8 μ l every 3 min. Measurements were corrected for dilution heats as determined by titration of peptide into buffer. The acquired data was processed with Nano-Analyse Software and fitted to a independent binding model.

2.2.23 Thermal denaturation assay

Thermal denaturation assays were carried out on a C1000 Thermal cycler with a CFX real-time system. 5 μ M recombinant protein in HSP70 buffer was supplemented with 10x SYPRO Orange in a 96-well PCR plate. Fluorescence of SYPRO Orange at 570 nm was monitored during stepwise increase of incubation heat from 20°C to 80°C. The resulting

relative fluorescence units (RFU) were corrected for controls lacking recombinant protein and melting temperatures (T_m) were identified as the highest part of the curve by plotting the first derivative of the fluorescence emission as a function of temperature (T):

$$T_m = \frac{\Delta RFU}{\Delta T}$$

2.2.24 Secreted placental alkaline phosphatase assay

SEAP assay was performed in triplicates with the NovaBright SEAP Enzyme Reporter Gene Chemiluminescent Detection System 2.0. 24 h after transfection 200 μ l growth medium was collected and centrifuged at 1000 x g for 10 min at 4°C. 25 μ l of the supernatant was transferred to a reaction tube, mixed with 25 μ l assay buffer (CompA) and incubated at 65°C for 5 min in a Thermoshaker. Following 50 μ l reaction buffer (CompB) was added, the suspension was transferred to a black flat-bottom 96-well plate and incubated at RT for 20 min. Luminescence was measured at a Tecan infinite M200 plate reader with 1 sec acquisition per well.

2.2.25 Luciferase reporter assay

The luciferase assay system from Promega was used. For the luciferase assays performed in parallel with SEAP assays transfected cells were washed twice with PBS before addition of 150 μ l luciferase lysis buffer. Cells were lysed by a freeze-thaw cycle at -80°C for 20 min. 50 μ l of lysate were mixed with luciferase assay buffer in a black 96-well plate immediately before luminescence measurement with a Tecan infinite M200 plate reader for 5 sec per well.

2.2.26 XTT cell proliferation assay

For XTT assays, 0.05×10^6 wild-type MEF cells and MEF K.O. cell were seeded in triplicates per well in a 24-well plate. Growth medium was aspirated \sim 12 h after seeding and exchanged by 500 μ l or 250 μ l DMEM supplemented with 25 mM HEPES-KOH pH 7.5. Following cells were subjected to heat stress at 43°C for 2 h while controls remained at 37°C. Medium was exchanged after heat shock by DMEM containing 0.3 mg/ml XTT and 12.5 μ g/ml 5-Methylphenazinium methyl sulfate (PMS) proceeding incubation for 1:30 h at 37°C and 5 % CO₂. Absorbance was measured at 475 nm and 660 nm for each well at a Tecan infinite M200 plate reader after orbital shaking for 5 sec with an amplitude of 3 mm. To ensure effective heat stress, only experiments that displayed 10-20 % viability in wells with 250 μ l during heat shock were taken into account. For determination of viability, absorbance at 660 nm was subtracted from absorbance at 475

nm from wells that contained 500 μ l during heat stress and normalized to controls not exposed to heat stress.

2.2.27 Mass spectrometry

Sample preparation

For interactome analysis cells were lysed with 300 μ l lysis buffer and DNA was sheared by sonication for 5s with a MS72 sonotrode at 50 % power. The lysate was cleared by centrifugation at 12,000 x g for 15 min at 4°C and protein amount was normalized with Bradford reagent to 1.25 μ g/ μ l using dilution buffer. Lysate was incubated with 20 μ l EGFP-Trap-M magnetic beads rotating for 90 min at 4°C. Beads were washed trice with dilution buffer and twice with MS wash buffer before snap-freezing with liquid nitrogen and storage at -80°C until further processing. Following processing of MS samples was done by Dr. Giulia Calloni. Beads were resuspended in 50 μ l 8 M urea in 50 mM TRIS-HCl pH 8.5, reduced with 10 mM DTT for 30 min and alkylated with 40 mM chloroacetamide for 20 min at 22°C. Urea concentration was diluted to 2 M using 25 mM TRIS-HCl pH 8.5 with 10 % (v/v) acetonitrile. Proteins were digested over night with trypsin/lysC at 24°C. Peptides were acidified with 0.1 % (v/v) trifluoroacetic acid, desalted and fractionated on combined C18/strong cation exchange StageTips. Finally peptides were dried and resuspended in 1 % acetonitrile, 0.1 % formic acid.

For proteome analysis of CHIP overexpression, cells sorted by FACS were lysed in 200 μ l lysis buffer and DNA was broken by sonication for 5 sec. The lysate was cleared by centrifugation and 100 μ g of total protein were diluted in 4 % (w/v) SDS, 100 mM HEPES-NaOH pH 7.6, 150 mM NaCl, 0.1 mM DTT and heated for 5 min at 95°C. Following processing of MS samples was done by Dr. Giulia Calloni. The samples were then mixed with 200 μ l 8 M urea in 50 mM TRIS-HCl pH 8.5 and loaded onto spin filters with 30kDa cut off (Microcon). The filter aided sample preparation protocol (FASP) was essentially followed ([113]). Proteins were digested overnight with trypsin (sequencing grade, Promega). According to ([114]), acidified peptides (0.1 % (v/v) trifluoroacetic acid final concentration) were desalted with C18 Stage Tips (3 M) and fractionated with strong cation exchange (SCX) StageTips. The C18 trans-elution fraction was combined with the first of 6 SXC fraction. Peptides were dried and resolved in 1 % (v/v) acetonitrile, 0.1 % (v/v) formic acid.

LC-MS/MS

LC-MS/MS was performed by Dr. Giulia Calloni on a Thermo Scientific™ Q Exactive Plus equipped with an ultra-high performance liquid chromatography unit (Thermo Scientific Dionex Ultimate 3000) and a Nanospray Flex Ion-Source (Thermo Scientific).

Peptides were loaded on a C18 reverse-phase pre-column (Thermo Scientific) and separated on an in-house packed column (100 μm inner diameter, 30cm length, 2.4 μm Reprosil C18 resin (Dr. Maisch GmbH, Germany)) using a two-step gradient from mobile phase A 1 % (4 % acetonitrile, 0.1 % formic acid) to 30 % mobile phase B (80 % acetonitrile, 0.1 % formic acid) for 30 min followed by a second step to 60 % B for 60 min, with a flow rate of 250 nl/min. MS data was recorded in data dependent mode selecting the 10 most abundant precursor ions for HCD fragmentation. The full MS scan range was set to 300 to 2,000 m/z with a resolution of 70,000. Ions with charge ≥ 2 were selected for MS/MS scan with a resolution of 17,500 and an isolation window of 2 m/z. Dynamic exclusion of selected ions was set to 30s. Data were acquired using Xcalibur software (Thermo Scientific). The LC Unit was controlled by Chromeleon Xpress software.

Data analysis

MS data files were analysed by Dr. Giulia Calloni using MAX Quant (version 1.5.3.30) [115]. For protein identification the spectra were compared with UniProtKB mouse FASTA database (Jan. 2016) with a false discovery rate of 1 %. Unidentified features were matched between runs in a time window of 2 min. Identified hits of the categories false positive, only identified by site and known contaminants were excluded from further analysis. For label-free quantification (LFQ) the minimal ratio count was set to 1. Bioinformatic analysis was performed with Perseus (1.5.2.6) [116]. Statistical analysis between different conditions was done on logarithmic LFQ intensities for quantified proteins found at least in four out of five biological replicates for the interactome analysis and at least three out of four times for the analysis of proteome changes. All mass spectrometry methods were applied and mostly written by Dr. Giulia Calloni.

Results

3.1 Chaperone-free CHIP interacts with cellular membranes *in vivo* and *ex vivo*

In order to investigate how the E3 ligase CHIP localisation participates in early stress response, murine embryonic fibroblasts (MEF) were subjected to heat stress, inducing a perturbation of cellular proteostasis. In live cell confocal fluorescence microscopy, localisation of transiently transfected EGFP-CHIP was observed at 43°C for a duration of 120 min. During the exposure a significant fraction of MEF cells (21 %) displayed a mobilization of cytosolic EGFP-CHIP to the plasma membrane. In a small fraction of cells (3.6 %), EGFP-CHIP was already present at the plasma membrane under physiological conditions. A mobilization to the plasma membrane due to the EGFP fusion could be excluded, as EGFP transfected cells did not display membrane localisation under physiological and stress conditions (Fig.11A).

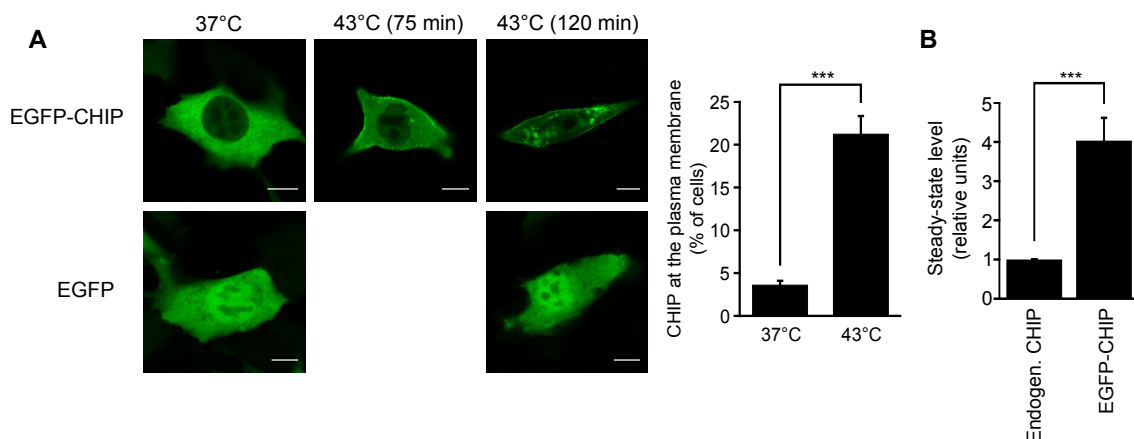


Figure 11. Heat stress induces CHIP mobilisation to cellular membranes *in vivo*. (A) Live cell microscopy of transiently transfected murine fibroblasts (MEF) during heat shock at 43°C for a duration of 120 min mobilised EGFP-CHIP to plasma membrane (mean \pm SD). One representative of three independent experiments is shown. Scale bar 10 μ m. *** p <0.001, chi-square analysis; N = 3 independent experiments. (B) Steady-state levels of endogenous CHIP and EGFP-CHIP 24 h after transfection (mean \pm SD). *** p <0.001, t-test analysis, N = 3 independent experiments.

For the quantification of cells with the membrane phenotype, an average of ninety cells was evaluated for each condition. Sufficient transfection efficiency was verified by western blot quantification of EGFP-CHIP expression levels. The transfected fusion protein displayed a four times increase over endogenous CHIP levels (Fig.11B). Due to the weak interaction between HSPs and CHIP [117], a preliminary hypothesis was established: Due to the stress induced disturbance of proteostasis, the chaperones would be channelled to unfolding proteins to prevent protein aggregation. During this immediate stress response holdase functions of the respective chaperones would be preferred over ubiquitylation and degradation of client proteins [1]. Thus, freeing CHIP to perform chaperone independent tasks until the HSP pool increases through transcriptional up-regulation.

To simulate the temporal deficiency of heat shock proteins *in vivo* and exclude the influence of metabolic changes on CHIP localisation during heat shock, EGFP-CHIP expressing murine fibroblasts were treated with specific inhibitors of HSP70 (VER-155008) and HSP90 (17-AAG) under quiescent conditions. A similar phenotype as in heat-stressed cells could be observed after 4 h treatment for both inhibitors in EGFP-CHIP transfected cells, but not in EGFP transfected controls (Fig.12). A sufficient knock-down of HSC70/HSP70 levels by means of siRNA, to supplement the results acquired by inhibitor treatment, could not be achieved (data not shown).

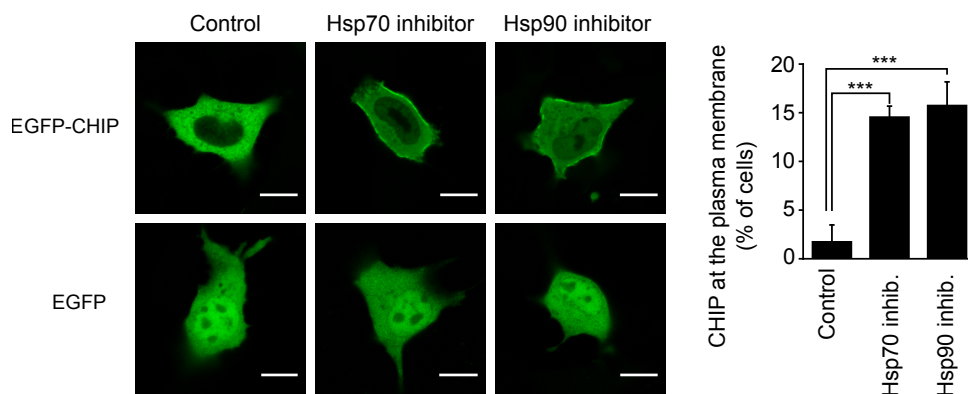


Figure 12. HSP70 and HSP90 inhibitor treatment induces CHIP localization to membranes. Intracellular localisation of CHIP changed, upon treatment for 4 h with HSP70 inhibitor (20 μ M VER-155008) or HSP90 inhibitor (20 μ M 17-AAG) to the plasma membrane of murine fibroblasts (mean \pm SD). EGFP-transfected cells were used as control. One representative experiment out of three is shown. Scale bar 10 μ m. *** p <0.001, chi-square analysis; N = 3 independent experiments.

The abundance and activity of chaperones was hypothesised to be a major determinate for the change in subcellular localisation of CHIP. Thus, supplementing cells with additional HSPs, could obstruct the transition to membranes during exposure to heat stress. Accordingly, heat shock at 43°C mobilized EGFP-CHIP to the plasma membrane in 16 % of cells, while membrane localisation was reduced by half in cells co-transfected with HSC70, as determined by live cell imaging (Fig.13A). The successful expression of transfected HSC70 surpassed endogenous protein levels by at least 2 fold, as shown by western blot analysis using anti-HSC70 specific antibody. GAPDH antibody was used as a control for equal loading of total protein (Fig.13B).

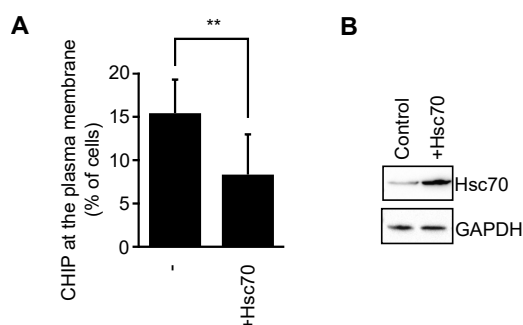


Figure 13. Chaperone abundance is linked to CHIP localisation *in vivo*. (A) Co-expression of HSC70 with EGFP-CHIP under heat shock conditions (43°C, 2 h) reduced translocation of cytosolic EGFP-CHIP to cellular membranes, as determined by live cell imaging (mean \pm SD). ** $p < 0.01$, chi-square analysis; $N = 3$ independent experiments. (B) Steady-state levels of HSC70 24 h after transfection, in murine fibroblasts, as determined by means of western blotting with anti-HSC70 antibody. One representative of two independent experiments is shown.

In order to determine if localisation of CHIP to cellular membranes was a general response to proteotoxic stress, different stressors were applied on MEF cells, transiently transfected with EGFP-CHIP. The toxic metalloid arsenite is a commonly applied chemical to induce proteotoxic stress, as it interferes with protein folding by acting on unfolded polypeptides and inducing protein aggregation. Moreover, arsenite induced aggregates might act as a seed promoting the aggregation of other labile proteins [118]. Treatment of murine fibroblasts with 0.5 mM arsenite for 30 min did not induce any mobilization of transiently transfected EGFP-CHIP to cellular membranes, nor did it affect EGFP-CHIP subcellular distribution in general. To ensure that proteostasis was challenged by arsenite treatment, the formation of stress granules was monitored in arsenite treated cells and control cells (Fig.14). Stress granules were observed only in arsenite treated cells by immunofluorescent staining of eukaryotic initiation factor-4A (eIF4A), a typical component of stress granules [22].

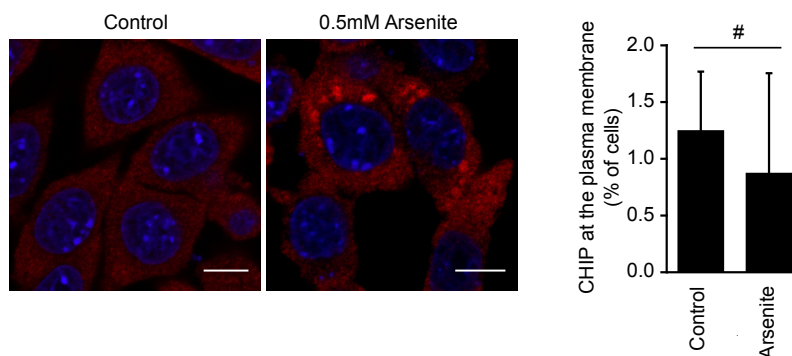


Figure 14. Arsenite treatment does not mobilise CHIP to membranes. Treatment of murine fibroblasts with 0.5 mM arsenite for 30 min did not induce EGFP-CHIP translocation to membranes, as determined by live cell imaging (mean \pm SD). #, no statistically significant difference according to chi-square analysis; N = 3 independent experiments. Immunofluorescent staining of eIF4A (red) was used to confirm proteotoxic stress and stress granule formation. DAPI staining in blue. Scale bar 10 μ m.

A different kind of stressor that disturbs proteostasis is the starvation for serum and amino acids, which induces several pathways of autophagy [119]. Localisation of EGFP-CHIP was investigated during starvation in Hank's balanced saline solution (HBSS), as CHIP has been reported to influence autophagic flux [120]. No mobilisation of EGFP-CHIP to cellular membranes was observed during 4 h starvation with HBSS. A redistribution of cytosolic CHIP to granule compartments in the cytosol and intranuclear bodies was observed (Fig.15). However, controls transfected with EGFP displayed similar distribution, suggesting a late stage of macroautophagy with unspecific encapsulations of cytosolic material [12].

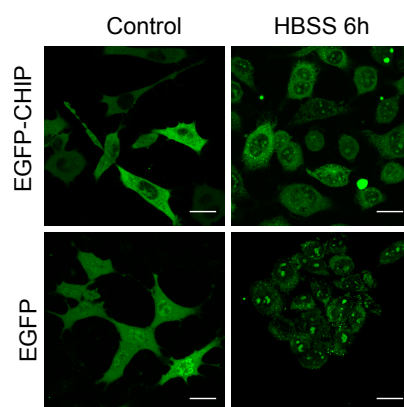


Figure 15. CHIP localisation during severe starvation. Murine embryonic fibroblasts (MEF) transiently transfected with EGFP-CHIP displayed increased granularity and localisation to intranuclear compartments after 6 h starvation in Hank's balanced saline solution (HBSS), as determined by live cell imaging. EGFP was used as control and displayed similar localisation. Scale bar 20 μ m. One representative of two independent experiments is shown.

In order to investigate subcellular localisation of CHIP biochemically and to further gain insight into possible CHIP oligomerization in membranes, subcellular fractionation was combined with chemical crosslinking. In the total lysate and the cytosol of MEF cells, endogenous CHIP appeared in high molecular weight species, when crosslinked with glutaraldehyde. These CHIP:chaperone/substrate complexes could be dissociated by addition of C-terminal HSP70 octapeptide (GPTIEEVD), yielding the chaperone-free, dimeric

form of CHIP. In the membrane fraction this "empty" CHIP dimer could be found even without the addition of HSP70 octapeptide. This result supports the microscopy findings that CHIP can localise at cellular membranes, even under physiological conditions and is, at least partially, chaperone-free (Fig.16A). In total lysate and in membrane fractions, but not in the cytosol, distinct high molecular-weight species of CHIP were observed, which were resistant to SDS solubilisation. The molecular weight according to the applied protein ladder ranged from 100 kDa to over 200 kDa. A successful separation of cytosol and membranes was controlled by GAPDH western blot. Similar observations were made by subcellular fractionation of transiently transfected CHIP, which was used to establish the conditions for successful fractionation. In contrast to the fractionation of endogenous CHIP, no SDS-insoluble CHIP complexes could be observed in transiently transfected MEF cells (Fig.16B).

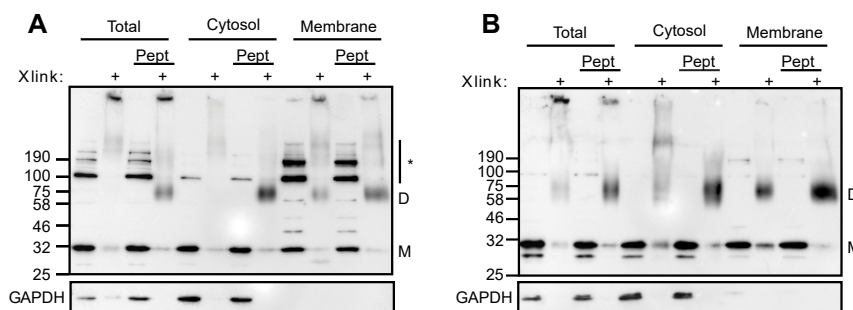


Figure 16. A fraction of cellular CHIP resides at membranes as chaperone-free dimer. Subcellular fractionation and chemical crosslinking of (A) endogenous CHIP and (B) transiently transfected CHIP in murine fibroblasts. Xlink, crosslinked samples; Pept, C-terminal HSP70 octapeptide (GPTIEEVD); *, SDS-insoluble CHIP oligomers; D, dimer; M, monomer. For endogenous CHIP one representative out of three experiments is shown.

In order to study the membrane localised CHIP in more detail and consolidate the hypothesis of its chaperone-independent function at membranes, mutagenesis was used to create a CHIP mutant that is unable to bind chaperones. A point mutation from lysine 30 to alanine (K30A) in the TPR domain of CHIP, is known to impede HSP70/90 association with CHIP and was confirmed by isothermal titration calorimetry (ITC) (Fig.17A). Subsequent titration of 200 μ M HSP70 octapeptide to 10 μ M recombinant wild-type CHIP saturated all available binding sites after 25 injections of 8 μ l, as indicated by the reduction of released heat rates. In contrast, titration of the octapeptide to 10 μ M recombinant CHIP-K30A resulted in little overall release of heat and a moderate slope of the curve towards saturation. The acquired heat rates were fitted by means of an independent binding model and K_D of wild-type CHIP and CHIP-K30A were calculated to be 5 μ M and 15 μ M respectively.

In order to identify possible differences in protein folding between mutant and wild-type protein, secondary structure content was compared by means of CD spectroscopy. Global α -helical content was similar in both proteins, confirming proper folding of the mutant protein (Fig.17B). Further assessment of the structural properties of the K30A mutant

revealed a reduced sensitivity to heat induced unfolding, as determined by thermal denaturation assay (Fig. 17C). The K30A mutant remained stable until 49.5°C while wild-type protein unfolded already at 45°C, as displayed by the increased binding of SYPRO Orange dye to exposed hydrophobic patches. The values acquired for wild-type CHIP and CHIP-K30A in the thermal denaturation assay matched previous examinations [86].

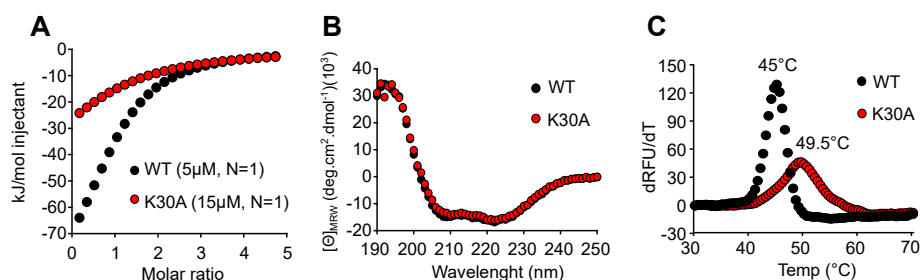


Figure 17. CHIP-K30A mutant resembles CHIP wild-type structurally but not functionally. (A) Mutation of lysine 30 to alanine in the TPR domain of CHIP aggravated binding of C-terminal HSP70 octapeptide to recombinant CHIP-K30A, as determined by isothermal titration calorimetry at 37°C. (B) Global secondary structure content of CHIP-K30A and wild-type CHIP protein were similar as shown by means of CD spectroscopy. (C) Thermal denaturation assay using SYPRO Orange revealed CHIP-K30A to be less sensitive to heat induced unfolding than wild-type CHIP.

After confirming structural integrity of CHIP-K30A, subcellular localisation was assessed by live cell confocal fluorescence microscopy. As expected, the chaperone-free EGFP-CHIP-K30A localised in 93 % of MEF cells to the plasma membrane, while EGFP-CHIP remained cytosolic. Similarly, to the data set from Fig. 11, about 3 % of wild-type EGFP-CHIP displayed membrane localisation. For both samples an average of 140 cells was evaluated. Differences in steady-state levels of the fusion-proteins could be excluded by western blot analysis 24 h after transfection. Fixation of EGFP-CHIP-K30A transfected cells for confocal fluorescence microscopy using 4 % paraformaldehyde resulted in a loss of the membrane localisation. As paraformaldehyde is a commonly applied method it offers an explanation why this striking phenotype was not observed so far. For a biochemical confirmation of CHIP-K30A membrane localisation, *ex vivo* fractionation was performed from MEF cells transiently transfected with a non-tagged CHIP-K30A. Steady-state protein levels of non-tagged, wild-type CHIP and CHIP-K30A were analysed by western blot 24 h after transfection, displaying no differences. Fractionation of MEF cells expressing CHIP-K30A confirmed membrane association of the mutant protein (Fig. 16B). In contrast to wild-type CHIP, but in agreement with the binding properties of CHIP-K30A, addition of HSP70 octapeptide could not completely release CHIP complexes into the dimeric form. This reflected also the microscopical observation that not the entire pool of EGFP-CHIP-K30A localised to the plasma membrane of the respective cell. With respect to the SDS-insoluble CHIP complexes, distinct bands were observed in total lysate and membrane fraction but not in the cytosol fraction of the subcellular fractionation, resembling the observation for endogenous CHIP in Fig. 16A.

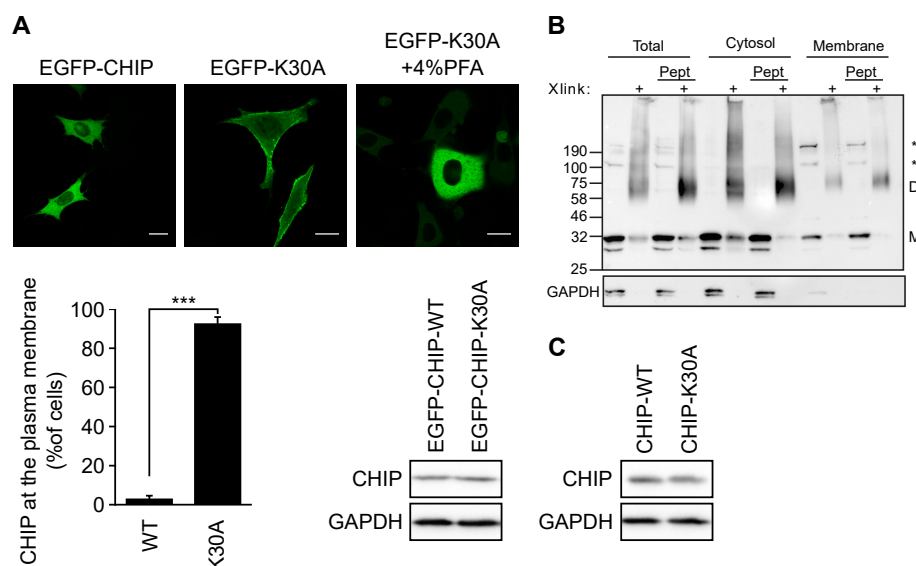


Figure 18. EGFP-CHIP-K30A localises to the plasma membrane of murine fibroblasts. (A) Transiently transfected EGFP-CHIP-K30A localised to plasma membranes of MEF cells in live cell confocal fluorescence microscopy (mean \pm SD). The localisation can not be observed in cells fixed with 4 % paraformaldehyde (PFA) for 20 min. One representative out of three independent experiments is shown. Scale bar 10 μ m. ***p<0.001, chi-square analysis; N = 3 independent experiments. Steady-state levels of EGFP-CHIP-WT and EGFP-CHIP-K30A 24 h after transfection as determined by western blotting. GAPDH was used as loading control. One representative out of three independent experiments is shown. (B) Sub-cellular fractionation and chemical crosslinking of transiently transfected MEF cells with CHIP-K30A. Xlink, crosslinked samples; Pept, C-terminal HSP70 octapeptide (GPTIEEVD); *, SDS insoluble CHIP complexes; D, dimer; M, monomer. (C) Steady-state levels of transfected non-tagged CHIP-K30A and CHIP-WT as determined by western blotting. GAPDH was used as loading control. One representative out of three independent experiments is shown.

In order to visualize the distribution of transiently transfected EGFP-CHIP-K30A on membranes *in vivo*, total internal reflection fluorescence (TIRF) microscopy was applied. Live cell TIRF microscopy is particularly suited to image proteins in close proximity to the plasma membrane, as TIRF is selectively illuminating regions within \sim 100 nm distance of the cover-slide, with fluorescence exponentially decaying for objects with growing distance to the evanescent field, which reduces background fluorescence [121][122]. TIRF has also been widely used to analyse membrane associated proteins and was applied here in order to reveal the characteristics of CHIP-K30A association with the plasma membrane *in vivo*. EGFP control displayed homogeneous distribution in epifluorescence and TIRF images. In EGFP-CHIP transfected cells a slight difference between epifluorescence and TIRF was observed, with CHIP displaying accumulation in small punctae in proximity to the nucleus (Fig.19, white arrows). EGFP-CHIP-K30A revealed a non-homogeneous distribution at the membrane in TIRF images. In the epifluorescence images, the membrane localised protein appeared as a near homogeneous green line, while being clearly separated into distinct punctae along the membrane (Fig.19).

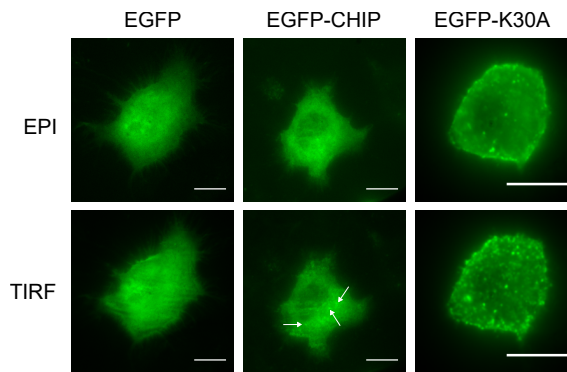


Figure 19. Distribution of EGFP-CHIP-K30A on the plasma membrane. TIRF microscopy of EGFP-CHIP revealed faint localisation to small punctae (white arrows). EGFP-CHIP-K30A displayed strong localisation to the plasma membrane and was separated into larger punctae along the membrane in MEF cells. EGFP controls displayed homogeneous distribution in epifluorescence and TIRF images. Scale bar 10 μ m. One representative out of two experiments is shown.

3.2 Lipid specificity of CHIP

To analyse the details of membrane interaction, an *in vitro* reconstitution was attempted utilizing recombinantly purified wild-type protein in lipid overlay assays and liposome co-sedimentation. The lipid specificity of CHIP was examined by lipid overlay assays using commercially available lipid strips, featuring the most abundant cellular lipids. Incubation of recombinant wild-type protein revealed a specific binding to phosphatidic acid, phosphatidylinositol-4-phosphate (PtdInositol-4-P) and phosphatidylinositol-4,5-bisphosphate (PtdInositol-4,5-bisP), but not to phosphatidylinositol-3,4,5-bisphosphate (PtdInositol-3,4,5-trisP) and phosphatidylserine (PS), arguing against a trivial electrostatic interaction. CHIP-K30A mutant utilized in microscopy experiments displayed the same lipid specificity, thus excluding the possibility of an artefactual binding to membranes *in vivo*, due to changed affinity towards cellular lipids and supporting the impact of chaperone association as the driving force for the phenomenon (Fig.20A).

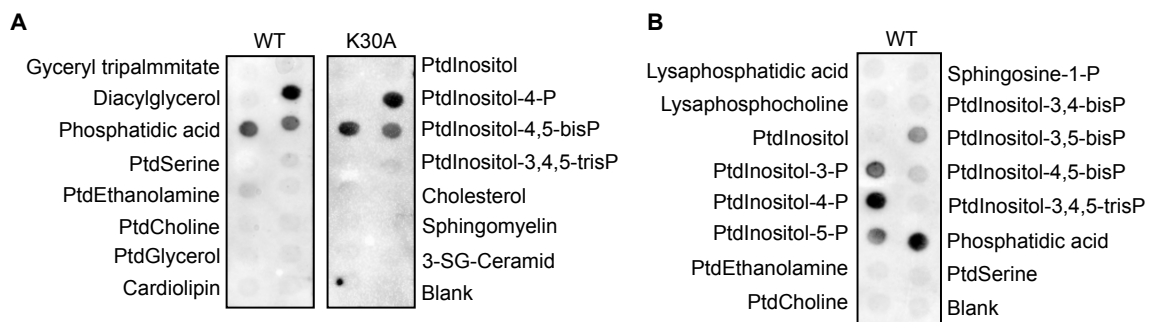


Figure 20. CHIP specifically binds to a subset of cellular phospholipids. Recombinant CHIP-WT and CHIP-K30A proteins bound specifically phosphatidic acid and phosphatidylinositol-monophosphates as determined by lipid overlay assay on commercial strips with a spectra of (A) General cellular lipids and (B) phosphatidylinositols. One representative result of three independent experiments is shown.

The spectra of lipid specificity was further defined by strips spotted with the most prominent cellular phosphatidylinositols (PIP-strips). Binding of CHIP to phosphatidic acid, phosphatidylinositol-4-phosphate and phosphatidylinositol-4,5-bisphosphate could be confirmed. Additionally, a binding to all phosphatidylinositol-monophosphates was observed, while increasing phosphorylation of inositol impeded CHIP binding such that phosphatidylinositol-3,4,5-tisphosphate displayed no binding. Similar to the previously used general lipid strip, signal intensities suggested an increased binding to phosphatidylinositol-4-phosphate and phosphatidic acid (Fig.20B). However, one has to be cautious to quantify binding affinities from lipid strips, as this has been reported to be error prone and the spotted lipids fail to naturally represent lipids in biological membranes [123][124]. This is supported by the fact that self-prepared lipid strips could reproduce CHIP binding to phosphatidic acid in a concentration-depend manner but binding to phosphatidylinositol-4-phosphate was absent (Fig.21). Thus, it was necessary to validate the findings from lipid overlay assays using liposomes.

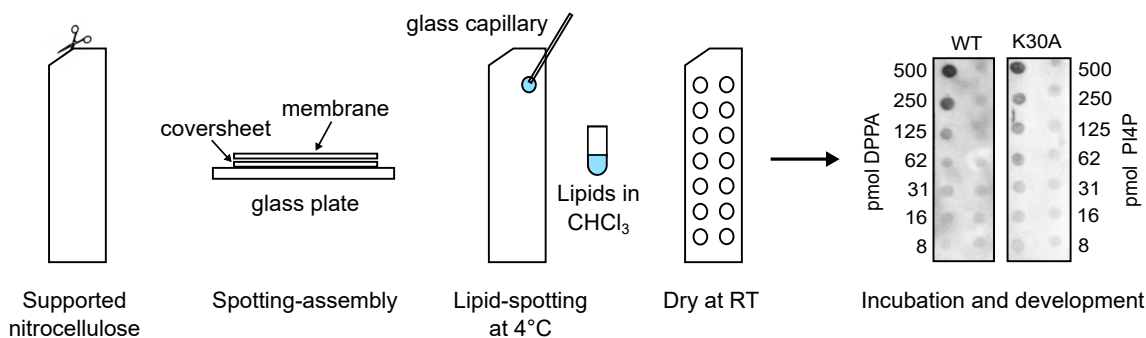


Figure 21. CHIP binds to phosphatidic acid spotted on nitrocellulose supported membranes. Recombinant wild-type CHIP and CHIP-K30A bound to phosphatidic acid (PA) but not phosphatidylinositol-4-phosphate (PI4P) manually spotted on supported nitrocellulose membranes.

Liposomes were prepared by thin-film hydration from chloroform stock solutions to a concentration of 10 mM with 1,2-Dioleoyl-sn-glycero-3-phosphocholine (DOPC). Following the specificity results from lipid overlay assays, the liposomes were supplemented with either 1 %, 5 % or 20 % of phosphatidic acid (PA) or phosphatidylinositol-4-phosphate (PI4P). Flotation assay was used in order to test CHIP binding to DOPC liposomes containing 20 % PA. Supporting the results from lipid overlay assays, CHIP displayed enhanced binding to liposomes spiked with PA, indicated by migration of CHIP to the top fraction of the applied sucrose gradient. This migration could not be observed for the gradient containing no liposomes, excluding a distribution of CHIP throughout the gradient by diffusion. Thus, the observed migration of CHIP in the gradient containing DOPC liposomes without PA must be due to interaction with these liposomes (Fig.22A). The amount of CHIP that migrated with DOPC liposomes was much less than in those supplemented with PA, reproducing the lack of binding of CHIP to phosphatidylcholine in lipid overlay assays. A significant difference of CHIP binding to PA containing liposomes compared to DOPC liposomes was confirmed and quantified by co-sedimentation

with about 58 % of CHIP bound to liposomes containing 20 % PA and only 13 % to liposomes without (Fig.22B). No significant difference between binding to liposomes with 1 % PI4P and DOPC liposomes could be observed. This could be due to insufficient occurrence of appropriate binding sites, possibly enhanced by sonication-induced ester hydrolysis [125]. Controls containing no liposomes confirmed that CHIP did not sediment on its own, but only in a liposome-dependent manner. Considering the intense binding of CHIP to PI4P in lipid overlay assays, the amount of PI4P supplemented to DOPC liposomes was increased to 5 % to overcome sensitivity limitations. Additionally, to enable a direct comparison in binding preferences, 5 % PA liposomes were used simultaneously with 5 % PI4P liposomes in a co-sedimentation assay. The interaction of CHIP with 5 % PA (11 %) was similar to DOPC liposomes (12 %), while 5 % PI4P supplemented liposomes displayed 51 % binding, which is similar to protein-binding observed for liposomes containing 20 % PA (Fig.22C). Thus, CHIP binding to membranes is more sensitive to the amount of PI4P present than to phosphatidic acid. However, a cooperative or synergistic effect of PA and PI4P could not be excluded at this point. To clarify a possible synergy of both lipids, mixed liposomes containing 5 % PA and 1 % PI4P were used in co-sedimentation assays. No effect neither additive nor synergistic could be determined between mixed liposomes and those containing only phosphatidic acid (Fig.23).

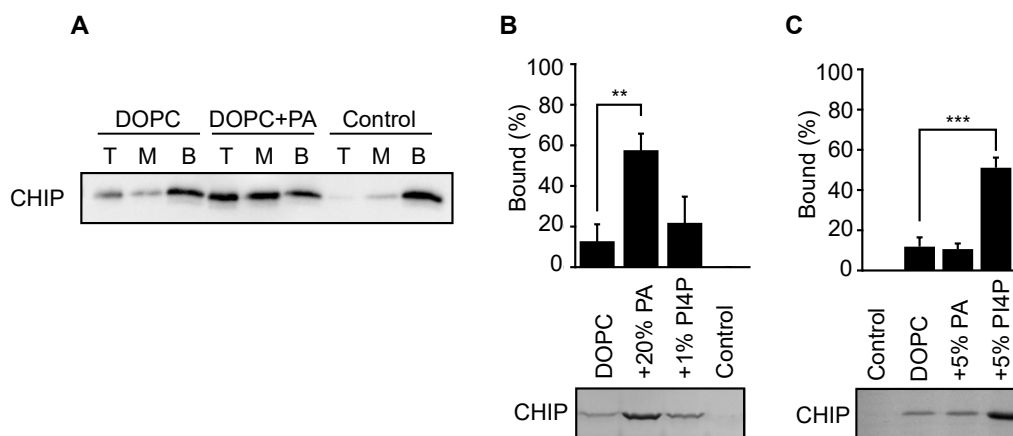


Figure 22. CHIP binds to liposomes spiked with phosphatidic acid (PA) and phosphatidylinositol-4-phosphate (PI4P). CHIP displayed enhanced binding to 1,2-Dioleoyl-sn-glycero-3-phosphocholine (DOPC) liposomes spiked with different amounts of phosphatidic acid (PA) or phosphatidylinositol-4-phosphate (PI4P) as determined by (A) flotation assay and (B,C) co-sedimentation assay (mean \pm SD). ** $p < 0.01$, *** $p < 0.001$, t-test analysis; N = 3 independent experiments. One representative western blot (A) or coomassie blue-stained gel (B,C) is shown.

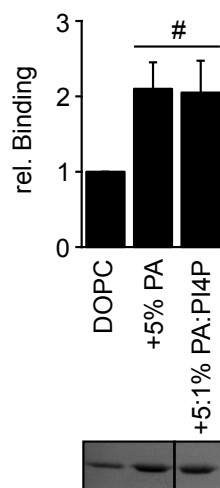


Figure 23. CHIP binding to mixed liposomes. Recombinant wild-type CHIP bound comparably strong to liposomes supplemented with only 5 % PA or both 5 % PA and 1 % PI4P. #, indicates no statistically significant difference. One representative coomassie blue-stained gel out of three independent experiments is shown.

After demonstrating CHIP specificity for phosphatidic acid and phosphatidylinositol-4-phosphate *in vitro*, it was aimed to deplete CHIP interacting lipids *in vivo* to reverse membrane association. For this purpose, membrane localised EGFP-CHIP-K30A mutant was transiently transfected to CHIP-deficient MEF cells (MEF K.O.). The CHIP knock-out cell lines were created with CRISPR/Cas9 by Mr. Wei-Han Lang and utilized in this setup to avoid cross-dimerisation of endogenous wild-type CHIP with transfected K30A. As anticipated, the mutant was localised to the plasma membrane of cells, but could be released into the cytosol by treatment with inhibitors of phospholipase D (PLD). The inhibition of phospholipase D blocks the hydrolysis of phosphatidylcholine to phosphatidic acid and thus reduces the pool of available binding sites for CHIP. Mammalian cells encode at least two isoforms of phospholipase D, PLD1 and PLD2, with specific inhibitors available for both isoforms [126]. Surprisingly, undocking of EGFP-CHIP-K30A from the plasma membrane could only be observed for the isoform-independent inhibitor FIPI and the PLD1 isoform-specific inhibitor (VU0155069) but not for the PLD2 specific inhibitor (CAY10594). The relocalisation to the cytosol was CHIP specific, as farnesylated EGFP (EGFP-F) remained at cellular membranes despite treatment with PLD inhibitors. The transition from membranes to the cytosol could be quantified by evaluating an average of 130 cells per condition, resulting in a significant localisation change in 13 % for VU0155069 treated cells (Fig.24A). Western blot analysis revealed no significant change in steady-state protein levels of CHIP upon PLD inhibitor treatment (Fig.24D).

A similar setup was utilized for the depletion of cellular PI4P levels by inhibition of the PI4P producing kinases (PI4K). There are four PI4Ks in mammals, two type II kinases (PI4KII α/β) and two type III kinases (PI4KIII α/β), residing at the plasma membrane, the golgi network and endosomal compartments and controlling local PI4P pools [127]. Wortmannin is a mycotoxin that acts as a specific inhibitor for phosphoinositol-3-kinase

(PI3K) at nanomolar concentrations but becomes an isoform independent inhibitor for type III phosphoinositol-4-kinases at micromolar concentrations [128]. Indeed, 10 μM wortmannin induced a significant mobilisation of EGFP-CHIP-K30A from membranes to the cytosol in a time dependent manner, while no significant change could be observed with a PI3K specific concentration, supporting the importance of PI4P specificity in CHIP localisation (Fig.24B). To further distinguish between the two PI4KIII isoforms, a PI4KIII- β specific inhibitor was applied for 20 min to EGFP-CHIP-K30A transfected cells and induced a significant reduction in membrane localisation. Unspecific toxic effects were excluded by EGFP-F control which did not change localisation despite inhibitor treatment (Fig.24C).

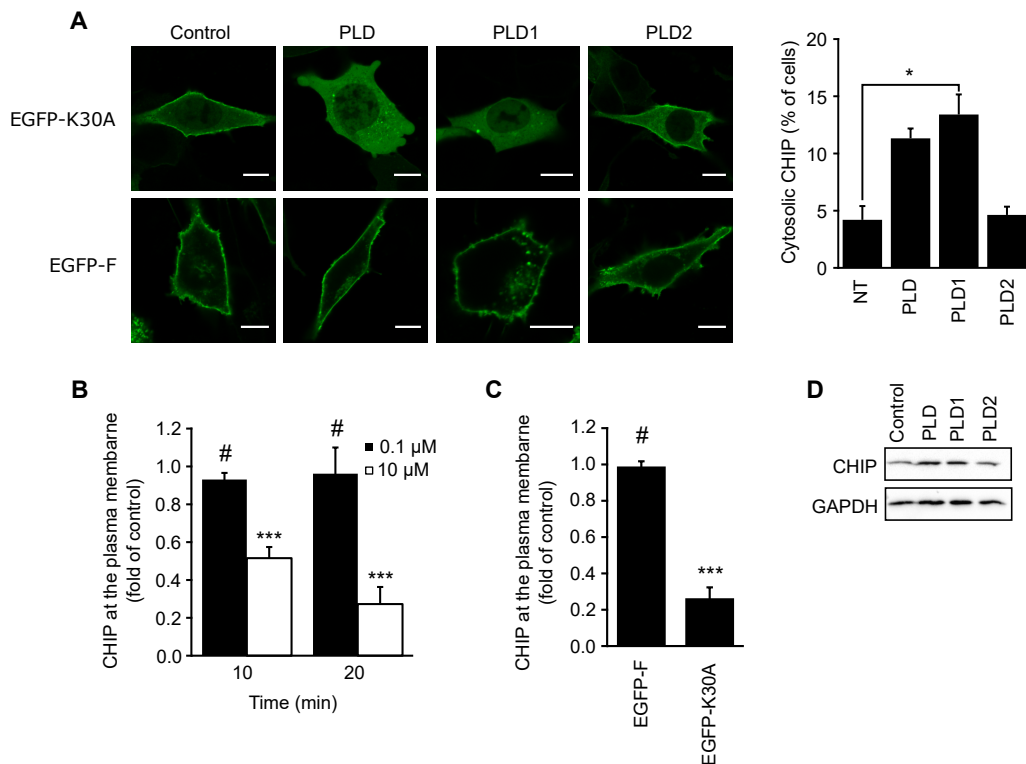


Figure 24. Depletion of PA and PI4P causes undocking of EGFP-CHIP-K30A from cellular membranes. (A) Inhibition of phospholipase D (PLD) for 12 h undocked EGFP-CHIP-K30A but not farnesylated EGFP (EGFP-F) from cellular membranes, as observed with live cell microscopy. FIPI, isoform independent inhibitor of PLD; VU0155069, CAY10594, specific inhibitors for PLD1 and PLD2, respectively (mean \pm SD). Scale bar 20 μm . * $p < 0.05$, chi-square analysis; $N = 4$ independent experiments. (B) Inhibition of type III phosphatidylinositol-4 kinases (PI4KIII) by wortmannin released EGFP-CHIP-K30A from cellular membranes (mean \pm SD). #, indicates no significant difference, *** $p < 0.001$, t-test analysis; $N = 3$ independent experiments. EGFP-F was used as control. (C) Inhibition of PI4KIII β by its specific inhibitor IN-10 for 20 min undocked EGFP-CHIP-K30A from cellular membranes (mean \pm SD). #, indicates no significant difference, *** $p < 0.001$, t-test analysis; $N = 3$ independent experiments. EGFP-F was used as control. (D) Steady-state levels of EGFP-CHIP-K30A were not significantly effected by PLD inhibitor treatment in MEF cells, as demonstrated by means of western blotting. One representative out of three western blots is shown.

The PLD inhibitor setup was subsequently used to clarify the impact of localisation changes on the interactome of CHIP-K30A. To this end, transiently transfected MEF K.O. cells were treated with PLD inhibitors, lysed and subjected to EGFP pulldown. Lysates were precleared by centrifugation, normalized and incubated on GFP-Trap-M magnetic beads for 90 min at 4°C. On-beads digestion for mass spectrometry analysis was resumed after all biological replicates were acquired. In label-free mass spectrometry performed by Dr. Giulia Calloni, 19 proteins were significantly enriched in control cells, whereas PLD treated cells displayed an increase to 47 significantly enriched proteins (Fig.25A). Among the 19 significantly enriched interactors of membrane localised EGFP-CHIP-K30A, most were plasma membrane proteins.

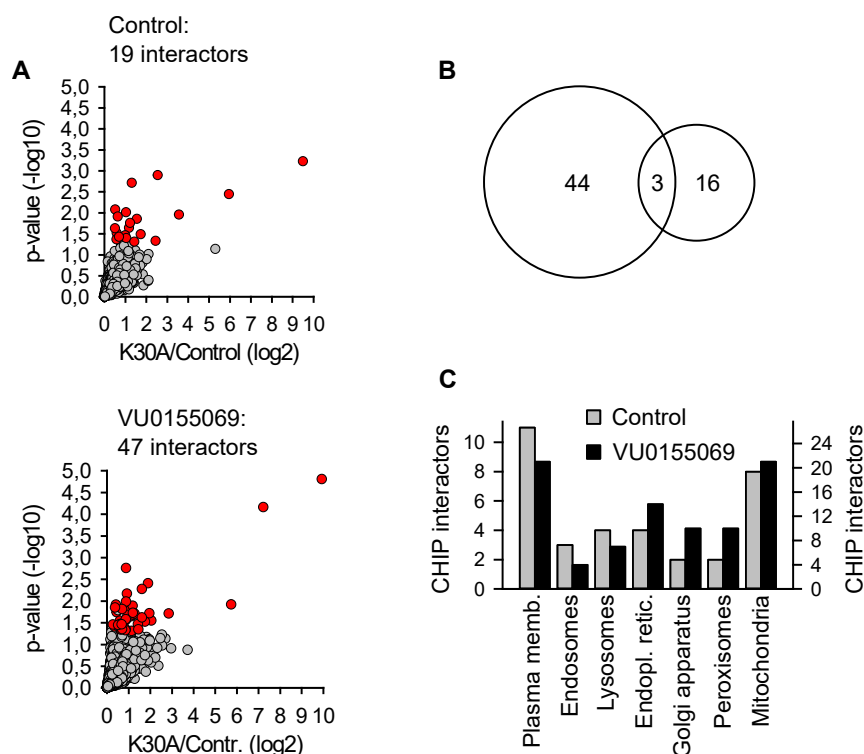


Figure 25. Interactome of chaperone-free CHIP at membranes. (A) Volcano plot of significantly changed EGFP-CHIP-K30A interactors (red) in control MEF K.O. cells and cells treated with 500 nM VU0155069. Label-free quantitative mass spectrometry was used and analysis was performed with MAX Quant (version 1.5.3.30). N = 5 biologically independent experiments. Significance was determined by two sample t-test $p < 0.05$. (B) Venn diagram displays minimal overlap between CHIP interactors of membranous and cytosolic EGFP-CHIP-K30A. (C) Subcellular localisation of EGFP-CHIP-K30A interactors of treated and control cells, assigned by GeneCards database (www.genecards.org). According to the database, proteins may display multiple localisations. The scales of y-axis were adjusted according to the interactome sizes (19 versus 47). MS evaluation was done by Dr. Giulia Calloni.

Additionally, proteins with reported localisation at the endosomes, the endoplasmic reticulum, and other membranous compartments were identified (Fig.25C). The identified interactors of PLD treated cells revealed little overlap with controls cells and contained typical cytosolic proteins, confirming the microscopically observed change in localisation (Fig.25B).

Next, the reconstitution of chaperone-lipid competition for CHIP binding was performed. For this purpose co-sedimentation assays using DOPC-20%PA liposomes and lipid overlay assays were combined with preincubation of CHIP with HSP70 octapeptide. As demonstrated in *ex vivo* subcellular fractionation, HSP70 octapeptide efficiently dispersed CHIP complexes. Thus, incubating the peptide with CHIP prior to co-sedimentation with liposomes, would possibly block CHIP-lipid interaction.

Analysis of coomassie blue-stained gels revealed, however, that even excessive amounts of 200 μ M octapeptide could reduce CHIP-liposome association only by 35 %. Lower concentration reduced association less efficiently (100 μ M) or not at all (50 μ M) (Fig.26A). Similar observations could be made from lipid overlay assays, incubating lipid strips with recombinant CHIP pre-incubated with HSP70 octapeptide. Since the strips are more sensitive than co-sedimentation assays, 10 μ M peptide were sufficient which corresponds to a 50 fold excess of peptide over recombinant protein used (Fig.26B).

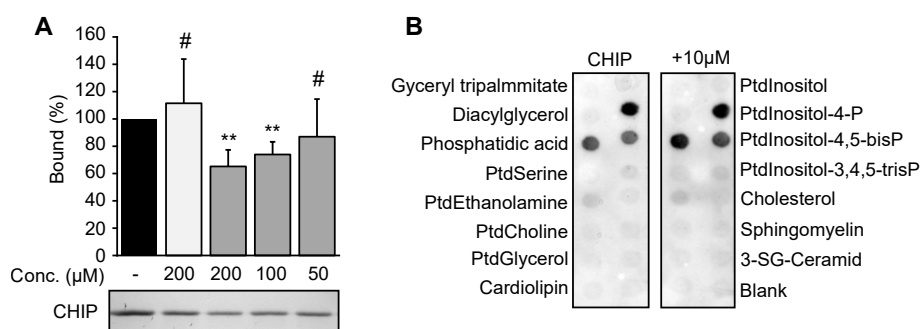


Figure 26. CHIP association to lipids is impaired by excessive amounts of C-terminal HSP70 octapeptide. (A) CHIP displayed reduced association with DOPC+20%PA liposomes at 50-100 times molar excess of C-terminal HSP70 octapeptide in co-sedimentation assays. #, no statistically significant difference, ** $p < 0.01$ according to t-test analysis; N = 4 independent experiments (mean \pm SD). (B) CHIP displayed no reduced association with lipids when bound to C-terminal HSP70 octapeptide in lipid overlay assays.

The insufficient blocking of CHIP-lipid association by the HSP70 octapeptide implied that additional residues of HSP70 are involved in CHIP binding, as it has been proposed previously [79]. These additional motifs could possibly cover the interface of CHIP-lipid interaction. Hence, a truncated version of HSP70 was cloned, encompassing the 260 C-terminal amino acids. This C-terminal HSP70 was recombinantly purified and used as competitor for CHIP-lipid interaction during co-sedimentation. Indeed, already a half-molar ratio of C-terminal HSP70 reduced CHIP association with DOPC+20%PA liposomes by 46 % and an equimolar ratio reduced docking to liposomes by 72 %, while similar concentrations of peptide displayed no significant reduction (Fig.27A). Supplementing the co-sedimentation, a qualitative assessment of CHIP binding in lipid over-

lay assays was examined. The use of 10-fold molar excess of C-terminal HSP70 completely abrogated the binding to phosphoinositol-monophosphates and phosphoinositol-4,5-diphosphate (Fig.27B). Only binding to phosphatidic acid could be detected but with clearly reduced intensities compared to wild-type CHIP binding (Fig.20B).

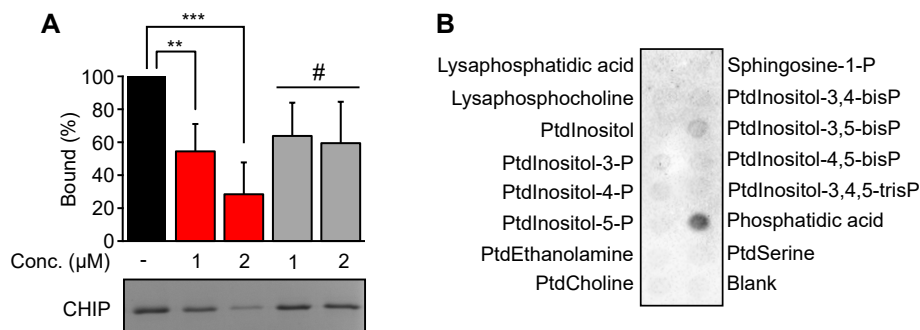


Figure 27. C-terminal HSP70 blocks CHIP association with liposomes. (A) CHIP association to DOPC+20%PA liposomes was reduced by pre-incubation with C-terminal HSP70 (260 amino acid fragment) as determined by co-sedimentation assay (mean \pm SD) . #, no statistically significant difference, *** $p < 0.001$, ** $p < 0.01$, t-test analysis; N = 4 independent experiments. One representative coomassie blue-stained gel is shown. (B) Ten-fold molar excess of C-terminal HSP70 blocked CHIP binding to phospholipids as determined by lipid overlay assay. One representative out of three independent experiments is shown.

3.3 Contact interfaces for lipid binding

Considering the results from competition experiments with C-terminal HSP70 (Fig.27), it is reasonable to assume that the TPR domain of CHIP is involved in the association with lipids, as obstruction of this domain by HSP70 octapeptide and C-terminal HSP70 binding blocked co-sedimentation of CHIP with liposomes. TPR domains are present in numerous proteins and usually mediate protein-protein interaction. However, one example of a TPR-mediated interaction with lipids was reported for protein phosphatase 5 [129]. Surprisingly, when trying to detect wild-type CHIP binding to lipid strips with a TPR sensitive antibody (recognizing 18-37 aa of CHIP), instead of the usually used C-terminal epitope (recognizing 251-268 aa of CHIP), it failed to detect any binding (Fig.28B). Given that C- and N-terminal antibody have similar sensitivity for recombinant CHIP, it was reasonable to assume that access of the N-terminal antibody to its epitope was obstructed by the contact of TPR domain with lipids or covered by the rest of CHIP though the lipid-binding induced orientation.

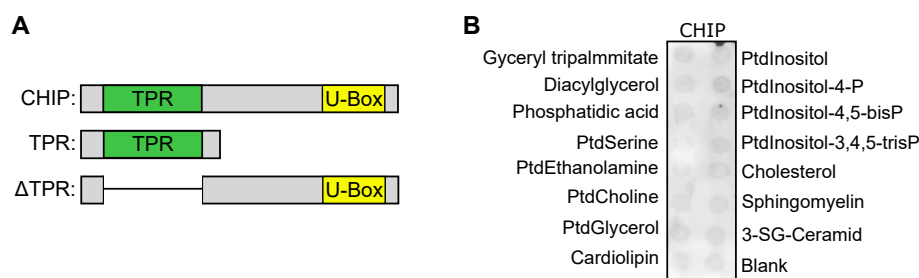


Figure 28. TPR domain mediates CHIP binding to lipids. (A) Schematic of recombinant protein variants used in liposome binding experiments to elucidate the impact of the TPR domain on lipid binding. (B) Wild-type CHIP could not be detected on commercial lipid strips by N-terminal CHIP reactive antibody. One representative out of three independent experiments is shown.

In order to confirm this assumption, isolated TPR domain and a TPR-free CHIP (Δ TPR) were cloned and purified. The neighbouring N- and C-terminal regions were included in the TPR construct to increase structural stability of the recombinant protein [89][77].

Indeed the requirement of the TPR domain for the lipid interaction of CHIP could be confirmed, as the TPR deletion displayed significantly reduced association with liposomes containing 20 % PA and 1 % PI4P. Both, the isolated TPR domain and the truncated deletion, remained soluble and did not pellet during ultracentrifugation excluding aggregation (Fig.29B). Notably, the isolated TPR domain bound even stronger to liposomes containing PA than the wild-type protein. The high amount of available phosphatidic acid seemed not to be the reason for this effect as the TPR domain still exceeded wild-type binding in liposomes with 5 % PA (Fig.29A). It is more likely that the asymmetric dimer of the full length protein exerts some degree of restraint on the otherwise very flexible TPR, influencing membrane association [89][77].

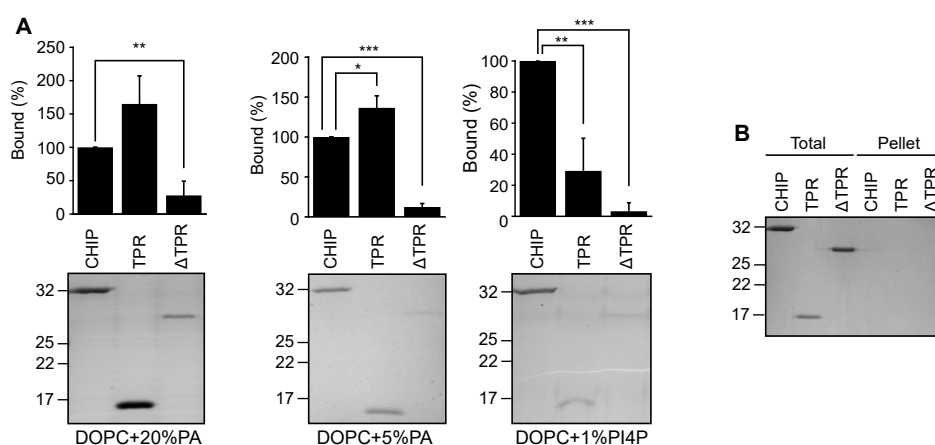


Figure 29. The TPR domain is a decisive determinant for liposome association of CHIP. (A) TPR domain was necessary for binding of CHIP to indicated liposomes, as determined by co-sedimentation (mean \pm SD). * $p < 0.05$, ** $p < 0.01$, *** $p < 0.001$, t-test analysis; $N = 3$ independent experiments. One representative coomassie blue-stained gel of three independent experiments is shown. (B) Indicated recombinant proteins did not pellet in co-sedimentation assays in the absence of liposomes. One representative coomassie blue-stained gel of three independent experiments is shown.

Indeed, a structural adaptation of isolated TPR domain upon liposome binding could be observed by means of CD spectroscopy. TPR domain displayed a reduction of secondary structures upon binding, independent of the presence of CHIP specific lipids. DOPC liposomes without PA induced a similar structural change as liposomes supplemented with 20 % PA, suggesting that the TPR domain is not providing lipid specificity (Fig.30A). The results from CD spectroscopy also offered an explanation for the excessive binding of isolated TPR to liposomes compared to wild-type. The unspecific interaction of the TPR domain enables binding not only to PA but to the entire liposome.

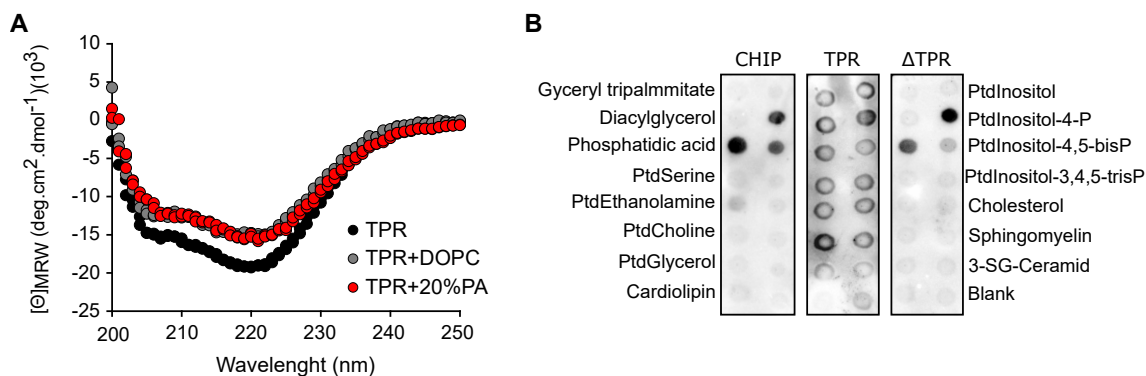


Figure 30. Isolated TPR domain displays reduced global secondary structure upon liposome association. (A) Global content of secondary structure elements was reduced for liposome-bound TPR domain, as determined by CD spectroscopy. Mean values of three independent experiments are plotted against respective wavelengths. (B) TPR domain displayed unspecific binding as determined by lipid overlay assay using a TPR reactive antibody (anti-N-terminal CHIP). Wild-type CHIP and Δ TPR were detected by C-terminal CHIP reactive antibody.

Next, the specificity of isolated TPR and truncated wild-type (Δ TPR) were examined by lipid overlay assays. In agreement with the results from co-sedimentation and CD spectroscopy, the isolated TPR domain bound unspecifically to all lipids on the strip. The TPR deletion, on the other side, exerted a similar binding pattern as the wild-type protein, suggesting that lipid specificity is mediated through an additional motif outside of the TPR domain (Fig.30B).

In search for the determinant mediating the residual lipid interaction of Δ TPR in co-sedimentation and lipid overlay assays, two positively charged patches in the hairpin middle domain of CHIP were identified as possible candidates. Often such patches of basic amino acids play an important role in the association with negatively charged phospholipids [130]. The two patches, named m1 (143-146: KKKR) and m2 (221-225: KRKKR), comprised lysine and arginine residues that were found to be evolutionary conserved (Fig.8). Mutation of the m1 site to alanines in EGFP-CHIP-K30A did not disturb the localisation to cellular membranes. However, partial exchange of m2 to alanines effectively released chaperone-free EGFP-CHIP-K30A from cellular membranes into the cytosol (Fig.31A). Additionally, EGFP-CHIP-K30A-m2 Δ was observed to mobilize the nucleus of transiently transfected MEF K.O. cells, a phenomenon absent in wild-type CHIP. A difference in localisation due to varying steady-state protein levels could be excluded by western blot analysis (Fig.31B).

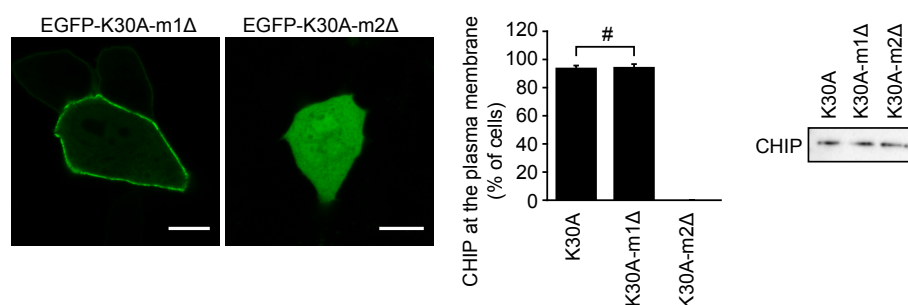


Figure 31. A positively charged patch in the middle domain is required for CHIP binding to membranes *in vivo*. (A) EGFP-CHIP-K30A-m2 Δ undocked from cellular membranes in live cell microscopy. Scale bar 10 μ m. #, no statistically significant difference according to chi-square analysis; N = 3 independent experiments (mean \pm SD). (B) There was no difference in protein levels between EGFP-CHIP-K30A, m1 Δ and m2 Δ mutants in MEF cells as determined by western blot analysis, using a hairpin-domain reactive CHIP antibody.

After *in vivo* confirmation of the involvement of the m2 patch in membrane association, lipid overlay assays and co-sedimentation were used to support the findings *in vitro*. For this purpose CHIP-m1 Δ and CHIP-m2 Δ were cloned and purified. Indeed, as expected m1 Δ displayed no difference in lipid association on strips compared to wild-type CHIP. Mutation of m2 Δ however did not bind phosphatidylinositol-diphosphates and had considerably weakened affinities for phosphatidylinositol-monophosphates and phosphatidic acid. This could be confirmed by co-sedimentation of CHIP-m2 Δ , where it showed reduced binding to liposomes containing 20 % PA. Surprisingly, an increase of unspecific binding to DOPC liposomes was observed, resembling the excessive binding to DOPC,

observed in co-sedimentation of isolated TPR. To check if CHIP-m2 Δ had similar characteristic as isolated TPR and to clarify the influence of the K30A mutation on K30A-m2 Δ localisation, EGFP-CHIP-m2 Δ was analysed microscopically and recombinant CHIP-m2 Δ was subjected to activity and stability analysis.

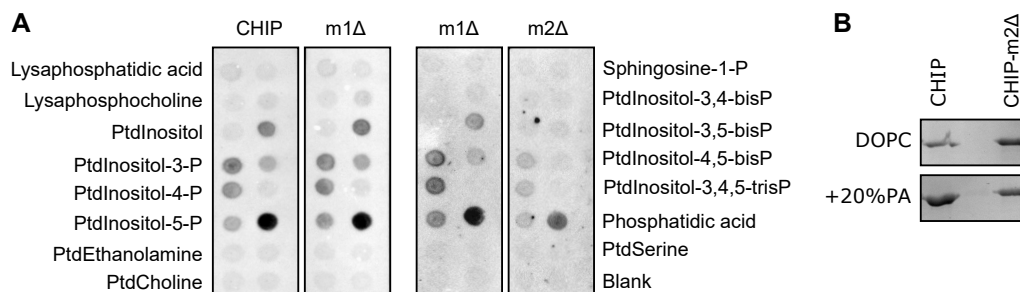


Figure 32. m2 mutation affects binding of CHIP to specific phospholipids *in vitro*. (A) Mutation of m2 reduced CHIP capability of binding phosphatidic acid and phosphatidylinositol-4-phosphate *in vitro* as determined by lipid overlay assay. One representative out of three independent experiments is shown. (B) Binding of CHIP-m2 Δ to phosphatidic acid (PA) containing liposomes was reduced, while binding to DOPC liposomes was enhanced as determined by co-sedimentation.

Chaperone-associated wild-type EGFP-CHIP and EGFP-CHIP-m2 Δ displayed the expected cytosolic localisation. Similarly to EGFP-CHIP-K30A-m2 Δ , EGFP-CHIP-m2 Δ additionally localised to the nucleus (Fig.33A). Thus, concluding that the transition to the nucleus is independent of CHIP association with chaperones and only induced by the mutation of the m2 patch. Thermal denaturation assay revealed that CHIP-m2 Δ is more sensitive to heat-induced unfolding with unfolding temperature shifted from 45°C to 39°C. The tendency to unfold at lower temperatures is an indication of a higher degree of structural flexibility. *In vitro* ubiquitylation assays showed that CHIP-m2 Δ lost its ability to ubiquitylate the model substrate NQO1. However, production of K63 ubiquitin chains was not impaired, arguing against general unfolding and destabilisation of CHIP-m2 Δ structure. Since the K30A mutation increased thermal stability (Fig.17), one could assume that CHIP-m2 Δ was stable and not misfolded.

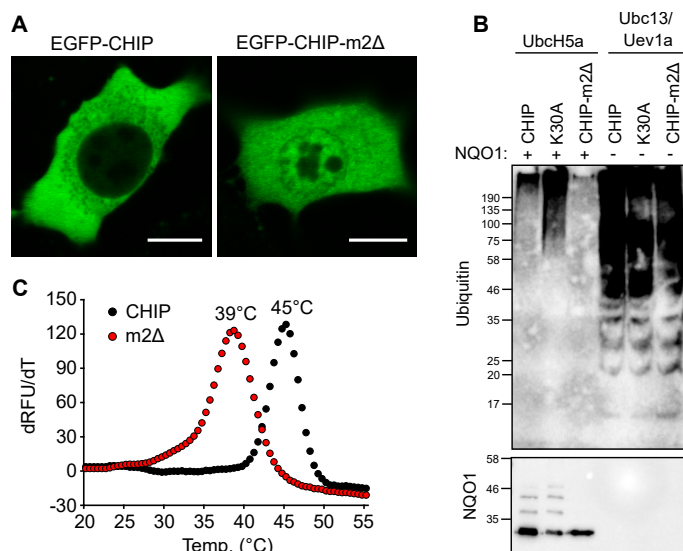


Figure 33. Wild-type CHIP-m2Δ *in vivo* and *in vitro*. (A) EGFP-CHIP-m2Δ localised to the nucleus of transiently transfected MEF cells, as determined by fluorescence microscopy. (B) CHIP-m2Δ was incapable of attaching K48 ubiquitin chains to the model substrate NQO1 but could produce free K63 chains in *in vitro* ubiquitylation assays. (C) CHIP-m2Δ was more sensitive to heat-induced unfolding as determined by thermal denaturation experiments.

3.4 CHIP structure and stability on membranes

In order to investigate the characteristics of CHIP-liposome association and to define liposome and CHIP properties that might influence the association, liposome preparations were subjected to Nanoparticle Tracking Analysis (NTA). The instrument tracked the movement of each particle in the flow chamber, based on its Brownian motion. This revealed size distribution of the unilamellar vesicles preparation after probe sonification. The diluted liposome preparation of both PA- and PI4P-supplemented liposomes displayed a near-homogeneous size distribution. The mode diameter of PA-containing liposomes was measured at 127 nm with slight tailing to 200 nm. PI4P-containing liposomes displayed a larger mode diameter at 161 nm with a second population of 230 nm diameter with about half abundance than the mode particle size. Thus, liposome preparations can be defined as large unilamellar vesicles (LUV) ranging from 100 nm to 200 nm diameter size (Fig.34A) [125].

To examine if CHIP binding to liposomes induced a change in size distribution, due to liposome fusion or fission, NTA was applied for liposomes containing 20 % PA, preincubated and co-sedimented with 10 μ M and 20 μ M CHIP respectively. Despite the appearance of smaller peaks beside the mode diameter, no significant shift could be observed, suggesting no influence of CHIP binding on liposome size. The smaller peaks possibly resulted from preparation heterogeneity and size variation induced by probe sonification (Fig.34B) [131].

In order to examine if liposome size is a determinant for CHIP binding, liposomes with

and without 20 % PA were subjected to size extrusion with 100 nm, 50 nm and 30 nm filters as well as probe sonification to produce LUV. Subsequently, the resulting liposomes were utilized in co-sedimentation assays with recombinant wild-type CHIP and quantified from coomassie blue-stained gels. It became obvious, that a diameter larger than 100 nm is required to detect statistically significant differences between pure DOPC and PA containing liposomes, because despite increased mean binding with decreasing liposome size, the system exhibited increasing fluctuation with repeated extrusions (Fig.34C).

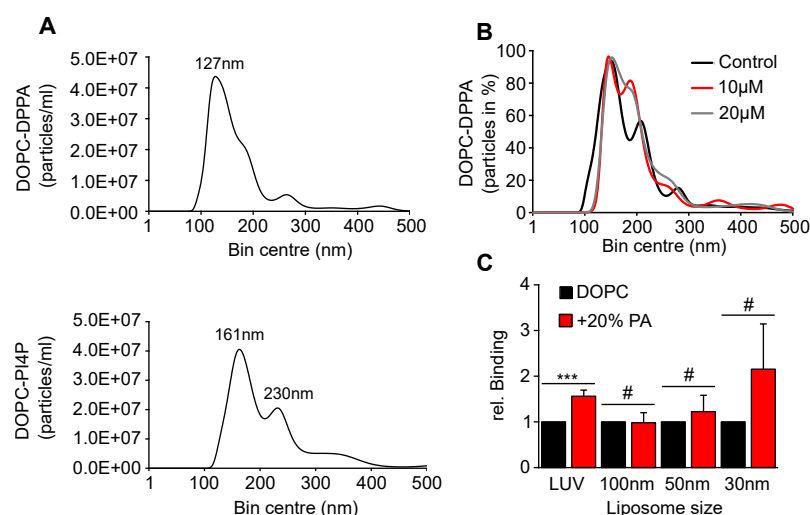


Figure 34. CHIP binding to PA-containing liposomes is size dependent and does not induce fission or fusion of liposomes. (A) Liposome size distribution after sonication was uniform as determined by particle analysis with Nanoparticle Tracking Analysis (NanoSight). (B) Wild-type CHIP binding to DOPC+20%PA did not significantly induce fission or fusion of liposomes, as determined by Nanoparticle Tracking Analysis (NanoSight). Mean abundance of particles is plotted against respective diameters from two independent experiments. (C) A liposome size larger than 100 nm is required to differentiate between binding to DOPC liposomes and liposomes supplemented with PA as determined by co-sedimentation. LUV, large unilamellar vesicle; N = 3 independent experiments (mean \pm SD).

After examining the impact of CHIP binding on liposomes and ensuring sufficient quality of liposome preparations, the impact of membrane association on CHIP structure and stability was assessed by means of CD spectroscopy and limited proteolysis. Global secondary structure of wild-type recombinant CHIP did not change in presence of liposomes, as determined by CD spectroscopy, measuring recombinant CHIP in solution with or without 2 mM DOPC+20%PA (Fig.35A). It has to be noted that CD spectroscopy in the presence of liposomes underlies limitations concerning the unfavourable influence of elevated liposome concentrations on HV values, which can reduce accuracy of the obtained data.

Similarly, no change during limited proteolysis was observed upon CHIP-membrane association *in vitro* (Fig.35B). Recombinant CHIP was subjected to co-sedimentation with DOPC+20%PA liposomes, followed by up to 10 min digestion with trypsin. The concentration of CHIP in control digestions, lacking liposomes, was estimated from previous co-sedimentation assays and quantification was achieved by measuring the fraction of CHIP that remained undigested after trypsin treatment.

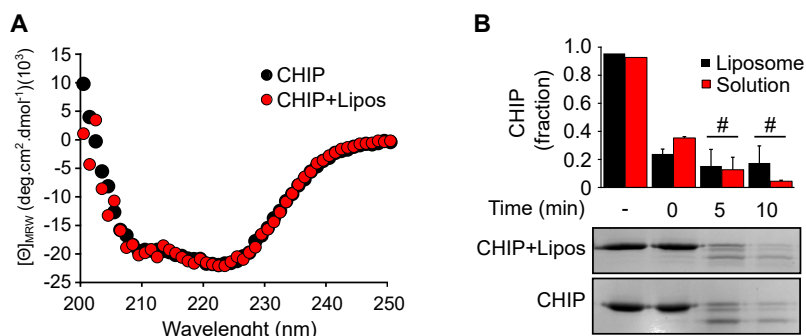


Figure 35. Characterisation of CHIP structure on liposomes. (A) CHIP (5 μ M) did not change its global content of secondary structures upon liposome binding, as determined by CD spectroscopy. Mean values of three independent experiments are plotted against the respective wavelengths. (B) CHIP binding to liposomes did not affect its sensitivity to proteolysis (mean \pm SD). #, indicates no statistically significant difference, t-test analysis; N = 3 independent experiments. One representative coomassie blue-stained gel of three independent experiments is shown.

In order to differentiate between insertion and transient attachment of proteins to membranes, a commonly used method subjects the bound protein to solutions of increasing ionic strength. Thus, if the interaction is electrostatically-driven and transient, the protein can be eluted from liposomes at high ion concentrations, whereas a resistance indicates an influence of hydrophobic effects, possibly through partial protein insertion into the membrane. Recombinant wild-type CHIP on DOPC+20%PA liposomes was collected by ultracentrifugation and the resulting pellet was sequentially washed with buffers of increasing sodium chloride concentrations. An increase to 500 mM NaCl released only 50 % of bound CHIP from DOPC+20%PA liposomes, indicating the involvement of hydrophobic interactions or a particularly strong electrostatic interaction.

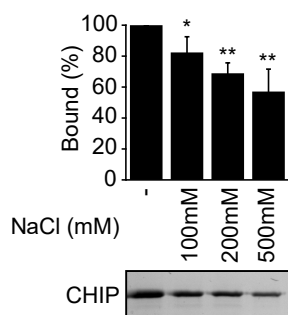


Figure 36. CHIP can not be entirely released from liposomes by increasing ionic strength. CHIP could not be released completely from liposomes by increasing sodium chloride concentrations, as determined by co-sedimentation assay (mean \pm SD). * $p < 0.05$, ** $p < 0.01$, t-test analysis; N = 3 independent experiments. One representative coomassie blue-stained gel of three independent experiments is shown.

3.5 CHIP oligomerization on membranes

CHIP has been reported to form high molecular weight oligomers stabilized by crosslinking with glutaraldehyde [90]. The function and significance of these oligomeric species remains largely elusive. The subcellular fractionation shown in Fig.16A displayed high molecular weight SDS-insoluble oligomers in membrane-containing fractions even without addition of crosslinker. One study reported the formation of these oligomers in response to oxidative stress [132]. This sparked the idea of a physiological function of CHIP oligomers at membranes. Although CHIP oligomers can only be detected at unphysiological high concentrations, membranes offer a relevant interface, enabling high local concentrations and functional assembly of cytosolic proteins [133]. Furthermore, stabilisation of oligomeric proteins through membrane association was reported previously [134].

In a first attempt to understand CHIP oligomerization, 5 μM recombinant wild-type CHIP was crosslinked with different amounts of glutaraldehyde for 10 min at 30°C. At the lowest concentration of crosslinker CHIP displayed monomeric conformation at ~ 32 kDa, dimeric form at about 63 kDa and also two distinct bands, corresponding to hexameric and higher-oligomeric states. By increasing the amount of glutaraldehyde, CHIP monomers disappeared and a third oligomeric conformation appeared above the already observed oligomers (Fig.37A).

Though commonly applied, chemical crosslinking can produce an artefactual representation of the situation in solution, as it influences the equilibrium distribution of species. To minimize, artificial crosslinks, zero-length crosslinker 1-ethyl-3-(3-dimethylaminopropyl)carbodiimide hydrochloride (EDC) in combination with N-hydroxysulfosuccinimide (Sulfo-NHS) was applied, which only crosslinks within the range of a hydrogen bond. Similarly to the crosslinking with glutaraldehyde, four conformations could be identified: a monomer, a dimer and two oligomers. In contrast to GA crosslinking, the sizes corresponded to tetrameric and hexameric oligomers. One can speculate that the different chemical properties of the crosslinkers, captured slightly distinct conformations with different access to SDS which resulted in the divergent migration in the gel.

In order to confirm the existence of oligomeric CHIP in solution, wild-type CHIP was analysed by means of native mass spectrometry in a collaboration with the laboratory of Dr. Nina Morgner (Goethe University Frankfurt). As expected, the dimeric form of CHIP was found to be most abundant in solution. Unexpectedly, also monomeric CHIP was found and a population of masses matching a tetrameric CHIP were identified in solution. Considering the low intensity of masses matching the tetramer, the data supported the idea, that CHIP oligomers are of negligible importance in solution [90]. The detection of monomers in solution offered an explanation for oligomer formation, as the asymmetric

dimer can not act as building block of tetrameric or higher oligomeric states due to steric constrains.

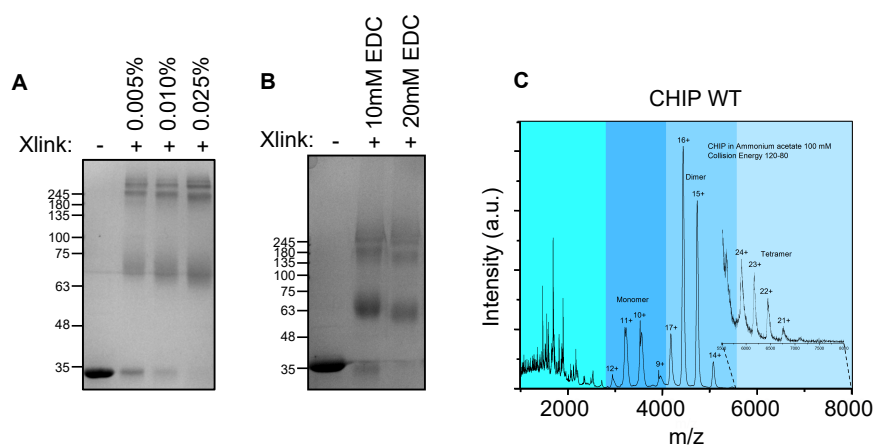


Figure 37. Oligomerization of CHIP in solution. (A) Chemical crosslinking of recombinant CHIP with glutaraldehyde. One representative coomassie blue-stained gel is shown. (B) Zero-length crosslinking of CHIP with EDC/Sulfo-NHS. One representative result of two independent experiments is shown. (C) Native mass spectrometry of untagged CHIP wild-type at 37°C, performed by Mr. Kudratullah Karimi. ESI with high collision energy was used to improve spectra resolution.

Following this hypothesis, monomerisation of CHIP was attempted by different treatments without introducing aggregation or misfolding. Among the tested monomerisation conditions, addition of the steroid deoxycholate effectively monomerised CHIP in agreement with previous studies [90]. In order to understand how deoxycholate affected secondary structural elements of CHIP, CD spectroscopy was performed in presence and absence of deoxycholate. The CD spectra of CHIP with 0.2 % deoxycholate displayed a partial reduction of secondary structure between 215 and 230 nm. Analysis of the spectra with the online tool BestSel predicted 84 % helical structures, 6.2 % turns and 9.7 % β -sheets under control conditions [135]. Even though CHIP does not have β -sheets it can be assumed that this prediction relates to the pair of β -hairpins present in the U-box [77]. Upon treatment with 0.2 % deoxycholate helices and β -structures transitioned into the prediction category "Others", which entails β -bridges, irregular/unstructured loops and hidden regions of the structure. Structures classified as turns remained unaffected. In agreement with the oligomerization initiated by monomers, native MS of deoxycholate-treated CHIP enabled the detection of hexameric CHIP in solution. The amount of DC used for MS was limited as it produced strong background signals at higher concentrations, preventing the direct comparison of oligomeric distributions in MS and the changes observed in CD spectroscopy. These preliminary results support the idea of oligomerization through CHIP monomers.

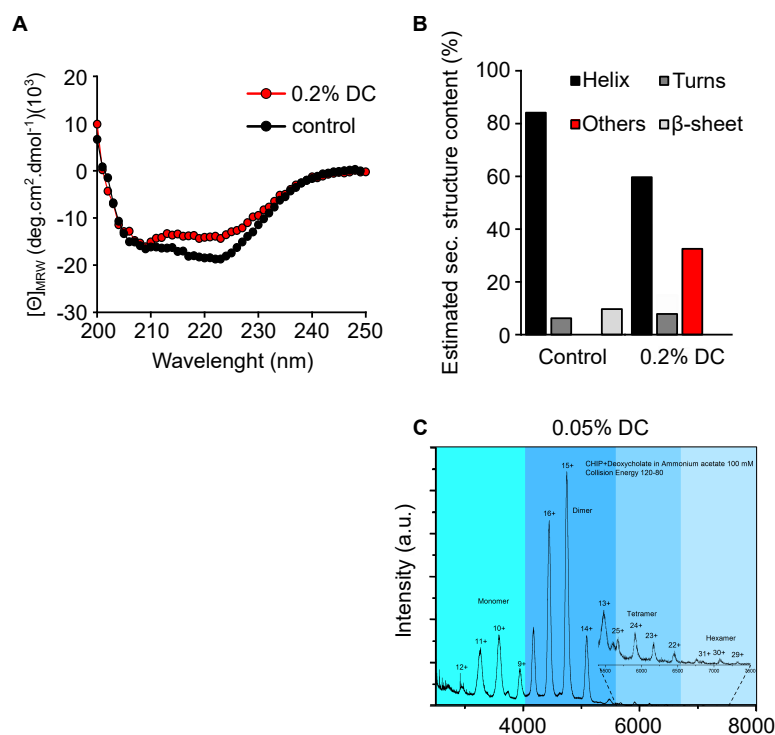


Figure 38. Deoxycholate-induced oligomerization of CHIP. (A) CD spectroscopy of wild-type CHIP in presence and absence of 0.2 % deoxycholate. (B) Estimation of secondary structures from CD-spectra using the online tool Bestsel [135]. (C) Native mass spectrometry of untagged CHIP wild-type at 37°C, in presence of 0.2 % deoxycholate performed by Mr. Kudratullah Karimi. ESI with high collision energy was used to improve spectra resolution.

Since deoxycholate is a steroid resembling the membrane component cholesterol, it can be hypothesised that the membrane association of CHIP facilitates or promotes formation of oligomers. Additionally, as already mentioned the membrane surface would enable high local protein concentrations, necessary for oligomer formation.

Chemical crosslinking experiments of liposome-bound CHIP showed that the fraction of oligomers increased, compared to CHIP in solution. It was speculated that especially the presumed hexamers might form a pore-like structure, in immediate stress response, due to the abrupt increase of chaperone-free CHIP at membranes. Subsequently those hexamers could increase membrane permeability, allowing the uncontrolled influx of extracellular ions and ultimately leading to cell death (Fig.39A). The hypothesis is supported by reports of increased oligomerization of CHIP through heat exposure [80][136]. Additionally, a CHIP-mediated alteration of membrane permeability was suggested in *Arabidopsis thaliana*, conferring an increased temperature sensitivity [137].

In an effort to analyse permeabilization *in vitro*, different experimental strategies with DOPC+5%PA liposomes were applied. It has to be noted that the setup was limited to a direct influence of CHIP on lipid and membrane properties, for examples by forming a pore-like complex or disturbing membrane integrity.

In a modification of the method of Wilschut et al. 1980, terbium (III) chloride (TbCl₃) was encapsulated as Tb(C₆H₅O₇)₃ in liposomes [138]. The liposomes were then mixed with a

buffer containing dipicolinic acid (DPA), which would form fluorescent Tb(DPA) complexes, if the encapsulated Tb($C_6H_5O_7$) would leak from the vesicles. To archive maximum release of the encapsulated material, liposomes would be lysed by the addition of 0.1 % Triton X-100. However, despite the combination of several stoichiometries of encapsulated Tb and exterior DPA, no substantial quantum yield could be measured. On the contrary, upon addition of Triton X-100 which should have resulted in a massive increase in fluorescence, quenching was observed. Different buffers were examined to exclude the possibility that components, like calcium, prevent complex formation even after liposome lysis. A remaining obstacle that was not intensively followed up, were osmolaric effects on the liposomes which could possibly have interfered with stable encapsulation.

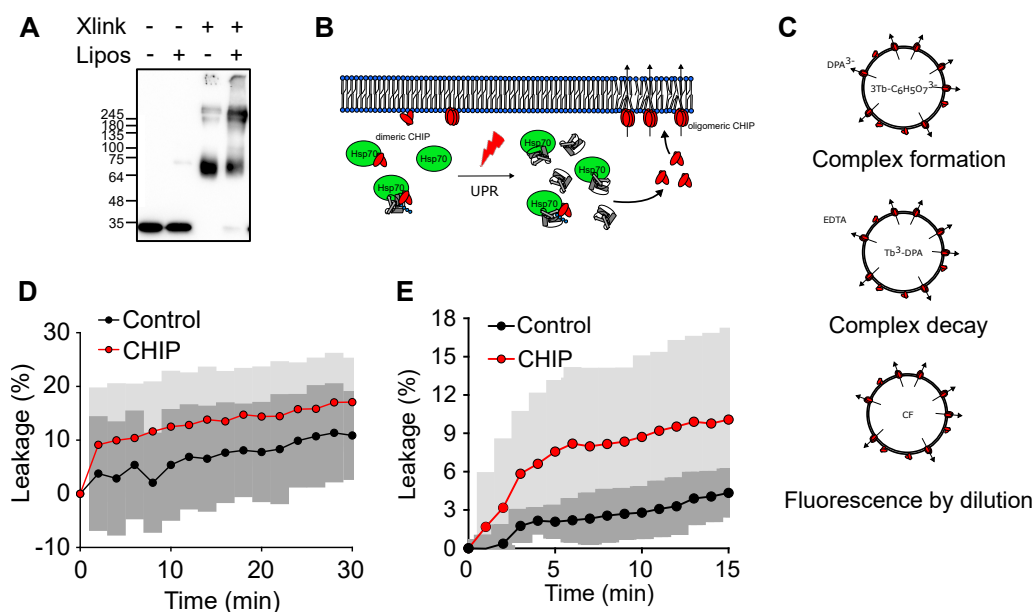


Figure 39. CHIP effects on membrane permeability *in vitro*. (A) Chemical crosslinking of CHIP with 0.025 % glutaraldehyde in presence of DOPC+20%PA liposomes displayed increased oligomerization. (B) Hypothesis of CHIP inducing membrane permeabilization. Chaperones are displayed in green, CHIP dimers and barrel-shaped oligomers in red. Unfolding/disordered proteins in grey. UPR, Unfolding protein response. (C) Strategies applied to investigate membrane permeability by CHIP oligomers. Liposomes are displayed as unilamellar bilayer spiked with red CHIP dimers and oligomers. Tb, terbium (III) ion; DPA, dipicolinic acid; $C_6H_5O_7$, citrate; CF, carboxyfluorescein. (D) CHIP-induced leakage of Tb(DPA) complexes from POPC+5%PA liposomes (mean \pm SD). (E) CHIP-induced leakage of CF from POPC+5%PA liposomes (mean \pm SD). SD of control, displayed in dark grey and SD of CHIP-containing samples in light grey.

As alternative, an opposite strategy was applied, were the Tb(DPA) complexes were encapsulated into liposomes. Upon release into a buffer containing a stronger chelator (EDTA) [112], they would decay and subsequently a fluorescence decrease would be measured. In this system, the assay principles worked properly, as addition of Triton X-100 abolished fluorescence completely, replacing the DPA in all Tb(DPA) complexes by EDTA. However, a constant leaking of Tb(DPA) was noticed, when controlling for the impermeability of DOPC+5%PA liposomes. A possible explanation offered the high degree of unsaturated fatty acids in the liposomes incorporated by 95 % DOPC, making the liposomes more susceptible to leakage induced by osmolaric fluctuations. In order to rigidify

the liposomes and increase their impermeability for Tb(DPA) complexes, DOPC was substituted with 1-palmitoyl-2-oleoyl-sn-glycero-3-phosphocholine (POPC) containing only one unsaturated fatty acid chain. Indeed, after substitution no leakage was observed in control conditions. However, in a setup to determine CHIP influence on liposome leakage, no significant difference was examined compared to control conditions (Fig.39D). Eventhough an initial increase to 10 % leakage after 2 min was observed in CHIP containing samples, the subsequent steepness of both curves was similar. Three independent experiments displayed huge fluctuations, resulting in overlapping standard deviations for both conditions.

Finally, a classical approach was followed, where the fluorophore carboxyfluorescein was encapsuled in liposomes. Carboxyfluorescein is quenched by dilution upon leaking from the liposome into the exterior buffer [112]. Addition of 10 μ M CHIP increased leakage to about 9 % after 15 min incubation but did not increase it further. Repetition revealed that the difference to controls was not significant. In conclusion, no effect of CHIP on membrane permeability could be detected in the used *in vitro* systems.

3.6 CHIP activity on membranes

With regard to the described increase in CHIP oligomerization at membranes, it was speculated that oligomers could display enhanced ubiquitylation of membrane localised substrates [133]. One might assume that CHIP oligomers form functional machineries, efficiently shuttling E2s from one U-box in the oligomer to another, producing large quantities of ubiquitin chains. To this end, the physiological impact of CHIP-mediated K63 ubiquitylation was investigated, as its functional consequences are insufficiently understood.

Recently, K63 ubiquitin chains have been found to act in various signalling events like NF- κ B (nuclear factor kappa enhancer binding protein) activation. NF- κ B is a transcription factor that controls many processes including immunity, inflammation and apoptosis. Its activation is regulated by a chain of kinases and E3 ubiquitin ligases [139]. The E3 RING ligase TRAF6 is one of these ligases and essential in the inflammatory pathways. It indirectly activates IKK by generation of K63-linked ubiquitin chains and TAK1 kinase activation [140]. One might speculate that K63 chains produced by CHIP oligomers serve a similar purpose.

In an initial experiment, a luciferase reporter plasmid containing NF- κ B binding sites, was co-transfected with CHIP and membrane localised CHIP-K30A in MEF cells. FLAG-tagged TRAF6 was used as a positive control. In MEF cells, a suppression rather than an activation of NF- κ B was observed for CHIP expressing cells (Fig.40A). Moreover, no TRAF6-induced activation of NF- κ B was observed in MEF cells, likely due to insufficient steady-state levels of TRAF6 (Fig.40B). The lack of a proper positive control prevented

the comparison with CHIP-transfected cells.

Since MEF cells proved to be an inadequate expression system for TRAF6 as a positive control of NF- κ B activation, Hek293T cells were utilized. Hek293T cells displayed high expression of TRAF6 (Fig.40) which strongly activated NF- κ B reporter. NF- κ B activation by CHIP expression was negligible (Fig.40A) and no difference between cytosolic CHIP and membrane-localised CHIP-K30A could be identified. It seems that K63 ubiquitin chains produced by CHIP have little influence on the NF- κ B signalling in the tested cell lines.

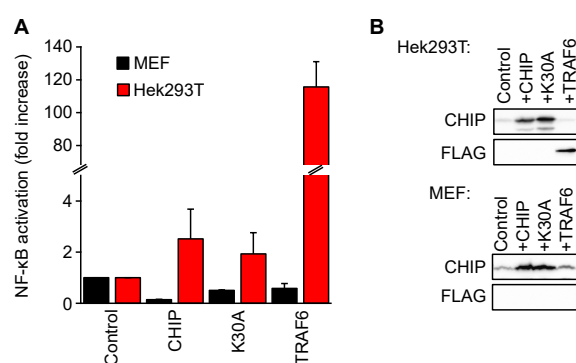


Figure 40. NF- κ B activation is not influenced by CHIP-mediated K63 ubiquitylation. (A) Luciferase reporter assay of MEF and Hek293T cells co-transfected with a NF- κ B reporter and CHIP, CHIP-K30A or FLAG-tagged TRAF6, respectively (mean \pm SD of two independent experiments). Controls of respective cell lines were set as 1. (B) Steady-state levels of CHIP and TRAF6 24 h after co-transfection, as determined by western blot analysis.

In order to examine if the presence of CHIP-interacting lipids had an influence on the capability of CHIP to ubiquitylate substrate proteins, DOPC+20%PA liposomes were added to *in vitro* ubiquitylation assays. As a model substrate, the human NAD(P)H:quinone oxidoreductase 1 P187S mutant was used because it has been reported to be a substrate of CHIP [141]. NQO1 is a flavoprotein which is important in maintaining the cellular redox-state. NQO1-P187S mutant is of special interest as it has been associated with increased susceptibility to various age-related pathologies and is increasingly ubiquitylated by CHIP compared to wild-type NQO1 [141].

Liposome-associated CHIP displayed no difference in K48 ubiquitylation of NQO1-P187S compared to CHIP in solution. An increase in CHIP auto-ubiquitylation could be observed in presence of UBCH5A, when DOPC+20%PA liposomes were supplemented to the reaction. Production of K63 ubiquitin chains was slightly impaired on liposomes, suggesting an obstruction of E2 binding sites through liposome binding. However, binding of UBCH5A was unaffected as demonstrated by efficient attachment of K48 chains to NQO1-P187S. Auto-ubiquitylation of CHIP was not observed in presence of the E2 heterodimer UBC13/UEV1A, consistent with observations from others [95].

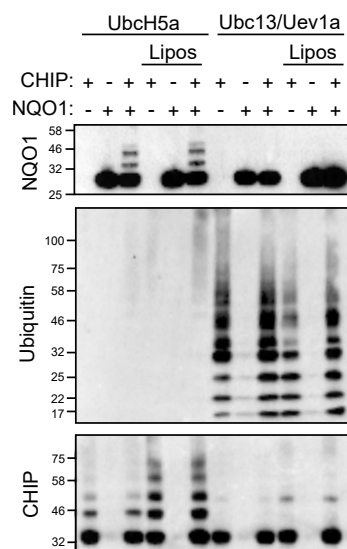


Figure 41. CHIP maintains its ubiquitylation activity on liposomes. CHIP bound to liposomes is capable of auto-ubiquitylation and can attach K48 ubiquitin chains to the pathogenic NAD(P)H:quinone oxidoreductase 1 P187S mutant (NQO1-P187S) in concert with the E2 UBCH5A. CHIP is able to synthesize free K63 chains in concert with E2 heterodimer UBC13/UEV1A when liposome bound, as determined by *in vitro* ubiquitylation assay. One representative out of three independent experiments is shown. The ubiquitylation assays in this figure were performed by Mr. Adrian Martínéz-Limon.

Since CHIP mobilisation to the plasma membrane was induced by heat stress, it was speculated that the presence of misfolded substrate proteins at membranes is necessary to trigger membrane-specific activity. Surprisingly, a striking difference in lipid binding was observed when comparing fatty acid-free bovine serum albumin (BSA) from Sigma Aldrich and Roche. The previously observed binding pattern could not be reproduced, when PIP-strips were developed with fatty acid-free BSA from Roche (Fig.42A). Analysis of the purification process of fatty acid-free BSA prompted a possible explanation.

While the exact process was not revealed by the companies, the data sheets suggested a heat shock fractionation for Sigma BSA, while no indication for heat exposure could be found for BSA from Roche. Assuming that Roche BSA was void of misfolded BSA species, present in Sigma BSA, a 3 % solution of Roche BSA was subjected to heat for 3 h at 65°C. It was safe to assume significant unfolding under the applied heat conditions, especially due to the visible formation of aggregates [142]. In the following development of a lipid strip with the heat-treated BSA from Roche, specific binding of CHIP to PA was observed, connecting the presence of misfolded proteins to CHIP association with lipids (Fig.42B).

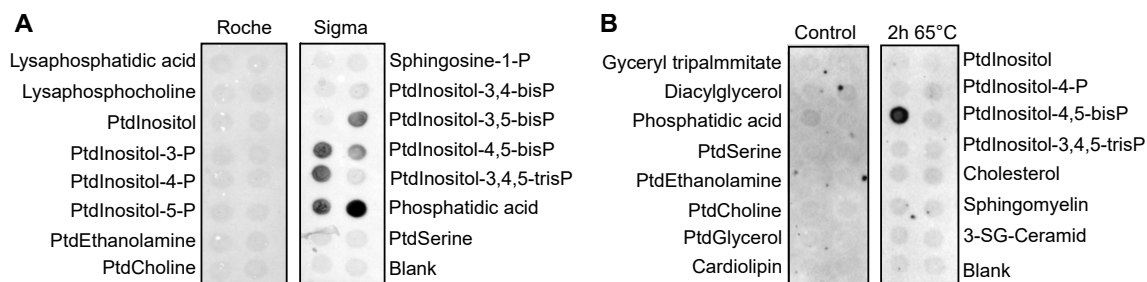


Figure 42. CHIP binding to lipids is enhanced by the presence of misfolded proteins. (A) CHIP bound to PIP-strips when using heated fatty acid-free BSA (Sigma Aldrich) during incubation but did not bind when fatty acid-free BSA from cold-ethanol purification (Roche) was used. One representative blot of two independent experiments is shown. (B) Heating of cold-ethanol purified BSA (Roche) restored CHIP binding to lipid strips. One representative blot of two independent experiments is shown.

In order to test if ubiquitylation activity of CHIP was enhanced on membranes in the presence of heated BSA, *in vitro* ubiquitylation assay was performed with DOPC+20%PA and DOPC liposomes. Fatty acid-free BSA from Roche was heated separately for 3 h at 65°C and centrifuged to remove visible aggregates. The treated and untreated BSA was incubated with liposomes at 37°C for 30 min to enable association. Next, the ubiquitylation mix containing CHIP was added and incubated for another 1 h at 37°C. Only heated BSA displayed significant ubiquitylation but with no sensitivity to the presence of liposomes (Fig.43A). The analysis with an ubiquitin-specific antibody displayed enhanced signal for all samples with heated BSA matching the result of the anti-BSA western blot. The slight increase in the sample with DOPC+20%PA is probably of little specificity, as it does not match with observations on BSA and was also observed for K48 ubiquitylation of NQO1-P187S mutant in Fig.41. The selective ubiquitylation of heated BSA could be assumed to be driven by the exposure of hydrophobic patches present in many unfolding proteins [143]. Since the mechanism of substrate recognition by CHIP is not clear to date, a final conclusion can not be drawn in this regard.

Flotation assays were applied to control for BSA binding to liposomes. The samples were treated similarly as the *in vitro* ubiquitylation, with the addition of CHIP after incubation of BSA and DOPC+20%PA liposomes. Association of BSA with liposomes was confirmed and a striking increase in association of heat shocked BSA was observed (Fig.43B). Determinants for BSA association with lipids remain to be clarified. There was no enhanced recruitment of CHIP to liposomes with heated BSA.

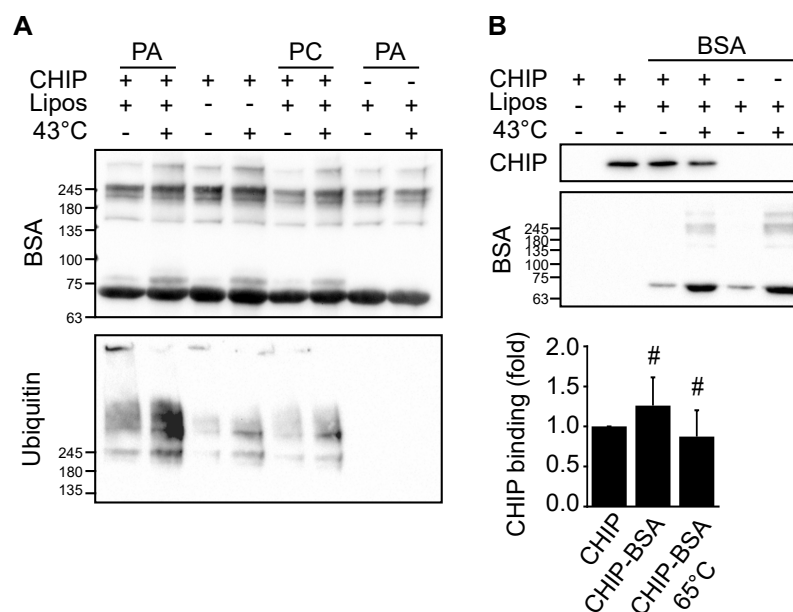


Figure 43. CHIP ubiquitylates heat-treated BSA independently of lipids. (A) *In vitro* ubiquitylation assay of CHIP, in concert with UBCH5A, displayed activity preferably on fatty acid-free BSA from Roche, subjected to 3 h 65°C heat shock. The presence of DOPC+20%PA or DOPC liposomes had no significant influence on the efficiency of ubiquitylation. One representative blot of two independent experiments is shown. (B) BSA subjected to heat treatment bound increasingly to DOPC+20%PA liposomes in flotation assays. No significant change of CHIP association with liposomes depending on amount or quality of BSA present, could be observed (mean \pm SD). Only the top fractions of the flotation gradients are shown. #, no statistically significant change according to t-test; N = 3. One representative blot of three independent experiments is shown.

With respect to a physiologically more relevant setup connected to heat-stress response, it was examined if ubiquitylation of a natural cytosolic substrate, would display a sensitivity to membrane presence. To this end, recombinant wild-type and P187S mutant NQO1 protein were heated at 43°C for 1 h in the presence of DOPC+20%PA and DOPC liposomes. It can be assumed that wild-type NQO1 is sufficiently affected by heating at 43°C, as melting temperatures have been determined previously and shown to be about 45°C [144]. Wild-type NQO1 was less ubiquitylated than mutant in solution under control conditions (Fig.44A). However, ubiquitylation of heated wild-type NQO1 was increased in the presence of DOPC+20%PA liposomes. Heated wild-type NQO1 supplemented with DOPC liposomes displayed no increased ubiquitylation by CHIP. In contrast, it led to a subtle but significant reduction of ubiquitylation. As already described, DOPC liposomes did not effectively associated with CHIP, thus it can be assumed that ubiquitylation was depended on the presence of the CHIP-specific lipid PA. The mutant protein displayed no sensitivity to the presence of membranes, probably because it is already less structured and partially unfolded under physiological conditions (Fig.44A) [144]. Yet, a decreased ubiquitylation could be observed in controls and DOPC containing samples, subjected to heat. One might speculate that upon heat exposure the already unstable NQO1 P187S aggregates reducing its access for CHIP.

To verify the presence of NQO1 on the utilized liposomes, co-sedimentation was ap-

plied under equal conditions as for the *in vitro* ubiquitylation. Both wild-type and mutant protein bound with high efficiency to DOPC+20%PA liposome. Contrary to wild-type NQO1, the mutant associated also with DOPC liposomes. Heat treatment induced increasing recruitment of both wild-type and mutant NQO1 to liposomes, resembling association-preference of heated BSA, also indicating unspecific interactions of motifs exposed by unfolding.

Through the increased ubiquitylation of unfolded wild-type NQO1 at CHIP-bound liposomes, the localisation change during heat shock can be connected to the effective processing of substrates.

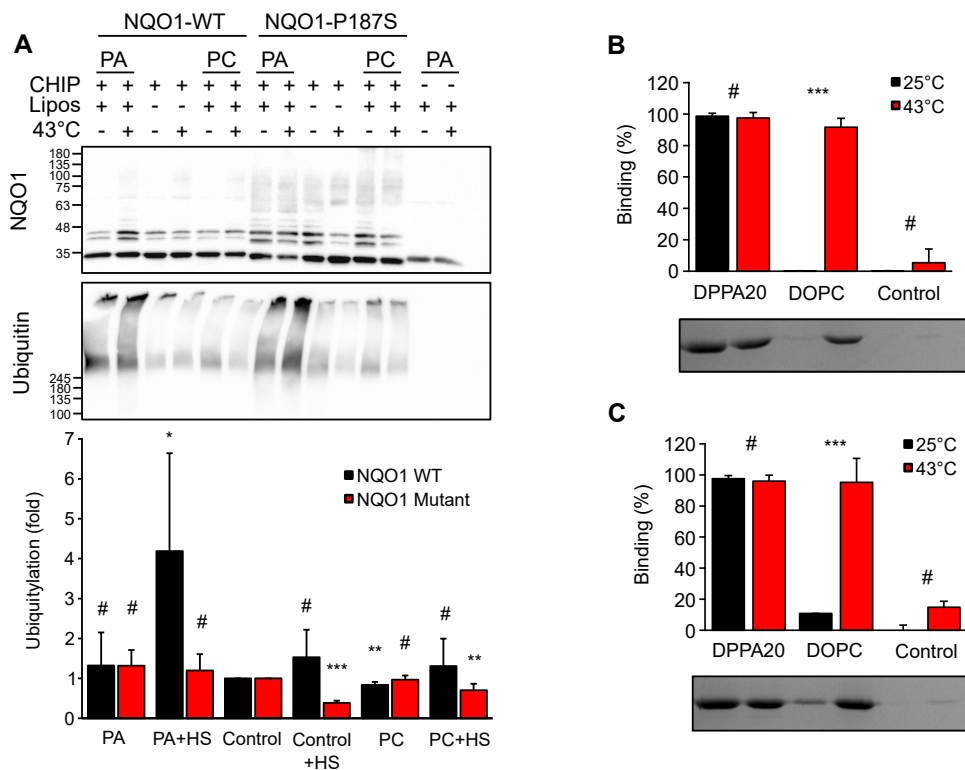


Figure 44. CHIP ubiquitylates unfolded proteins on PA-containing liposomes. (A) CHIP bound to DOPC+20%PA liposomes displayed increasing attachment of K48 ubiquitin chains to heated wild-type NQO1. NQO1 P187S was more efficiently ubiquitylated than wild-type but showed no sensitivity to the presence of PA-containing liposomes and reduced ubiquitylation when exposed to heat at 43 °C for 1 h (mean \pm SD). * $p < 0.05$, ** $p < 0.01$, *** $p < 0.001$, t-test analysis; N = 3 independent experiments. One representative out of three independent experiments is shown. (B) Wild-type and mutant NQO1 bound to DOPC+20%PA liposomes, but only NQO1 P187S bound to DOPC liposomes in co-sedimentation. Heat treatment at 43 °C for 1 h unspecifically increased binding of wild-type and mutant NQO1 to liposomes.

3.7 Physiological consequences of CHIP association with membranes

3.7.1 CHIP influences cellular architecture

After finding chaperone-free CHIP at cellular membranes and characterisation of the CHIP-lipid interaction *in vitro*, the physiological consequences were investigated. It has already been clarified, that heat stress mobilized CHIP to the plasma membrane due to reduced chaperone association. The plasma membrane localisation was further validated by the discovery of lipid specificity of CHIP, as PA and PI4P are abundant phospholipids in the plasma membrane. Another organelle that has characteristically high amounts of phosphoinositol-monophosphates, especially PI4P, is the Golgi apparatus. Thus, it was intriguing to examine the influence of chaperone-free CHIP on the Golgi apparatus.

In a first approach, the effect of CHIP overexpression on the proteome of transiently transfected MEF cells after 24 h was quantified by label-free mass spectrometry. To selectively analyse CHIP expressing cells, MEF cells were co-transfected with EGFP and sorted by FACS. The lysates were prepared for MS using the filter-aided sample preparation protocol (FASP). Final sample preparation, operating and analysis of mass spectrometry was performed by Dr. Giulia Calloni.

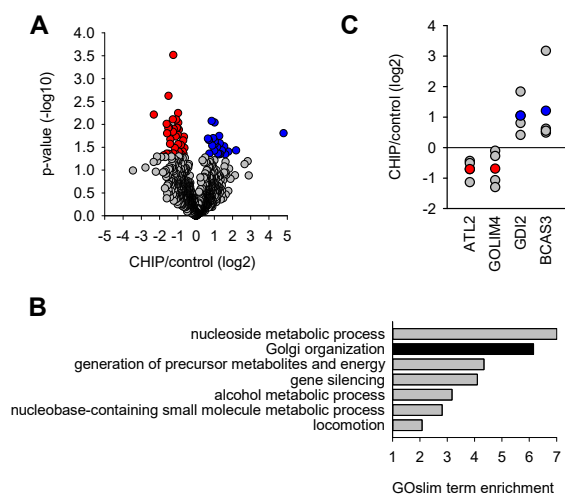


Figure 45. Label-free quantitative mass spectrometry shows specific proteome changes in MEFs upon overexpression of CHIP. (A) Volcano plot of significantly changed protein levels upon CHIP overexpression in MEF cells. Red marks significantly reduced, blue significantly enriched proteins, as determined by two sample t-test ($p\text{-value} < 0.05$, $N = 4$ biologically independent experiments). (B) GOBPslim terms revealed Golgi organisation proteins to be enriched above two in the group of proteins significantly changed upon CHIP overexpression. Fisher exact test was used to determine statistical significance. (D) Examples of significantly changed proteins with connection to Golgi morphology. MS measurement, analysis and blots were prepared by Dr. Giulia Calloni.

Among the 59 significantly changed proteins, 19 were upregulated upon CHIP overexpression and 40 were downregulated (Fig.45A). In agreement with PI4P localisation and CHIP specificity, GO term analysis of CHIP interactors scored "Golgi-organisation" as second highest enrichment among the significantly changed proteins (Fig.45B). Amongst the proteins linked to "Golgi-organisation" in GO term analysis, Golgi integral membrane protein 4 (GOLIM4) was reduced to 62 % of its physiological level, while other protein levels, like Rab GDP dissociation inhibitor beta (GDI2) doubled. Interestingly, proteins that scored in "Golgi-organisation" and exhibited reduced levels upon CHIP overexpression are often connected to the maintenance of cellular architecture and membrane tethering, like Golgi phosphoprotein 3 (GOLPH3), GRIP and coiled-coil domain-containing protein 2 (GCC2) and atlastin-2 (ATL2) [145][146].

To verify the effect of CHIP overexpression on the Golgi apparatus, CHIP was co-transfected with the Golgi marker β -1,4-galactosyltransferase1-EGFP in MEF cells. A significant fragmentation of Golgi stacks was observed 24 h after CHIP transfection in 30 % of cells, reflecting a 3-fold increase of disrupted Golgi architecture compared to control conditions (Fig.46A). For quantification, an average of 211 cells were analysed for their Golgi apparatus morphology.

The fragmentation of Golgi structure was especially interesting, as it is known to dissociate under heat stress conditions, which would connect to the observed release of CHIP from chaperones under heat [147]. To test this idea, Golgi morphology was analysed under 43°C treatment for 2 h in wild-type MEF cells (WT) and CHIP-deficient MEF cells (CHIP K.O.). A 6-fold increase of Golgi dissociation could be observed in wild-type MEF cells after heat shock but no significant change was present in MEF K.O. cells, affirming the participation of CHIP in this phenomenon (Fig.46B).

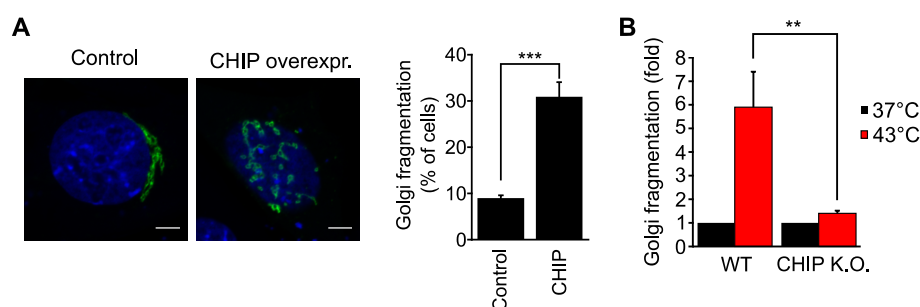


Figure 46. Chaperone-free CHIP distorts Golgi morphology. (A) Morphology change of the Golgi apparatus upon transient CHIP overexpression, monitored by co-transfection of an EGFP-tagged Golgi marker (mean \pm SD). DAPI stain of the nucleus in blue. Scale bar 5 μ m. *** p <0.001, chi-square analysis; N = 3 independent experiments. (B) Disruption of Golgi apparatus in MEF wild-type (WT) and CHIP knock-out (CHIP K.O.) cells after heat shock. Values are normalised for Golgi fragmentation at 37°C. Increase of cells with fragmented Golgi after 30 min at 43°C are plotted as mean \pm SD from three independent experiments. ** p <0.01, t-test analysis.

In a complementary setup, HSP70 was co-transfected with CHIP and the Golgi marker to rescue Golgi morphology. The addition of excessive HSP70 should saturate the chaperone-free CHIP in the cell, thus abrogating CHIP binding to Golgi and preventing subsequent fragmentation. Indeed, simultaneous overexpression of CHIP and HSP70 significantly reduced the abundance of dissociated Golgi apparatus compared to control conditions (Fig.47A). For quantification of microscopy pictures an average of 137 cells were evaluated with ImageJ. Western blot analysis was used to confirm successful overexpression of HSP70. To control the specificity of the observed rescue of the Golgi apparatus through HSP70, a mutant HSP70 was created lacking the C-terminal aspartate. This mutant is supposed to have low affinity to CHIP [148][149]. As expected, the mutant HSP70 could not rescue Golgi fragmentation (Fig.47A).

In an attempt to connect lipid specificity of CHIP with the effect on the Golgi apparatus, the CHIP-m2 Δ mutant was co-transfected with the Golgi marker in MEF K.O. cells. As expected, no significant distortion of Golgi stacks could be observed for this mutant, as it can not associate with PI4P on the Golgi apparatus. However, examination of protein levels revealed CHIP-m2 Δ expression to be only about 25 % of wild-type CHIP, rendering a comparison of the effect on Golgi morphology not straight forward (Fig.47B).

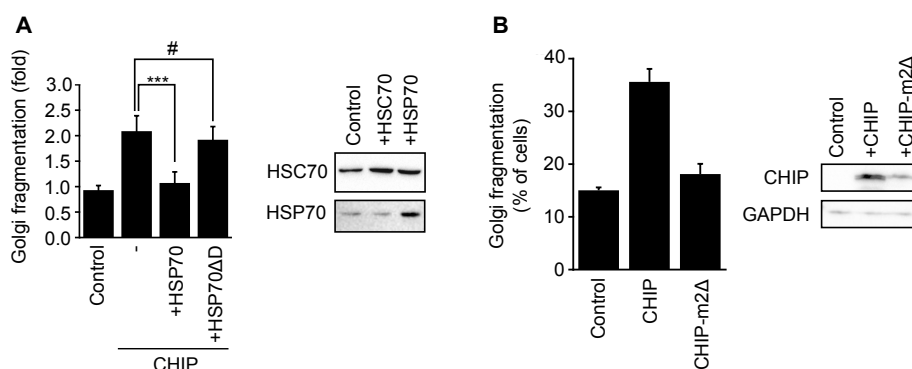


Figure 47. Excessive HSP70 rescues Golgi apparatus from CHIP-induced distortion. (A) Golgi fragmentation by transient overexpression of CHIP was reduced by co-transfection of HSP70 but not by CHIP-binding-impaired HSP70 Δ D in MEF cells (mean \pm SD). #, no statistically significant difference, *** p <0.001, chi-square analysis; N = 3 independent experiments. Expression levels determined by means of western blotting. (B) CHIP-m2 Δ displayed reduced Golgi fragmentation and protein levels in CHIP knock-out MEF cells 24 h after transfection (mean \pm SD of three independent experiments). Protein steady-state levels determined by means of western blotting.

In an effort to uncover the physiological consequences of CHIP-induced Golgi distortion, an effect on the secretion system of the cell seemed plausible. The Golgi apparatus is a major organelle involved in the shuttling and processing of cargo proteins to the plasma membrane, thus one can speculate that its structural disintegration has detrimental effects on protein secretion [150].

For this purpose, a chemiluminescence-based reporter system, measuring secretion of placental alkaline phosphatase (SEAP) was utilized. SEAP is a truncated form of the human placental alkaline phosphatase (PLAP), which is secreted into the cell culture medium. MEF K.O cells were co-transfected with CHIP and a SEAP-containing reporter plasmid.

In order to examine secretion defects the medium of transfected cells was mixed with assay buffers, containing CSPD[®] chemiluminescent substrate Emerald-III[™] luminescence enhancer, 24 h past transfection. The amount of SEAP induced luminescence measured in the growth medium was reduced by about 80 % in CHIP expressing cells, supporting the CHIP-induced inhibition of secretion. However, a luciferase reporter assay performed by lysis of the remaining cells, displayed similar reduction of luciferase luminescence upon CHIP overexpression. Since both luciferase and SEAP were regulated by the same promoter, a transcriptional effect of CHIP overexpression on SEAP levels could not be excluded.

A complementary analysis of SEAP and luciferase transcripts with real-time quantitative PCR (qPCR) would have been necessary to evaluate the results. Moreover, luciferase is a known substrate of CHIP and the reduced luciferase levels might result from by CHIP-mediated degradation [33]. Treatment with the proteasome inhibitor MG132 would provide an indication of luciferase degradation.

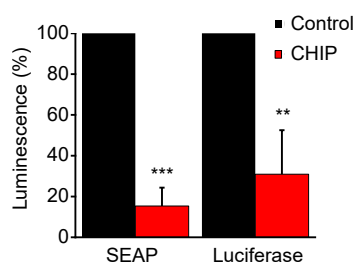


Figure 48. Overexpression of CHIP impairs SEAP secretion in MEF cells. NovaBright reporter gene detection system 2.0 from invitrogen was used to measure transiently transfected SEAP in growth medium 24 h after transfection in MEF K.O. cells. Significant reduction of SEAP luminescence in cells transfected with CHIP was observed. Luciferase activity, measured in parallel to SEAP from lysate of adherent cells displayed a similar reduction (mean \pm SD). *** $p < 0.001$, ** $p < 0.01$, t-test analysis; N = 3 independent experiments.

3.7.2 Membrane localisation of CHIP is linked to cell survival

One possible reason of CHIP mobilisation to cellular membranes is its involvement in cellular survival. A protective role against cell death has been reported for CHIP in several occasions [151][107]. However, recent work in cells treated with staurosporine indicate that CHIP has the capability to enhance cell death [152].

The CHIP-induced dispersion of the Golgi apparatus was an indication that supported the later, as disassembly of Golgi stacks was reported to be a symptom of apoptosis [153]. Hence, cell viability of wild-type MEF cells and MEF K.O. cells subjected to 2 h 43°C heat shock treatment was examined. As reported previously in this work, CHIP transitioned to the plasma membrane of wild-type MEF cells when exposed to heat stress (Fig.11). Observations of stressed cells with brightfield microscopy revealed a drastically different cell morphology of wild-type MEF and CHIP deficient MEF K.O. cells immediately after heat exposure. While wild-type MEF cells were severely affected by heating, displaying shrinking and rounding of almost all cells, the CHIP deficient MEF K.O. cells remained mostly unaffected (Fig.49A).

In a similar setup, the increased resistance to heat stress of cells lacking CHIP could be confirmed by an XTT assay. CHIP deficient MEF K.O. cells displayed statistically significant increased cell viability immediately after heat stress compared to wild-type MEF, supporting the idea of CHIP as a key component of cell survival in early stress response (Fig.49B).

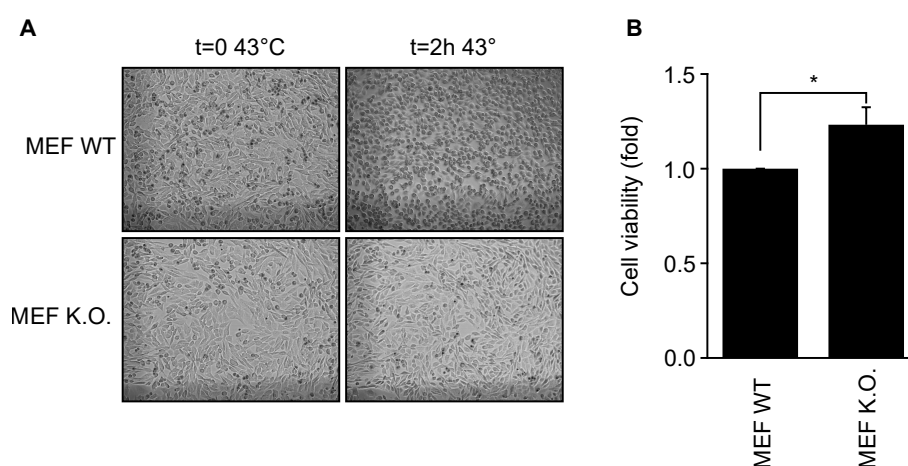


Figure 49. The presence of CHIP negatively influences cell viability in MEF cells exposed to heat stress. (A) Brightfield microscopy of wild-type MEF and CHIP-deficient MEF K.O. cells before and after heat stress for 2 h at 43°C. Images were taken on the same spot of the plate, indicated by a cross marking on the plate (shadows in the left and lower corners of each image), before and after treatment. One representative of three independent experiments is shown. (B) Quantification of heat induced cell death after 2 h 43°C by means of XTT assay, showed a statistically significantly more cell viability in CHIP deficient MEF K.O. compared to wild-type cells (mean \pm SD). * $p < 0.01$, t-test analysis; N = 3 independent experiments.

To specify the relationship between membrane-associated CHIP and decreased cell survival, EGFP-CHIP localisation during apoptosis induction was observed. Wild-type MEF cells were treated for 12 hours with 2 μ M staurosporine, a common inducer of apoptotic cell death and a stressor that has been directly linked to CHIP-promoted cell death [152]. Transiently transfected EGFP-CHIP migrated to the plasma membrane after staurosporine exposure, similar to the phenotype observed for heat stress (Fig.50). In EGFP-transfected cells, no change in subcellular localisation could be observed, excluding an unspecific mobilization due to EGFP.

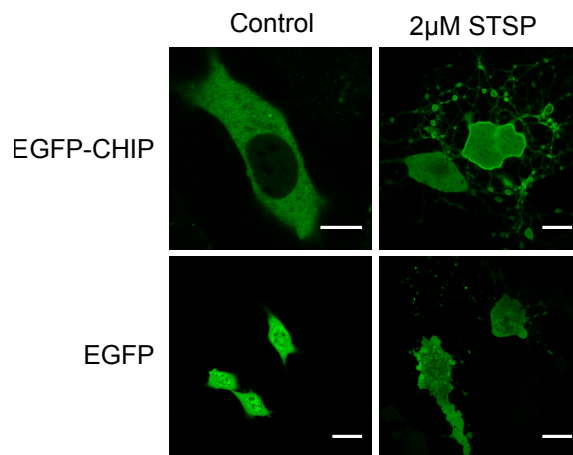


Figure 50. Induction of apoptosis correlates with the plasma membrane localisation of CHIP in MEF cells. Live cell imaging of transiently transfected EGFP-CHIP displayed transition from the cytosol to the plasma membrane in wild-type MEF cells treated with 2 μ M staurosporine (STSP) for 12 h. Controls transfected with EGFP did not display changed localisation upon treatment with staurosporine. Scale bar 10 μ m.

To further confirm the importance of CHIP localisation on cell viability, the chaperone-free and membrane-localised mutant EGFP-CHIP-K30A was transiently transfected into MEF cells. However, staining with 7-Aminoactinomycin (7-AAD) and subsequent FACS analysis revealed no significant change in cell viability 24 h after transfection (data not shown). The processing of samples for FACS could be one reason for the absence of an effect, as cells that died and detached from the flask were not included in the analysis. Another possibility for the absence of an effect could be the relatively low amount of protein expressed in MEF cells, which was not sufficient to generate a cell death-inducing signal. Especially, considering that a portion of transfected EGFP-CHIP-K30A possibly cross-dimerised with endogenous CHIP, reducing effective membrane localisation.

In order to circumvent the effects of relatively low protein expression, CHIP-K30A mutant was transfected into Hek293T cells, which have a highly active translation and metabolism. It was speculated that the amount and speed of CHIP overexpression could be enough to collapse the PN and trigger a signal for cell death. Transfection of EGFP-CHIP-K30A in HEK293T cells confirmed its membrane localisation (Fig.51A). In contrast to MEF cells, EGFP-CHIP-K30A displayed a more heterogeneous distribution at the plasma membrane, concentrating to distinct spots at the plasma membrane. In brightfield

microscopy it became apparent that cells expressing CHIP-K30A displayed increased cell death, while the cytosolic localised wild-type CHIP had no significant effect on viability (Fig.51B). This observation could be confirmed by FACS analysis of transfected cells. To analyse these cells and avoid procedure-related fluctuations, CHIP-K30A was co-transfected with EGFP. Apoptosis was detected by staining with 7-AAD. For quantification purposes, only cells that showed both 7-AAD and EGFP fluorescence, were counted by FACS. In agreement with the visual assessment using brightfield microscopy, membrane localised CHIP-K30A increased cell death significantly 24 h after transfection (Fig.51C). Even though CHIP-K30A displayed only about half of steady-state levels of wild-type protein, it induced a more pronounced effect on cell survival, supporting that CHIP-induced cell death depends on CHIP dissociation from chaperones and changed subcellular localisation (Fig.51D).

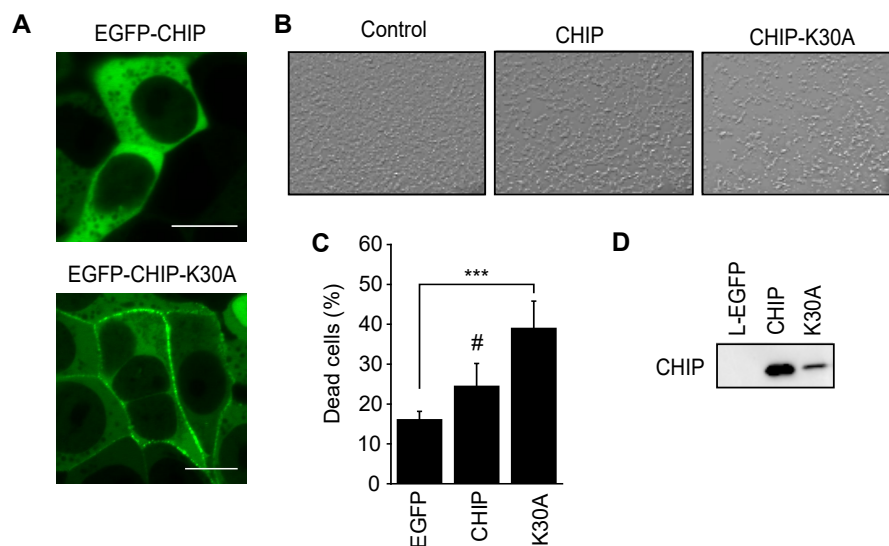


Figure 51. Membrane-localised CHIP-K30A induces cell death in Hek293T. (A) Live cell microscopy of Hek293T stable cell line expressing EGFP-CHIP or EGFP-K30A. Scale bar 10 μ m. (B) CHIP-K30A reduced cell population 24 h after transient transfection as displayed by brightfield microscopy of a representative spot on the plate. (C) Cell death in Hek293T co-transfected with EGFP and CHIP or CHIP-K30A respectively, determined by 7-AAD staining and FACS analysis 24 h after transfection (mean \pm SD). *** p <0.001, t-test analysis; N = 3 independent experiments. (D) Steady-state levels of CHIP, CHIP-K30A in Hek293T cells 24 h after transfection analysed by means of western blot analysis.

Discussion

4.1 Research question and working hypothesis

The purpose of this study was to understand how the E3 ligase CHIP, an essential guardian of proteostasis, participates in acute stress response and how a link between proteostasis and the adaptation of cellular architecture during stress response is established. With growing evidence of cellular structures which participate in the spatial sequestration of misfolded proteins, the mechanisms of the PN that mediate this interplay need to be identified [14]. In this regard, localisation changes of CHIP, an E3 ligase with a diverse substrate pool in multiple pathways in the cell, might provide such a link.

Additionally, the aim was to collect information on the chaperone-dependency of CHIP in this context, as there is a yet unresolved discussion about the bilateral regulation of chaperones and CHIP and how vital chaperone-independent processes are for cellular homeostasis.

To address these questions, the following was considered. In quiescent conditions, the PN of mammalian cells maintains the balance of folding and degradation with the help of molecular chaperones. Among them, the most abundant are HSP70 and HSP90 with their co-chaperones, such as CHIP, tightly associated to regulate their activity. In face of acute stress, cells would channel the HSPs to the accumulating amount of misfolded proteins to prevent or mitigate aggregation [8]. Until the transcriptional up-regulation can compensate the relative chaperone deficit, interactors of these chaperones are freed exposing compartment-specific determinants and allowing them to localise to new destinations within the cell. The changed localisation enables these proteins to engage a compartment-specific interactome which they can modify to possibly compensate stress-induced shortcomings or initiate disposal of cells that are not able to adapt.

In order to test this hypothesis, the localisation of E3 ligase CHIP was analysed during acute stress response, as it interacts with both major chaperones and is a central node in the protein triage and the PN [33][73]. In addition, the association of CHIP and HSPs has been reported to be rather weak [117], thus one can assume that sequestration of chaperones to aggregates could easily yield chaperone-free CHIP *in vivo*. Moreover, CHIP has been

reported to act on membrane localised proteins and influence cell survival [154] [155].

4.2 Chaperone independent CHIP recruitment to cellular membranes

In agreement with the hypothesis, EGFP-CHIP mobilized to new cellular sites in early stress response, when the chaperone system was challenged. Heat shock mobilized CHIP to the plasma membrane of MEF cells, a subcellular localisation that has not been reported for CHIP so far (Fig.11). The plasma membrane is a reasonable target as a novel effector site, as CHIP has been reported to regulate the turnover of many membrane-localised proteins. For example, CHIP mediates ubiquitylation of the misfolded cystic fibrosis transmembrane conductance regulator (CFTR Δ F508), a mutant which abundance at the plasma membrane is inversely proportional to the severity of cystic fibrosis [156]. Like most defective membrane proteins, CFTR Δ F508 is removed by the endoplasmic-reticulum-associated protein degradation (ERAD). In particular CFTR Δ F508 is recognized by HSC70 and subsequently ubiquitylated by CHIP amongst other E3 ligases [80]. The partially misfolded receptor can however escape ERAD and is then shuttled to the plasma membrane. There, it is recognized by HSC70:HOP:HSP90 complex, recruiting CHIP during prolonged interaction. Subsequent ubiquitylation leads to clathrin-dependent internalisation and lysosomal degradation [157]. Additionally, CHIP mediates ubiquitylation of conformationally defective vasopressin V-2 receptor (V2R) and dopamine D4.4 receptor (DRD4), initiating their disposal from the plasma membrane. Both proteins are associated with human diseases [158][159]. What unites all these reports, is the chaperone-dependency of CHIP recruitment to the membrane-localised substrates. As summarized in the introduction, the role of chaperone-independent CHIP activity needs further investigations and some of the mentioned studies hint that chaperone-independent processes might be active at membranes [157][136].

This study provides evidence that supports chaperone-independent activity of CHIP, as the observed localisation of EGFP-CHIP to the plasma membrane during heat stress was inverse proportional to the pool of available chaperones. The co-expression of additional HSC70 reduced the plasma membrane localisation of EGFP-CHIP during stress exposure (Fig.13). Moreover, the heat-induced phenomenon could be mimicked by blocking of HSP70 and HSP90 activity. Treatment with HSP70/90 specific inhibitors recruited EGFP-CHIP to the plasma membrane of MEF cells (Fig.12). Hence, metabolic changes during heat shock could be excluded as the cause for the translocation. The stalling in one conformation of the HSP activity cycle possibly occluded binding of CHIP, thus enabling a part of the cellular CHIP pool to move to the plasma membrane. Due to the supstoichiometric amounts of HSP/HSC70 and HSP90 with respect to cellular CHIP

levels, it is not surprising that only a fraction of cytosolic CHIP migrated to the plasma membrane during heat stress. Similarly, the phenotype upon inhibitor treatment could only be observed for a partially affected HSP70/90 pool, as inhibition of the majority of these essential chaperones is lethal. The observed membrane localisation of EGFP-CHIP in about 4% of cells under control conditions points to an inherent disturbance of the PN in the respective cells and argues against an artificially induced mobilisation of CHIP to the plasma membrane (Fig.11; Fig.18).

To determine if the stress-induced membrane localisation of CHIP was due to a specific reaction to heat stress or a disturbance of proteostasis, different proteotoxic stressors were applied. Arsenite treatment did not induce the localisation change even though a proteotoxic stress was present (Fig.14). This might question the generality of the hypothesis of CHIP translocalisation due to the accumulation of misfolded proteins. However, it has been shown in previous studies that arsenite follows an aggregation pathway distinct from heat-induced misfolding [118]. While heat stress unfolds existing native protein structures, arsenite induces aggregation by interference with the *de novo* folding process. Furthermore, it was argued that the resulting aggregates might be fundamentally dissimilar and HSP presence did not provide as much protection against arsenite aggregates compared to heat induced damage.

Another type of stress disturbing proteostasis is starvation which was induced by cultivation of MEF cells in serum-free and amino acid-deprived conditions [119]. Transfected EGFP-CHIP accumulated in the nucleoli and in small foci in the cytosol, instead of localising to the plasma membrane (Fig.15). This effect might be attributed to the involvement of CHIP in autophagy, which is the dominant response during starvation [120]. However, the identity of the cytosolic foci was not confirmed by specific markers, leaving specification of the observed dots speculative. Regardless of the identity of the EGFP-CHIP dots, it supports the assumption that plasma membrane localisation is a heat-specific stress response. It could be summarized that translocation is most likely a reaction to structural perturbation of the existing proteome which is sensible to the abundance of stress-induced chaperones.

In addition, a subcellular fractionation of unstressed cells showed a chaperone-free CHIP dimer in the membrane fraction. The appearance of endogenous CHIP in the membrane fraction of MEF cells further substantiates cellular membranes as a natural localisation of CHIP. Moreover, the occurrence of the "naked" dimer in the membrane fraction, without addition of HSP70 octapeptide, suggests that at least a fraction of CHIP is not associated with chaperones at membranes.

In order to further investigate the mutually exclusive binding of CHIP to chaperones or membranes, a mutant which is unable to bind HSP70/90 was utilized. The mutation of lysine30 to alanine was used previously to investigate possible allosteric effects of the TPR domain on CHIP activity, as it displayed reduced TPR flexibility compared to

wild-type CHIP [86][160]. Physicochemical properties of the recombinant CHIP-K30A utilized in this study match data from previous studies and confirm its reduced capacity to associate with chaperones and exclude non-native folding of the mutant. In fact, K30A appeared to be more stable than the wild-type in thermal denaturation assays, possibly due to the rigidification of the TPR domain [86]. The accrued dissociation constants for the HSP70 C-terminal peptide:CHIP/K30A complex were higher than in previous reports, which calculated a K_D of $2\mu\text{M}$ for CHIP binding to HSP70 octapeptide [161]. However, the ITC experiment were performed at 25°C , while the values of this study were calculated from data acquired at 37°C . Variations to the published K_D values are likely to result from the different acquisition temperatures. At physiological temperature, an increase of K_D can be expected to result from the overall increase in thermal motion of the molecules, compared to 25°C .

In accordance with the hypothesis, the chaperone-free EGFP-CHIP-K30A mutant was localised to the plasma membrane in over 93% of MEF cells. Any remaining cytosolic EGFP-CHIP-K30A is likely to originate from heterodimerisation of endogenous CHIP with the transfected CHIP-K30A mutant or from saturation of available binding sites. The possibility of a mutation-induced artificial localisation determinant was excluded as wild-type and mutant protein displayed similar lipid specificity *in vitro* (Fig.20A).

Evaluation of EGFP-CHIP-K30A distribution on membranes by means of TIRF microscopy is physically restricted to the contact-interface of the cell and the cover-slide due to the extent of the evanescent field [122]. Even though clear differences were visible between wild-type CHIP and K30A in TIRF microscopy, the identity of the punctae could not be determined as the need for live cell imaging prevented the use of immunofluorescence methods. One can speculate that at the imaged contact-interface of cell and glass slide, the dots correspond to an association of EGFP-CHIP-K30A with integrins, as co-localisation and turnover of integrin-linked kinase (ILK), was demonstrated to be mediated by the CHIP:HSP90 complex [162]. It would, however, imply CHIP binding to ILK in a chaperone-independent manner as CHIP-K30A can not bind HSP90. Another explanation would be the association with lipid microdomains accompanied by oligomerization or the assembly of functional complexes [134][133]. However, the underlying mechanisms for formation and protein association with lipid microdomains remain largely elusive and isolation proves to be difficult [163]. Because of the possible association of CHIP with cellular adherence complexes one has to be careful to assume a granular distribution of CHIP-K30A throughout the entire plasma membrane. In order to verify this several adhesion proteins need to be cloned with fluorescence tags to investigate possible co-localisation *in vivo*. Another possibility would be the isolation of lipid microdomains (lipid rafts) which could give another explanation for the observed punctae. Preliminary results from a lipid raft isolation following the protocol from Deborah A. Brown did not identify CHIP on lipid rafts (data not shown)[164].

Surprisingly, subcellular fractionation of transfected CHIP-K30A did not reproduce the microscopic observations. The expected accumulation of CHIP in the membrane fraction could not be identified, though it did confirm the impaired chaperone binding of CHIP-K30A, as addition of HSP70 peptide could not release substrate complexes, as it was observed for endogenous CHIP. Concerning the lack of accumulation of K30A in the *ex vivo* membrane fraction, an explanation might be the transient nature of the association of CHIP with cellular membranes. During the process of separating cellular compartments, it seems likely that the association is partially lost due to changing ionic buffer strength and the presence of detergents. This argument is supported by the fact that membrane association can not be observed in samples fixed with paraformaldehyde, a method commonly applied in fluorescence microscopy, but which perturbs cellular morphologies [165][166]. One could speculate that the membrane association of endogenous CHIP and transfected CHIP is somewhat different, with transfected CHIP being transiently associated and endogenous CHIP more tightly tethered to membranes or organised in complexes.

The competitive nature of chaperones and lipids for CHIP binding could also be confirmed by *in vitro* association with liposomes and lipid strips. Both, C-terminal HSP70 peptide and a truncated version of HSP70, inhibited binding of CHIP to liposomes. Notably, the HSP70 octapeptide, which is sufficient for CHIP binding to HSP70, only competed with lipid binding at unphysiologically high concentrations. The results suggest that the TPR domain is a main, but not the exclusive determinant of lipid binding, as demonstrated by the increased effectiveness of the truncated HSP70 protein. The additional C-terminal residues of HSP70 possibly shield additional residues on CHIP, which participate in lipid binding.

If CHIP is not recruited to membranes by chaperones, it is essential to uncover which determinant is responsible for the changed localisation of CHIP. A novel direct association with lipids was hypothesised, even though the sequence of human CHIP does not entail any conserved lipid-binding domains. To analyse the details of the association with membranes, binding was reconstituted *in vitro* by means of commercial lipid strips and liposomes. It was also aimed to establish a lipid overlay assay with self-made lipid strips, but the preparation exhibited significant fluctuations.

On commercial lipid strips, CHIP displayed specific binding to phosphatidic acid (PA) and phosphatidylinositol monophosphates, especially to PI4P. Comparison of liposomes spiked with equal amounts of PA or PI4P displayed specific association only with PI4P, suggesting that it may be the main determinant for membrane association or at least has the higher affinity towards CHIP. However, the necessity of PA for CHIP membrane association can not be excluded, as PA levels are considerably higher than PI4P levels *in vivo* and can vary significantly in response to stress. Fitting to the observed membrane localisation during heat stress, an increase of PA levels was reported for heat challenged

plants, which would provide the necessary additional binding sites for CHIP [167]. Additionally, only one type of PA, that with two saturated alanyl chains, was tested in liposomes and it has been suggested that PA species that are produced by distinct pathways *in vivo* vary at sn-1 and sn-2 positions resulting in very different effects on protein association [168]. Unspecific binding due to trivial electrostatic attraction could be excluded, as increasing charge, provided by poly-phosphorylation of inositols, displayed reduced binding in lipid overlay assays. Similarly, other phospholipids with a negative net charge, like phosphatidylserine did not show binding on commercial lipid strips, supporting a stereospecific recognition of lipids. Both, PA and PI4P can be found in the plasma membrane of mammalian cells [169][170].

Verification of CHIP specificity for PA and PI4P, was provided by depletion of the respective lipid levels *in vivo*. Treatment with specific inhibitors initiated the expected relocalisation of EGFP-CHIP-K30A to the cytosol, due to reduction of available binding sites. Notably, only the isoform-unspecific PLD inhibitor FIPI and the PLD1-specific inhibitor, but not the PLD2-specific inhibitor, relocalised EGFP-CHIP-K30A from the membrane into the cytosol. This appears to be counter intuitive as PLD2 is the isoform that resides mainly at the plasma membrane and has a strong intrinsic catalytic activity, while PLD1 has been reported at various cellular sites and needs to be activated by the presence of effector proteins, like protein kinase C α [171]. A reasonable explanation could be that in MEF cells PLD1 is exclusively localised to the plasma membrane. Accordingly, studies support an exclusive membrane localisation of PLD1 in fibroblasts [172][171]. Another option would be that PLD1 is actively mobilized to the plasma membrane, as the presence of CHIP-K30A at cellular membrane artificially generates a stimulus, similar as induced by external stressors. A stimuli-dependent translocation of PLD1 to the plasma membrane has been observed in RBL-2H3 cells [172]. The impact and specificity of PLD is of special interest, as their isoforms have been implicated in diverse pathologies, like Alzheimer's disease and cancer, in which CHIP is involved as well [173].

The lipid specificity has several interesting implications for effector sites of CHIP within the cell and requires further investigations. For example, the understanding of PA functions in cellular processes has increased significantly over the recent years. It has become apparent that PA not only serves as building block for other phospholipids but also exerts regulatory functions in various processes, such as cell survival, signal transduction, membrane trafficking, secretion, stress response and cytoskeletal rearrangement, in plants and mammals. Furthermore, a protein-tethering function of PA has been reported to initiate the assembly of cytosolic proteins to specific membranes or regions on membranes, where those complexes participate in critical cellular processes [168]. The steady-state levels of PA in cellular membranes are relatively low compared to phosphatidylcholine (less than 5%) but can change significantly depending on metabolic state or stress exposure [174]. This gives additional reason for a stress-induced change of CHIP to specific subcellular

locations.

Specificity of PI4P binding could be confirmed by relocalisation of EGFP-CHIP-K30A upon wortmannin and PI4KIII β inhibitor treatment. Even though PIPs are less abundant than PA, they are essential for organelle identity. PI4P is enriched in the Golgi apparatus and the plasma membrane, while PI3P can be found in early endosomes and PI5P in membranes of late endosomes. Their specific subcellular distribution and their high turnover make PIPs optimal mediators of signalling events and they have been implicated in nearly all processes of cell physiology [175]. The binding to PI3P and PI5P appeared to be weaker in lipid overlay assays and is possibly an evolutionary byproduct of the PI4P specificity with little biological impact, as PI3P and PI5P are ten and hundred times less abundant than PI4P [176].

At submicromolar concentrations, wortmannin acts as a specific PI3K inhibitor and had no effect on EGFP-CHIP-K30A localisation, which confirms the insignificant role of PI3P for CHIP association with the plasma membrane *in vivo*. However, as PI3P is predominately accumulated in endosomes, it might be interesting to investigate if CHIP is recruited to endosomes, dependent on PI3P levels. At higher concentrations, wortmannin becomes a potent inhibitor of type III but not type II PI4Ks [177]. The treatment of MEF cells with 10 μ M successfully depleted EGFP-CHIP-K30A from the plasma membrane. Thus, it can be assumed that type III PI4K provides the pool of CHIP interacting PI4P at the plasma membrane. Importance of PI4P produced by type III PI4K could be further supported by the relocalisation of EGFP-CHIP-K30A to the cytosol in response to PI4KIII β -specific inhibitor treatment.

The interactome analysis of pulldowns from EGFP-CHIP-K30A transfected cells confirmed the effective relocalisation of CHIP to the cytosol upon PLD treatment, as interactomes displayed minimal overlap. Moreover, for the first time, a high confidence identification of chaperone-free interactors of CHIP at the plasma membrane could be provided. Several interactors were assigned to other organelles, like endosomes and the Golgi apparatus, which indicates the possibility of a broad spectrum of cellular sites modified by membrane-localised CHIP. In contrast to the *in vitro* experiments, the identification of interactors involved in endosomal pathways hint to a relative importance of PI3P and PI5P in targeting CHIP to endosomal membranes.

4.3 Structural determinants for CHIP binding to membranes

As argued in competition experiments and as a prerequisite for the initial hypothesis, the TPR domain of CHIP was considered to be the main lipid-binding interface. Co-sedimentation of liposomes with truncated CHIP versions and the inability to detect CHIP on lipid strips with a TPR-reactive antibody supported this idea. The binding of isolated TPR domain displayed pronounced binding to liposomes while Δ TPR associated only minimally. The exceeding binding of the isolated TPR domain compared to wild-type CHIP probably resulted from the high flexibility of the isolated domain, enabling also unspecific lipid binding. A high flexibility of TPR domain has been shown before [89] and it seems reasonable to assume that the flexibility is further enhanced in the isolated domain, which lacks the allosteric control from the rest of the molecule [92]. This was supported by CD spectroscopy which uncovered reduced secondary structure content upon liposome binding, independent of PA presence, and by the unspecific binding of TPR on lipid strips. The truncated Δ TPR protein displayed residual binding on liposomes as well as specific binding on lipid strips, suggesting an additional lipid-binding determinant in CHIP.

Sequence analysis revealed two positively charged patches (m1 (143-146 aa:KKKR); m2 (221-225 aa: KRKKR)) in the CC-domain as promising candidates. Mutation to alanine of the m2 patch, but not the m1 patch, resulted in a complete abrogation of the EGFP-K30A-m2 Δ membrane association. It remains unclear why neighbouring m1 patch, despite the obvious similarities, seemed to have no impact on the localisation. One can speculate that the two sites differ in lipid accessibility due to the asymmetry of the CHIP dimer. The importance of the m2 patch in lipid binding was verified in lipid overlay assays, with the mutant displaying reduced association. In a co-sedimentation assay, recombinant CHIP-m2 Δ displayed reduced association with PA-spiked liposomes compared to wild-type CHIP, further substantiating m2 importance in membrane association. However, the binding to DOPC liposomes was enhanced compared to wild-type CHIP and no difference between PA-spiked and DOPC liposomes was observed for CHIP-m2 Δ . This resembles the unspecific binding of the isolated TPR domain on lipid strips. A factor that might impact the increased binding to DOPC could originate from differences in physicochemical properties of the recombinant CHIP-m2 Δ protein. It was significantly more susceptible to thermal unfolding, suggesting reduced structural stability. *In vitro* ubiquitylation argues against mutation induced unfolding, as despite the inhibited K48 ubiquitylation of the model substrate NQO1, the production of K63 chains was not impaired.

Previous comparisons of other PA binding regions in different proteins revealed that there is no common conserved motif, except the presence of basic amino acids like Lys, Arg,

or His, which are also abundant in the the proposed binding sites of CHIP [168]. One can envision that, similar to other PA binding proteins, structural rearrangements are necessary to enable the exposure of PA binding sites in the CC-domain of CHIP [168]. Even though the exact mechanism remains unclear this seems possible, considering the highly dynamic nature of the asymmetric CHIP dimer [93]. The details of how m2 and the TPR domain mediate lipid association remain unclear and further investigations need to be conducted to conclude how they mediate lipid specificity and if dimer allostery controls their accessibility.

Interactions between proteins and membranes can be bivalent. Membrane association often initiates changes in protein structure or activity and, on the other hand, proteins can change membrane properties, such as lipid composition or curvature [178][169]. Especially due to the addition of PA, there is an increased probability of altered membrane structure which might induce liposome fusion [168]. Size distribution of liposomes analysed by NanoSight did not reveal a pronounced effect of CHIP binding on the size of PA-spiked liposomes. The variations in mean diameter can be attributed to the liposome preparation, when using probe sonication instead of extrusion with filters of specific diameter [179]. Comparison of liposomes of different sizes prepared by extrusion revealed that only LUVs with a diameter greater than 100nm displayed a significant difference in CHIP association between PA-spiked and DOPC liposomes. It is possible that formation of PA microdomains is necessary, which is facilitated on LUVs because they provide the necessary surface and stability. The formation of microdomains is supported by the weak interaction of DOPC with high melting lipids, such as DPPA, which promotes coalescence to macroscopic PA domains [180][181]. The necessity of microdomain formation for CHIP binding to lipids might also offer an explanation why no specific interaction was detected for liposomes containing only 1% PI4P. Additionally, smaller liposomes (30-50nm) containing 20% PA might be more affected by the curvature stress and possible packing defects induced by PA, explaining the increasing fluctuation in CHIP binding observed for extruded liposomes (Fig.34C) [168]. Another explanation might be that the initial shape of extruded liposomes is cylindrical, which reduces the available contact sites. Furthermore, extruded liposomes have the tendency to exhibit age related effects, which possibly obliterate the differences between PA-spiked and pure DOPC liposomes [182].

The already mentioned transient nature of CHIP association with membranes could be supported by limited digestion *in vitro*, as no differences between liposome-bound CHIP and CHIP in solution could be found. An insertion of an amphipathic helix for example would have protected parts of the protein from degradation, yielding a divergent degradation pattern [183]. Similarly, CD spectroscopy of wild-type CHIP did not display an increase or decrease of overall secondary structure elements, which are usually observed for proteins inserting into membranes. However, structural rearrangements can not be

excluded because changes, as observed for CD of the isolated TPR domain, could be allosterically compensated by the rest of the molecule, especially considering the proposed flexibility of the CHIP dimer [93]. Additionally, CD spectroscopy is limited in the observation of liposome-induced changes. Higher amounts of liposomes increase turbidity and, consequently, the voltage applied to the photon multiplier (HT-value), which makes the resulting data not interpretable. The results from the high-salt wash argue against the experiments that support an exclusively transient association of CHIP with membranes, as the increasing ionic strength should be able to release the protein if it is only bound through electrostatic forces to the lipid headgroups [179]. However, considering that the majority of experiments is supporting a transient interaction, it could be reasoned that CHIP harbours at least two sites of membrane association, which can stabilize the binding enough to maintain association under the applied ionic conditions. An influence of hydrophobic forces could not be finally excluded and the proportion of possibly unspecific interactions of the TPR domain has to be taken into consideration.

Surprisingly, fractionation of endogenous CHIP displayed SDS-insoluble oligomers of distinct size, predominantly in the membrane fraction. Similar SDS-insoluble oligomers have been reported for H₂O₂-treated CHIP [132]. Fractionation was performed under reducing conditions and fractions from transiently transfected cells did not yield a comparable amount of the oligomers, pointing towards a phenomenon specific for endogenous CHIP. One could imagine that there is a limited amount of binding sites at membranes, saturated by endogenous CHIP in oligomeric conformations. Hence, supplementing additional CHIP by transfection can not increase these oligomeric species. The combination of oligomeric state and membrane tethering might protect these endogenous complexes from sufficient SDS solubilisation.

The analysis of CHIP oligomers and a possible connection to membrane binding was investigated due to their predominant appearance in *ex vivo* membrane fractions. The oligomers observed in chemical crosslinking of recombinant protein match previous observations and are not artefacts of unspecific crosslinks, as zero-length crosslinker displayed a similar pattern [90]. However, the ratios of dimers and oligomers displayed in chemical crosslinking are not representative for the situation in solution, as native MS revealed only a minor fraction of CHIP corresponding to a tetrameric form and no oligomers of higher order were identified. Notably, this is the first time that human CHIP oligomers could be shown in solution. Surprisingly, native MS identified the presence of CHIP monomers, which has not been reported so far and suggests a possible pathway for CHIP oligomerization. In agreement with this assumption, addition of the monomerizing agent desoxycholate (DC) enabled the identification of a population matching hexameric CHIP in native MS [90]. The exact mechanism of the DC-induced monomerisation and how CHIP monomers assemble into tetrameric and hexameric oligomers remains to be determined. A recent study confirmed the presence of an oligomeric and monomeric CHIP

species in solution using SEC [184]. Additionally, they managed to shift the equilibrium towards oligomers using site-directed mutagenesis and reasoned that at least some diseases are mediated by the oligomeric state of CHIP. In a similar attempt, a self-cast column was combined with continuous heating to increase oligomeric species, in order to purify CHIP oligomers for structural analysis. However, despite several conditions it was not possible to acquire a fraction sufficiently enriched in oligomers (data not shown), pointing to a low stability of oligomers and an immediate restoration of equilibrium conditions during sampling.

The importance of CHIP oligomers was previously neglected due to the need of unphysiological high concentrations. Yet cellular membranes provide a surface where local concentrations can be significantly higher than in the cytosol [133]. The effect of the cholesterol-resembling steroid DC on CHIP, together with the natural occurrence of endogenous CHIP oligomers in *ex vivo* membrane fractions, indicate the possible importance of membranes in CHIP oligomerization. Crosslinking of recombinant CHIP on liposomes provided additional evidence that membranes can provide a relevant scaffold to increase oligomerization.

With respect to the stress-induced mobilisation of CHIP at membrane, it is reasonable to assume that a sudden increase in local concentration at membranes promotes formation of CHIP oligomers. To this end, it was speculated that especially hexamers, if assuming a ring-like shape with a central cavity, could form a pore that would increase membrane permeability [185]. Despite the application of several strategies to investigate liposome leakage, no significant influence of CHIP on liposome permeability could be concluded.

In another approach, it was speculated that CHIP oligomers might form functional machineries that shuttle E2s from U-box to U-box to enhance production of ubiquitin chains. Especially K63 ubiquitylation seemed to be a promising example to test the hypothesis, as *in vitro* ubiquitylation with UBC13-UEV1A was shown to produce free poly-ubiquitin chains [77]. Since the UBC13-UEV1A heterocomplex together with TRAF6 has been reported to mediate K63 ubiquitylation in the NF- κ B signalling pathway, it was investigated if K63 ubiquitylation mediated by CHIP had similar effects and if those are dependent on CHIP localisation to membranes [139]. However, no significant activation of NF- κ B signalling could be found in Hek293T cells, and in MEF cells a suppressive effect was observed. Such a suppressive effect of CHIP on NF- κ B signalling was reported previously [186]. The cause for the suppression was found to be CHIP mediated K48 ubiquitylation of NIK (NF- κ B-inducing kinase). Thus, the functional importance of CHIP oligomers remains enigmatic, as MEF cells proved to be an inadequate expression system and the results obtained with Hek293T cells, as well as the ubiquitylation assay in the presence of liposomes, argued against the increase of K63 ubiquitylation at cellular membranes.

4.4 Physiological implications of CHIP localisation to cellular membranes

In search for the functional consequences of CHIP localisation to membranes, *in vitro* ubiquitylation was investigated in presence and absence of PA-spiked and DOPC liposomes. The ubiquitylation of the model substrate NQO1-P187S was not impaired or enhanced on liposomes containing 20% PA. In contrast K63 ubiquitylation was slightly affected when CHIP was bound to liposomes, possibly due to an impaired access of the UEV1A/UBC13 heterocomplex. Autoubiquitylation of CHIP was enhanced on liposomes, however, with no apparent regulatory effect on ubiquitylation activity. It has been suggested that autoubiquitylation of CHIP could regulate its activity, as it has been reported for other E3 ligases like the HECT E3 ligase Rsp5 [187]. In agreement with the published data, the increased auto-ubiquitylation is accompanied by enhanced oligomerization of CHIP on membranes, as demonstrated by crosslinking on liposomes. However, CHIP K48 activity was unaffected. A simple explanation for the increased auto-ubiquitylation would be the relative proximity of CHIP proteins on the liposome compared to CHIP in solution, which might promote recognition of CHIP as its own substrate. With the combined indications from lipid strips and *in vitro* ubiquitylation of heated BSA, it was assumed that CHIP might clear mislocalised proteins in order to maintain protein homeostasis at membranes. BSA and NQO1 both displayed increased association with liposomes after heating with no specificity for the lipid composition, suggesting an unspecific binding of proteins to membranes upon unfolding. Interestingly, NQO1 was reported to relocate to the inner leaflet of the plasma membrane during oxidative stress. Since NQO1 is a natural substrate of CHIP, this might offer an explanation why it displays membrane specific ubiquitylation by CHIP, while BSA does not [188]. The results acquired by co-sedimentation suggested that the association of NQO1 might also be determined by PA levels in the plasma membrane, as wild-type NQO1 selectively bound to PA-spiked liposomes. In plants an increase of PA during oxidative stress has been reported which would fit to the observed specificity of NQO1 and a possible transition to the plasma membrane [168]. In mammals an increased PLD activity in response to oxidative stress points towards a similar enrichment of PA [189]. Future studies need to reveal if the turnover of other membrane-localised substrates is specific for membrane-localised CHIP.

In order to identify other possible cellular sites where CHIP might exert a specific function at membranes, the Golgi apparatus was identified to be significantly affected by chaperone-free CHIP. The Golgi apparatus has characteristically high levels of PI4P, which makes it a reasonable target of CHIP, considering its lipid specificity [190]. Golgi morphology was significantly disrupted by chaperone-free CHIP, as demonstrated by

CHIP overexpression and comparison of MEF WT and MEF K.O. cells under heat stress conditions. Additionally, the disassembled Golgi phenotype could be rescued by co-expression of HSP70, supporting the competitive role of chaperones and membranes for binding to CHIP.

The Golgi requires its cisternal-stacking morphology in order to mediate proper secretion, trafficking and post-translational processing of proteins [191][192]. Mechanisms causing morphological defects of the Golgi apparatus have become of significant importance in the understanding of many neurodegenerative diseases, such as Alzheimer's [193], amyotrophic lateral sclerosis [194][195] and Huntington's [196]. In all these diseases Golgi fragmentation and dispersal precedes neuronal cell death. It was suggested that the Golgi might even serve a common sensor of stress signals in cell death pathways [197]. This thesis work suggests that CHIP also participates in cell death via the disassembly of the Golgi. Thus, one can imagine that increasing CHIP activity or abundance for therapeutic purposes might have detrimental side effects. On the other side, CHIP has been reported in neurodegenerative diseases to confer protection against neuronal cell death by preventing the formation of toxic aggregates [198][199][200]. Thus, the exact role of CHIP in cell death pathways remains to be established as there are opposing studies reporting cytotoxic and cytoprotective effects. For example, CHIP protects cells against necroptosis by degradation of RIPK3 [201]. It was also reported to confer protection against thermal stress and apoptosis by activation of HSF1 [107]. In contrast, CHIP exerts cytotoxic effect through degradation of cell proliferation- and survival-related proteins, including ErBb2 [202] and HIF1- α [203]. In neuroblastoma cells treated with staurosporine, CHIP enhanced cytotoxicity by ubiquitylation and subsequent degradation of PINK1, a positive regulator of neuronal cell survival [152]. In agreement with these results, MEF K.O. cells displayed decreased cytotoxic effects after stress exposure. MEF K.O. displayed more resilience to heat shock, while CHIP localisation to membranes during heat shock increased cell death in wild-type MEF cells. Moreover, localisation to the plasma membrane was observed during treatment with the apoptosis inducing agent staurosporine in MEF cells, which supports the idea of membrane-localised CHIP participating in cell death. The specific localisation of CHIP during staurosporine treatment goes in line with the reported increase of cellular PA levels upon staurosporine treatment [204].

Another direct indication of membrane-localised CHIP participating in cell death is provided by the significant increase in cell death upon overexpression of the chaperone-free CHIP-K30A in Hek293T cells. One could hypothesise that the protective nature of CHIP is mostly in concert with associated chaperones, while the detrimental effect on cell survival CHIP might be a unique feature of the chaperone-free ligase.

The results of this study offer new possibilities to explain the inconsistent effects observed for CHIP on cell death pathways. Seemingly opposing functions of CHIP in cell survival might depend not only on the diversity of its downstream targets but on the localisation

of the ligase and chaperone association as well. Since localisation to membranes is only possible if the ligase is free from chaperone association, CHIP might act as a sensor for the severity of damage and for the strength of the stress reaction. For the sake of the whole organism, metazoans might need to sacrifice cells which have failed to adapt and CHIP might act as a key sensor in this scenario.

Bibliography

- [1] Dietmar Kültz. MOLECULAR AND EVOLUTIONARY BASIS OF THE CELLULAR STRESS RESPONSE. *Annual Review of Physiology*, 67(1):225–257, mar 2005.
- [2] Bruce Alberts, Alexander Johnson, Julian Lewis, Martin Raff, Keith Roberts, and Peter Walter. *Molecular Biology of the Cell, Fourth Edition*. Garland Science, 2002.
- [3] Yujin E. Kim, Mark S. Hipp, Andreas Bracher, Manajit Hayer-Hartl, and F. Ulrich Hartl. Molecular chaperone functions in protein folding and proteostasis. *Annual Review of Biochemistry*, 82(1):323–355, jun 2013.
- [4] Anne Gershenson, Lila M Gierasch, Annalisa Pastore, and Sheena E Radford. Energy landscapes of functional proteins are inherently risky. *Nature Chemical Biology*, 10(11):884–891, oct 2014.
- [5] R. John Ellis and Allen P. Minton. Protein aggregation in crowded environments. *Biological Chemistry*, 387(5), jan 2006.
- [6] Monica Bucciantini, Elisa Giannoni, Fabrizio Chiti, Fabiana Baroni, Lucia Formigli, Jesús Zurdo, Niccolò Taddei, Giampietro Ramponi, Christopher M. Dobson, and Massimo Stefani. Inherent toxicity of aggregates implies a common mechanism for protein misfolding diseases. *Nature*, 416(6880):507–511, apr 2002.
- [7] W. E. Balch, R. I. Morimoto, A. Dillin, and J. W. Kelly. Adapting proteostasis for disease intervention. *Science*, 319(5865):916–919, feb 2008.
- [8] D. Balchin, M. Hayer-Hartl, and F. U. Hartl. In vivo aspects of protein folding and quality control. *Science*, 353(6294):aac4354–aac4354, jun 2016.
- [9] Fabrizio Chiti and Christopher M. Dobson. Protein misfolding, functional amyloid, and human disease. *Annual Review of Biochemistry*, 75(1):333–366, jun 2006.
- [10] Nadja Kettern, Michael Dreiseidler, Riga Tawo, and Jörg Höhfeld. Chaperone-assisted degradation: multiple paths to destruction. *Biological Chemistry*, 391(5), jan 2010.

- [11] Avram Hershko and Aaron Ciechanover. THE UBIQUITIN SYSTEM. *Annual Review of Biochemistry*, 67(1):425–479, jun 1998.
- [12] M. P. Jackson and E. W. Hewitt. Cellular proteostasis: degradation of misfolded proteins by lysosomes. *Essays In Biochemistry*, 60(2):173–180, oct 2016.
- [13] Stéphanie Escusa-Toret, Willianne I M Vonk, and Judith Frydman. Spatial sequestration of misfolded proteins by a dynamic chaperone pathway enhances cellular fitness during stress. *Nature cell biology*, 15:1231–1243, October 2013.
- [14] Emily M Sontag, Willianne IM Vonk, and Judith Frydman. Sorting out the trash: the spatial nature of eukaryotic protein quality control. *Current Opinion in Cell Biology*, 26:139–146, feb 2014.
- [15] Daniel Kaganovich, Ron Kopito, and Judith Frydman. Misfolded proteins partition between two distinct quality control compartments. *Nature*, 454(7208):1088–1095, aug 2008.
- [16] Beidong Liu, Lisa Larsson, Antonio Caballero, Xinxin Hao, David Öling, Julie Grantham, and Thomas Nyström. The polarisome is required for segregation and retrograde transport of protein aggregates. *Cell*, 140(2):257–267, jan 2010.
- [17] D. Venton. Highlight: The chaperone network–evolution's helping hand. *Genome Biology and Evolution*, 4(5):626–627, may 2012.
- [18] Steffen Preissler and Elke Deuerling. Ribosome-associated chaperones as key players in proteostasis. *Trends in Biochemical Sciences*, 37(7):274–283, jul 2012.
- [19] Alice Y Yam, Yu Xia, Hen-Tzu Jill Lin, Alma Burlingame, Mark Gerstein, and Judith Frydman. Defining the TRiC/CCT interactome links chaperonin function to stabilization of newly made proteins with complex topologies. *Nature Structural & Molecular Biology*, 15(12):1255–1262, nov 2008.
- [20] Wilhelm Voth and Ursula Jakob. Stress-activated chaperones: A first line of defense. *Trends in Biochemical Sciences*, 42(11):899–913, nov 2017.
- [21] Klaus Richter, Martin Haslbeck, and Johannes Buchner. The heat shock response: Life on the verge of death. *Molecular Cell*, 40(2):253–266, oct 2010.
- [22] J. Ross Buchan and Roy Parker. Eukaryotic stress granules: The ins and outs of translation. *Molecular Cell*, 36(6):932–941, dec 2009.
- [23] Zsolt Török, Tim Crul, Bruno Maresca, Gerhard J. Schütz, Felix Viana, Laura Dindia, Stefano Piotto, Mario Brameshuber, Gábor Balogh, Mária Péter, Amalia Porta, Alfonso Trapani, Imre Gombos, Attila Glatz, Burcin Gungor, Begüm Peksel,

- László Vigh, Bálint Csoboz, Ibolya Horváth, Mathilakath M. Vijayan, Phillip L. Hooper, John L. Harwood, and László Vigh. Plasma membranes as heat stress sensors: From lipid-controlled molecular switches to therapeutic applications. *Biochimica et Biophysica Acta (BBA) - Biomembranes*, 1838(6):1594–1618, jun 2014.
- [24] Balint Csoboz, Gabor E. Balogh, Erzsebet Kusz, Imre Gombos, Maria Peter, Tim Crul, Burcin Gungor, Lajos Haracska, Gordana Bogdanovics, Zsolt Torok, Ibolya Horvath, and Laszlo Vigh. Membrane fluidity matters: Hyperthermia from the aspects of lipids and membranes. *International Journal of Hyperthermia*, 29(5):491–499, jul 2013.
- [25] F. Ritossa. A new puffing pattern induced by temperature shock and DNP in drosophila. *Experientia*, 18(12):571–573, dec 1962.
- [26] F Ritossa. Discovery of the heat shock response. *Cell stress & chaperones*, 1:97–98, June 1996.
- [27] Florian H. Schopf, Maximilian M. Biebl, and Johannes Buchner. The HSP90 chaperone machinery. *Nature Reviews Molecular Cell Biology*, 18(6):345–360, apr 2017.
- [28] Jürgen Radons. The human HSP70 family of chaperones: where do we stand? *Cell Stress and Chaperones*, 21(3):379–404, feb 2016.
- [29] Matthias P. Mayer and Roman Kityk. Insights into the molecular mechanism of allostery in hsp70s. *Frontiers in Molecular Biosciences*, 2, oct 2015.
- [30] Eugenia M. Clerico, Joseph M. Tilitsky, Wenli Meng, and Lila M. Gierasch. How hsp70 molecular machines interact with their substrates to mediate diverse physiological functions. *Journal of Molecular Biology*, 427(7):1575–1588, apr 2015.
- [31] Nadinath B. Nillegoda and Bernd Bukau. Metazoan hsp70-based protein disaggregases: emergence and mechanisms. *Frontiers in Molecular Biosciences*, 2, oct 2015.
- [32] M. P. Mayer and B. Bukau. Hsp70 chaperones: Cellular functions and molecular mechanism. *Cellular and Molecular Life Sciences*, 62(6):670–684, mar 2005.
- [33] C A Ballinger, P Connell, Y Wu, Z Hu, L J Thompson, L Y Yin, and C Patterson. Identification of chip, a novel tetratricopeptide repeat-containing protein that interacts with heat shock proteins and negatively regulates chaperone functions. *Molecular and cellular biology*, 19:4535–4545, June 1999.

- [34] Mathias Gehrmann, Gerhard Liebisch, Gerd Schmitz, Robin Anderson, Claudia Steinem, Antonio De Maio, Graham Pockley, and Gabriele Multhoff. Tumor-specific hsp70 plasma membrane localization is enabled by the glycosphingolipid gb3. *PLoS ONE*, 3(4):e1925, apr 2008.
- [35] Mathias Gehrmann, Stefan Stangl, Andreas Kirschner, Gemma A. Foulds, Wolfgang Sievert, Brigitte T. Doß, Axel Walch, Alan G. Pockley, and Gabriele Multhoff. Immunotherapeutic targeting of membrane hsp70-expressing tumors using recombinant human granzyme b. *PLoS ONE*, 7(7):e41341, jul 2012.
- [36] Victor Lopez, David M. Cauvi, Nelson Arispe, and Antonio De Maio. Bacterial hsp70 (DnaK) and mammalian hsp70 interact differently with lipid membranes. *Cell Stress and Chaperones*, 21(4):609–616, apr 2016.
- [37] Gabrielle Armijo, Jonathan Okerblom, David M. Cauvi, Victor Lopez, Diana E. Schlamadinger, Judy Kim, Nelson Arispe, and Antonio De Maio. Interaction of heat shock protein 70 with membranes depends on the lipid environment. *Cell Stress and Chaperones*, 19(6):877–886, may 2014.
- [38] Ajay K. Mahalka, Thomas Kirkegaard, Laura T.I. Jukola, Marja Jäättelä, and Paavo K.J. Kinnunen. Human heat shock protein 70 (hsp70) as a peripheral membrane protein. *Biochimica et Biophysica Acta (BBA) - Biomembranes*, 1838(5):1344–1361, may 2014.
- [39] Kateryna Morozova, Cristina C. Clement, Susmita Kaushik, Barbara Stiller, Esperanza Arias, Atta Ahmad, Jennifer N. Rauch, Victor Chatterjee, Chiara Melis, Brian Scharf, Jason E. Gestwicki, Ana-Maria Cuervo, Erik R. P. Zuiderweg, and Laura Santambrogio. Structural and biological interaction of hsc-70 protein with phosphatidylserine in endosomal microautophagy. *Journal of Biological Chemistry*, 291(35):18096–18106, jul 2016.
- [40] Valerie Uytterhoeven, Elsa Lauwers, Ine Maes, Katarzyna Miskiewicz, Manuel N. Melo, Jef Swerts, Sabine Kuenen, Rafaël Wittocx, Nikky Corthout, Siewert-Jan Marrink, Sebastian Munck, and Patrik Verstreken. Hsc70-4 deforms membranes to promote synaptic protein turnover by endosomal microautophagy. *Neuron*, 88(4):735–748, nov 2015.
- [41] Bin Chen, William H. Piel, Liming Gui, Elspeth Bruford, and Antónia Monteiro. The HSP90 family of genes in the human genome: Insights into their divergence and evolution. *Genomics*, 86(6):627–637, dec 2005.
- [42] Mikko Taipale, Irina Krykbaeva, Martina Koeva, Can Kayatekin, Kenneth D. Westover, Georgios I. Karras, and Susan Lindquist. Quantitative analysis of hsp90-client

- interactions reveals principles of substrate recognition. *Cell*, 150(5):987–1001, aug 2012.
- [43] Pablo C. Echeverría, Andreas Bernthaler, Pierre Dupuis, Bernd Mayer, and Didier Picard. An interaction network predicted from public data as a discovery tool: Application to the hsp90 molecular chaperone machine. *PLoS ONE*, 6(10):e26044, oct 2011.
- [44] E. Pick, Y. Kluger, J. M. Giltane, C. Moeder, R. L. Camp, D. L. Rimm, and H. M. Kluger. High HSP90 expression is associated with decreased survival in breast cancer. *Cancer Research*, 67(7):2932–2937, apr 2007.
- [45] Anna Rodina, Tai Wang, Pengrong Yan, Erica DaGama Gomes, Mark P. S. Dunphy, Nagavarakishore Pillarsetty, John Koren, John F. Gerecitano, Tony Taldone, Hongliang Zong, Eloisi Caldas-Lopes, Mary Alpaugh, Adriana Corben, Matthew Riolo, Brad Beattie, Christina Pressl, Radu I. Peter, Chao Xu, Robert Trondl, Hardik J. Patel, Fumiko Shimizu, Alexander Bolaender, Chenghua Yang, Palak Panchal, Mohammad F. Farooq, Sarah Kishinevsky, Shanu Modi, Oscar Lin, Feixia Chu, Sujata Patil, Hediye Erdjument-Bromage, Pat Zanzonico, Clifford Hudis, Lorenz Studer, Gail J. Roboz, Ethel Cesarman, Leandro Cerchietti, Ross Levine, Ari Melnick, Steven M. Larson, Jason S. Lewis, Monica L. Guzman, and Gabriela Chiosis. The epichaperome is an integrated chaperome network that facilitates tumour survival. *Nature*, 538(7625):397–401, oct 2016.
- [46] Linda K. Nicholson, Chunyu Wang, Jun Xi, and Tadhg P. Begley. Solution structure of this and implications for the evolutionary roots of ubiquitin. *Nature Structural Biology*, 8(1):47–51, jan 2001.
- [47] Cecile M. Pickart and Michael J. Eddins. Ubiquitin: structures, functions, mechanisms. *Biochimica et Biophysica Acta (BBA) - Molecular Cell Research*, 1695(1-3):55–72, nov 2004.
- [48] Masato Akutsu, Ivan Dikic, and Anja Bremm. Ubiquitin chain diversity at a glance. *Journal of Cell Science*, 129(5):875–880, feb 2016.
- [49] Yong Tae Kwon and Aaron Ciechanover. The ubiquitin code in the ubiquitin-proteasome system and autophagy. *Trends in Biochemical Sciences*, 42(11):873–886, nov 2017.
- [50] Linda Hicke and Rebecca Dunn. Regulation of membrane protein transport by ubiquitin and ubiquitin-binding proteins. *Annual Review of Cell and Developmental Biology*, 19(1):141–172, nov 2003.

- [51] Annemarie G. van der Veen and Hidde L. Ploegh. Ubiquitin-like proteins. *Annual Review of Biochemistry*, 81(1):323–357, jul 2012.
- [52] Hermann-Josef Meyer and Michael Rape. Enhanced protein degradation by branched ubiquitin chains. *Cell*, 157(4):910–921, may 2014.
- [53] L. Herhaus and I. Dikic. Expanding the ubiquitin code through post-translational modification. *EMBO reports*, 16(9):1071–1083, aug 2015.
- [54] Joanna R. Morris and Alexander J. Garvin. SUMO in the DNA double-stranded break response: Similarities, differences, and cooperation with ubiquitin. *Journal of Molecular Biology*, may 2017.
- [55] Michael W. Lake, Margot M. Wuebbens, K. V. Rajagopalan, and Hermann Schindelin. Mechanism of ubiquitin activation revealed by the structure of a bacterial MoeB–MoaD complex. *Nature*, 414(6861):325–329, nov 2001.
- [56] Antje Schäfer, Monika Kuhn, and Hermann Schindelin. Structure of the ubiquitin-activating enzyme loaded with two ubiquitin molecules. *Acta Crystallographica Section D Biological Crystallography*, 70(5):1311–1320, apr 2014.
- [57] G. Markson, C. Kiel, R. Hyde, S. Brown, P. Charalabous, A. Bremm, J. Semple, J. Woodsmith, S. Duley, K. Salehi-Ashtiani, M. Vidal, D. Komander, L. Serrano, P. Lehner, and C. M. Sanderson. Analysis of the human e2 ubiquitin conjugating enzyme protein interaction network. *Genome Research*, 19(10):1905–1911, jun 2009.
- [58] Yihong Ye and Michael Rape. Building ubiquitin chains: E2 enzymes at work. *Nature Reviews Molecular Cell Biology*, 10(11):755–764, nov 2009.
- [59] Shaun K. Olsen and Christopher D. Lima. Structure of a ubiquitin e1-e2 complex: Insights to e1-e2 thioester transfer. *Molecular Cell*, 49(5):884–896, mar 2013.
- [60] Wei Li, Mario H. Bengtson, Axel Ulbrich, Akio Matsuda, Venkateshwar A. Reddy, Anthony Orth, Sumit K. Chanda, Serge Batalov, and Claudio A. P. Joazeiro. Genome-wide and functional annotation of human e3 ubiquitin ligases identifies mulan, a mitochondrial e3 that regulates the organelle dynamics and signaling. *PLoS ONE*, 3(1):e1487, jan 2008.
- [61] Lori Buetow and Danny T. Huang. Structural insights into the catalysis and regulation of e3 ubiquitin ligases. *Nature Reviews Molecular Cell Biology*, 17(10):626–642, aug 2016.

- [62] Jonathan N. Pruneda, Peter J. Littlefield, Sarah E. Soss, Kyle A. Nordquist, Walter J. Chazin, Peter S. Brzovic, and Rachel E. Klevit. Structure of an e3:e2~ub complex reveals an allosteric mechanism shared among RING/u-box ligases. *Molecular Cell*, 47(6):933–942, sep 2012.
- [63] Ali A Yunus and Christopher D Lima. Lysine activation and functional analysis of e2-mediated conjugation in the SUMO pathway. *Nature Structural & Molecular Biology*, 13(6):491–499, may 2006.
- [64] Shigetsugu Hatakeyama, Masayoshi Yada, Masaki Matsumoto, Noriko Ishida, and Kei-Ichi Nakayama. U box proteins as a new family of ubiquitin-protein ligases. *Journal of Biological Chemistry*, 276(35):33111–33120, jul 2001.
- [65] Martin Scheffner and Olivier Staub. HECT e3s and human disease. *BMC Biochemistry*, 8(Suppl 1):S6, 2007.
- [66] Stanley Lipkowitz and Allan M. Weissman. RINGs of good and evil: RING finger ubiquitin ligases at the crossroads of tumour suppression and oncogenesis. *Nature Reviews Cancer*, 11(9):629–643, aug 2011.
- [67] M. B. Metzger, V. A. Hristova, and A. M. Weissman. HECT and RING finger families of e3 ubiquitin ligases at a glance. *Journal of Cell Science*, 125(3):531–537, feb 2012.
- [68] Hari B. Kamadurai, Judith Souphron, Daniel C. Scott, David M. Duda, Darcie J. Miller, Daniel Stringer, Robert C. Piper, and Brenda A. Schulman. Insights into ubiquitin transfer cascades from a structure of a UbcH5b~ubiquitin-HECTNEDD41 complex. *Molecular Cell*, 36(6):1095–1102, dec 2009.
- [69] Elena Maspero, Eleonora Valentini, Sara Mari, Valentina Cecatiello, Paolo Soffientini, Sebastiano Pasqualato, and Simona Polo. Structure of a ubiquitin-loaded HECT ligase reveals the molecular basis for catalytic priming. *Nature Structural & Molecular Biology*, 20(6):696–701, may 2013.
- [70] Hari B Kamadurai, Yu Qiu, Alan Deng, Joseph S Harrison, Chris MacDonald, Marcelo Actis, Patrick Rodrigues, Darcie J Miller, Judith Souphron, Steven M Lewis, Igor Kurinov, Naoaki Fujii, Michal Hammel, Robert Piper, Brian Kuhlman, and Brenda A Schulman. Mechanism of ubiquitin ligation and lysine prioritization by a HECT e3. *eLife*, 2, aug 2013.
- [71] Indranil Paul and Mrinal K. Ghosh. The e3 ligase CHIP: Insights into its structure and regulation. *BioMed Research International*, 2014:1–12, 2014.

- [72] Vibhuti Joshi, Ayeman Amanullah, Arun Upadhyay, Ribhav Mishra, Amit Kumar, and Amit Mishra. A decade of boon or burden: What has the CHIP ever done for cellular protein quality control mechanism implicated in neurodegeneration and aging? *Frontiers in Molecular Neuroscience*, 9, oct 2016.
- [73] Holly McDonough and Cam Patterson. Chip: a link between the chaperone and proteasome systems. *Cell stress & chaperones*, 8:303–308, 2003.
- [74] Cam Patterson, Patrice Connell, Carol A. Ballinger, Jihong Jiang, Yaxu Wu, Larry J. Thompson, and Jörg Höhfeld. The co-chaperone chip regulates protein triage decisions mediated by heat-shock proteins. *Nature Cell Biology*, 3(1):93–96, dec 2000.
- [75] C. A. Loureiro, A. M. Matos, A. Dias-Alves, J. F. Pereira, I. Uliyakina, P. Barros, M. D. Amaral, and P. Matos. A molecular switch in the scaffold NHERF1 enables misfolded CFTR to evade the peripheral quality control checkpoint. *Science Signaling*, 8(377):ra48–ra48, may 2015.
- [76] Shigeo Murata, Yasufumi Minami, Michiko Minami, Tomoki Chiba, and Keiji Tanaka. CHIP is a chaperone-dependent e3 ligase that ubiquitylates unfolded protein. *EMBO reports*, 2(12):1133–1138, dec 2001.
- [77] Minghao Zhang, Mark Windheim, S. Mark Roe, Mark Peggie, Philip Cohen, Chrisostomos Prodromou, and Laurence H. Pearl. Chaperoned ubiquitylation-crystal structures of the CHIP u box e3 ubiquitin ligase and a CHIP-ubc13-uev1a complex. *Molecular Cell*, 20(4):525–538, nov 2005.
- [78] Matthew C. Smith, K. Matthew Scaglione, Victoria A. Assimon, Srikanth Patury, Andrea D. Thompson, Chad A. Dickey, Daniel R. Southworth, Henry L. Paulson, Jason E. Gestwicki, and Erik R. P. Zuiderweg. The e3 ubiquitin ligase CHIP and the molecular chaperone hsc70 form a dynamic, tethered complex. *Biochemistry*, 52(32):5354–5364, aug 2013.
- [79] Huaqun Zhang, Joseph Amick, Ritu Chakravarti, Stephanie Santarriaga, Simon Schlanger, Cameron McGlone, Michelle Dare, Jay C. Nix, K. Matthew Scaglione, Dennis J. Stuehr, Saurav Misra, and Richard C. Page. A bipartite interaction between hsp70 and CHIP regulates ubiquitination of chaperoned client proteins. *Structure*, 23(3):472–482, mar 2015.
- [80] Y. Matsumura, J. Sakai, and W. R. Skach. Endoplasmic reticulum protein quality control is determined by cooperative interactions between hsp/c70 protein and the CHIP e3 ligase. *Journal of Biological Chemistry*, 288(43):31069–31079, aug 2013.

- [81] Sarah E. Soss, Kristie L. Rose, Salisha Hill, Sophie Jouan, and Walter J. Chazin. Biochemical and proteomic analysis of ubiquitination of hsc70 and hsp70 by the e3 ligase CHIP. *PLOS ONE*, 10(5):e0128240, may 2015.
- [82] Yu Shang, Xinghui Zhao, Xialian Xu, Hong Xin, Xueni Li, Yonggong Zhai, Dacheng He, Baoqing Jia, Wei Chen, and Zhijie Chang. CHIP functions an e3 ubiquitin ligase of runx1. *Biochemical and Biophysical Research Communications*, 386(1):242–246, aug 2009.
- [83] Taishi Yonezawa, Hirotaka Takahashi, Shiori Shikata, Xiaoxiao Liu, Moe Tamura, Shuhei Asada, Tsuyoshi Fukushima, Tomofusa Fukuyama, Yosuke Tanaka, Tatsuya Sawasaki, Toshio Kitamura, and Susumu Goyama. The ubiquitin ligase STUB1 regulates stability and activity of RUNX1 and RUNX1-RUNX1t1. *Journal of Biological Chemistry*, page jbc.M117.785675, may 2017.
- [84] Riga Tawo, Wojciech Pokrzywa, Éva Kevei, Melek E. Akyuz, Vishnu Balaji, Svenja Adrian, Jörg Höhfeld, and Thorsten Hoppe. The ubiquitin ligase CHIP integrates proteostasis and aging by regulation of insulin receptor turnover. *Cell*, 169(3):470–482.e13, apr 2017.
- [85] L. Wang, Y.-T. Liu, R. Hao, L. Chen, Z. Chang, H.-R. Wang, Z.-X. Wang, and J.-W. Wu. Molecular mechanism of the negative regulation of smad1/5 protein by carboxyl terminus of hsc70-interacting protein (CHIP). *Journal of Biological Chemistry*, 286(18):15883–15894, mar 2011.
- [86] Vikram Narayan, Vivien Landré, Jia Ning, Lenka Hernychova, Petr Muller, Chandra Verma, Malcolm D. Walkinshaw, Elizabeth A. Blackburn, and Kathryn L. Ball. Protein-protein interactions modulate the docking-dependent e3-ubiquitin ligase activity of carboxy-terminus of hsc70-interacting protein (CHIP). *Molecular & Cellular Proteomics*, 14(11):2973–2987, sep 2015.
- [87] Yuzuru Imai, Mariko Soda, Shigetsugu Hatakeyama, Takumi Akagi, Tsutomu Hashikawa, Kei Ichi Nakayama, and Ryosuke Takahashi. Chip is associated with parkin, a gene responsible for familial parkinson’s disease, and enhances its ubiquitin ligase activity. *Molecular cell*, 10:55–67, July 2002.
- [88] Lakshmiapuram Seshadri Swapna, Kuchi Srikeerthana, and Narayanaswamy Srinivasan. Extent of structural asymmetry in homodimeric proteins: Prevalence and relevance. *PLoS ONE*, 7(5):e36688, may 2012.
- [89] Christian Graf, Marta Stankiewicz, Rainer Nikolay, and Matthias P. Mayer. Insights into the conformational dynamics of the e3 ubiquitin ligase CHIP in complex with chaperones and e2 enzymes. *Biochemistry*, 49(10):2121–2129, mar 2010.

- [90] Rainer Nikolay, Thomas Wiederkehr, Wolfgang Rist, Günter Kramer, Matthias P. Mayer, and Bernd Bukau. Dimerization of the human e3 ligase CHIP via a coiled-coil domain is essential for its activity. *Journal of Biological Chemistry*, 279(4):2673–2678, nov 2003.
- [91] Indranil Paul and Mrinal K. Ghosh. A CHIPotle in physiology and disease. *The International Journal of Biochemistry & Cell Biology*, 58:37–52, jan 2015.
- [92] Zhen Xu, Karl I. Devlin, Michael G. Ford, Jay C. Nix, Jun Qin, and Saurav Misra. Structure and interactions of the helical and u-box domains of chip, the c terminus of hsp70 interacting protein. *Biochemistry*, 45(15):4749–4759, apr 2006.
- [93] Zhaofeng Ye, Patrick G. Needham, Samuel K. Estabrooks, Susan K. Whitaker, Brandon L. Garcia, Saurav Misra, Jeffrey L. Brodsky, and Carlos J. Camacho. Symmetry breaking during homodimeric assembly activates an e3 ubiquitin ligase. *Scientific Reports*, 7(1), may 2017.
- [94] Zoi Erpapazoglou, Olivier Walker, and Rosine Haguenaer-Tsapis. Versatile roles of k63-linked ubiquitin chains in trafficking. *Cells*, 3(4):1027–1088, nov 2014.
- [95] Zhen Xu, Ekta Kohli, Karl I Devlin, Michael Bold, Jay C Nix, and Saurav Misra. Interactions between the quality control ubiquitin ligase CHIP and ubiquitin conjugating enzymes. *BMC Structural Biology*, 8(1):26, 2008.
- [96] J. Jiang. CHIP is a u-box-dependent e3 ubiquitin ligase. IDENTIFICATION OF hsc70 AS a TARGET FOR UBIQUITYLATION. *Journal of Biological Chemistry*, 276(46):42938–42944, sep 2001.
- [97] Junwei Guo, Fangli Ren, Yinyin Wang, Shan Li, Zhengrong Gao, Xiaoyan Wang, Hongxiu Ning, Jianguo Wu, Yi Li, Zhao Wang, Shek Man Chim, Jiake Xu, and Zhijie Chang. miR-764-5p promotes osteoblast differentiation through inhibition of CHIP/STUB1 expression. *Journal of Bone and Mineral Research*, 27(7):1607–1618, jun 2012.
- [98] K. Matthew Scaglione, Eszter Zavodszky, Sokol V. Todi, Srikanth Patury, Ping Xu, Edgardo Rodríguez-Lebrón, Svetlana Fischer, John Konen, Ana Djarmati, Junmin Peng, Jason E. Gestwicki, and Henry L. Paulson. Ube2w and ataxin-3 coordinately regulate the ubiquitin ligase CHIP. *Molecular Cell*, 43(4):599–612, aug 2011.
- [99] Seiko Shimamoto, Yasuo Kubota, Fuminori Yamaguchi, Hiroshi Tokumitsu, and Ryoji Kobayashi. Ca²⁺/s100 proteins act as upstream regulators of the chaperone-associated ubiquitin ligase chip (c terminus of hsc70-interacting protein). *Journal of Biological Chemistry*, 288(10):7158–7168, jan 2013.

- [100] Youngah Shin, Jochen Klucken, Cam Patterson, Bradley T. Hyman, and Pamela J. McLean. The co-chaperone carboxyl terminus of hsp70-interacting protein (CHIP) mediates α -synuclein degradation decisions between proteasomal and lysosomal pathways. *Journal of Biological Chemistry*, 280(25):23727–23734, apr 2005.
- [101] V. M. Miller. CHIP suppresses polyglutamine aggregation and toxicity in vitro and in vivo. *Journal of Neuroscience*, 25(40):9152–9161, oct 2005.
- [102] Shigetsugu Hatakeyama, Masaki Matsumoto, Takumi Kamura, Miyuki Murayama, Du-Hua Chui, Emmanuel Planel, Ryosuke Takahashi, Keiichi I. Nakayama, and Akihiko Takashima. U-box protein carboxyl terminus of hsc70-interacting protein (CHIP) mediates poly-ubiquitylation preferentially on four-repeat tau and is involved in neurodegeneration of tauopathy. *Journal of Neurochemistry*, 91(2):299–307, oct 2004.
- [103] Masashi Kajiro, Ryuichi Hirota, Yuka Nakajima, Kaori Kawanowa, Kae So-ma, Ichiaki Ito, Yuri Yamaguchi, Sho hei Ohie, Yasuhito Kobayashi, Yuko Seino, Miwako Kawano, Yoh ichi Kawabe, Hiroyuki Takei, Shin ichi Hayashi, Masafumi Kurosumi, Akiko Murayama, Keiji Kimura, and Junn Yanagisawa. The ubiquitin ligase CHIP acts as an upstream regulator of oncogenic pathways. *Nature Cell Biology*, 11(3):312–319, feb 2009.
- [104] Kefah Mokbel, Neill Patani, Wen Jiang, and Robert Newbold. Prognostic implications of carboxyl-terminus of hsc70 interacting protein and lysyl-oxidase expression in human breast cancer. *Journal of Carcinogenesis*, 9(1):9, 2010.
- [105] Eva Ruckova, Petr Muller, Rudolf Nenutil, and Borivoj Vojtesek. Alterations of the hsp70/hsp90 chaperone and the HOP/CHIP co-chaperone system in cancer. *Cellular and Molecular Biology Letters*, 17(3), jan 2012.
- [106] Syed Feroj Ahmed, Satamita Deb, Indranil Paul, Anirban Chatterjee, Tapashi Mandal, Uttara Chatterjee, and Mrinal K. Ghosh. The chaperone-assisted e3 ligase c terminus of hsc70-interacting protein (CHIP) targets PTEN for proteasomal degradation. *Journal of Biological Chemistry*, 287(19):15996–16006, mar 2012.
- [107] Q. Dai. CHIP activates HSF1 and confers protection against apoptosis and cellular stress. *The EMBO Journal*, 22(20):5446–5458, oct 2003.
- [108] J.-N. Min, R. A. Whaley, N. E. Sharpless, P. Lockyer, A. L. Portbury, and C. Patterson. CHIP deficiency decreases longevity, with accelerated aging phenotypes accompanied by altered protein quality control. *Molecular and Cellular Biology*, 28(12):4018–4025, apr 2008.

- [109] Wojciech Pokrzywa and Thorsten Hoppe. CHIPped balance of proteostasis and longevity. *Oncotarget*, oct 2017.
- [110] Chaokun Li, Aiyun Wen, Benchang Shen, Jia Lu, Yao Huang, and Yongchang Chang. FastCloning: a highly simplified, purification-free, sequence- and ligation-independent PCR cloning method. *BMC Biotechnology*, 11(1):92, 2011.
- [111] F Ann Ran, Patrick D Hsu, Jason Wright, Vineeta Agarwala, David A Scott, and Feng Zhang. Genome engineering using the CRISPR-cas9 system. *Nature Protocols*, 8(11):2281–2308, oct 2013.
- [112] Nejat Düzgüneş, Henrique Faneca, and Maria C. Pedroso de Lima. Methods to monitor liposome fusion, permeability, and interaction with cells. In *Methods in Molecular Biology*, pages 209–232. Humana Press, nov 2009.
- [113] Jacek R Wiśniewski, Alexandre Zougman, Nagarjuna Nagaraj, and Matthias Mann. Universal sample preparation method for proteome analysis. *Nature Methods*, 6(5):359–362, apr 2009.
- [114] Nils A Kulak, Garwin Pichler, Igor Paron, Nagarjuna Nagaraj, and Matthias Mann. Minimal, encapsulated proteomic-sample processing applied to copy-number estimation in eukaryotic cells. *Nature Methods*, 11(3):319–324, feb 2014.
- [115] Jürgen Cox and Matthias Mann. MaxQuant enables high peptide identification rates, individualized p.p.b.-range mass accuracies and proteome-wide protein quantification. *Nature Biotechnology*, 26(12):1367–1372, nov 2008.
- [116] Stefka Tyanova, Tikira Temu, Pavel Sinitcyn, Arthur Carlson, Marco Y Hein, Tamar Geiger, Matthias Mann, and Jürgen Cox. The perseus computational platform for comprehensive analysis of (prote)omics data. *Nature Methods*, 13(9):731–740, jun 2016.
- [117] Victoria A. Assimon, Daniel R. Southworth, and Jason E. Gestwicki. Specific binding of tetratricopeptide repeat proteins to heat shock protein 70 (hsp70) and heat shock protein 90 (hsp90) is regulated by affinity and phosphorylation. *Biochemistry*, 54(48):7120–7131, nov 2015.
- [118] T. Jacobson, C. Navarrete, S. K. Sharma, T. C. Sideri, S. Ibstedt, S. Priya, C. M. Grant, P. Christen, P. Goloubinoff, and M. J. Tamas. Arsenite interferes with protein folding and triggers formation of protein aggregates in yeast. *Journal of Cell Science*, 125(21):5073–5083, sep 2012.

- [119] L. Shang, S. Chen, F. Du, S. Li, L. Zhao, and X. Wang. Nutrient starvation elicits an acute autophagic response mediated by ulk1 dephosphorylation and its subsequent dissociation from AMPK. *Proceedings of the National Academy of Sciences*, 108(12):4788–4793, mar 2011.
- [120] Dongkai Guo, Zheng Ying, Hongfeng Wang, Dong Chen, Feng Gao, Haigang Ren, and Guanghui Wang. Regulation of autophagic flux by CHIP. *Neuroscience Bulletin*, 31(4):469–479, jul 2015.
- [121] A. L. Mattheyses, S. M. Simon, and J. Z. Rappoport. Imaging with total internal reflection fluorescence microscopy for the cell biologist. *Journal of Cell Science*, 123(21):3621–3628, oct 2010.
- [122] Jyoti K. Jaiswal and Sanford M. Simon. *Total Internal Reflection Fluorescence Microscopy for High-Resolution Imaging of Cell-Surface Events*, chapter Volume 1, pages 4.12.1–4.12.15. John Wiley & Sons, Inc., 2001.
- [123] Jong W Yu, Jeannine M Mendrola, Anjon Audhya, Shaneen Singh, David Keleti, Daryll B DeWald, Diana Murray, Scott D Emr, and Mark A Lemmon. Genome-wide analysis of membrane targeting by *s. cerevisiae* pleckstrin homology domains. *Molecular cell*, 13:677–688, March 2004.
- [124] Priya Putta, Johanna Rankenberg, Ruud A. Korver, Ringo van Wijk, Teun Munnik, Christa Testerink, and Edgar E. Kooijman. Phosphatidic acid binding proteins display differential binding as a function of membrane curvature stress and chemical properties. *Biochimica et Biophysica Acta (BBA) - Biomembranes*, 1858(11):2709–2716, nov 2016.
- [125] Abolfazl Akbarzadeh, Rogaie Rezaei-Sadabady, Soodabeh Davaran, Sang Woo Joo, Nosratollah Zarghami, Younes Hanifehpour, Mohammad Samiei, Mohammad Kouhi, and Kazem Nejati-Koshki. Liposome: classification, preparation, and applications. *Nanoscale Research Letters*, 8(1):102, 2013.
- [126] Paige E. Selvy, Robert R. Lavieri, Craig W. Lindsley, and H. Alex Brown. Phospholipase d: Enzymology, functionality, and chemical modulation. *Chemical Reviews*, 111(10):6064–6119, oct 2011.
- [127] Ludwig Heilmeyer, György Vereb, György Vereb, Annamária Kakuk, and Ilona Szivák. Mammalian phosphatidylinositol 4-kinases. *IUBMB Life*, 55(2):59–65, feb 2003.
- [128] S. Nakanishi, K. J. Catt, and T. Balla. A wortmannin-sensitive phosphatidylinositol 4-kinase that regulates hormone-sensitive pools of inositolphospholipids. *Proceedings of the National Academy of Sciences*, 92(12):5317–5321, jun 1995.

- [129] Mao Xiang Chen and Patricia T.W Cohen. Activation of protein phosphatase 5 by limited proteolysis or the binding of polyunsaturated fatty acids to the TPR domain. *FEBS Letters*, 400(1):136–140, jan 1997.
- [130] Robert V. Stahelin, Jordan L. Scott, and Cary T. Frick. Cellular and molecular interactions of phosphoinositides and peripheral proteins. *Chemistry and Physics of Lipids*, 182:3–18, sep 2014.
- [131] Monique M. Lapinski, Angelines Castro-Forero, Aaron J. Greiner, Robert Y. Ofoli, and Gary J. Blanchard. Comparison of liposomes formed by sonication and extrusion: rotational and translational diffusion of an embedded chromophore. *Langmuir*, 23(23):11677–11683, nov 2007.
- [132] Matthew J. LaVoie, Giuseppe P. Cortese, Beth L. Ostaszewski, and Michael G. Schlossmacher. The effects of oxidative stress on parkin and other e3 ligases. *Journal of Neurochemistry*, 103(6):2354–2368, dec 2007.
- [133] Osman N. Yogurtcu and Margaret E. Johnson. Cytosolic proteins can exploit membrane localization to trigger functional assembly. *PLOS Computational Biology*, 14(3):e1006031, mar 2018.
- [134] Robert V. Stahelin. Monitoring peripheral protein oligomerization on biological membranes. In *Methods in Cell Biology*, pages 359–371. Elsevier, 2013.
- [135] András Micsonai, Frank Wien, Linda Kernya, Young-Ho Lee, Yuji Goto, Matthieu Réfrégiers, and József Kardos. Accurate secondary structure prediction and fold recognition for circular dichroism spectroscopy. *Proceedings of the National Academy of Sciences*, 112(24):E3095–E3103, jun 2015.
- [136] M. F. N. Rosser, E. Washburn, P. J. Muchowski, C. Patterson, and D. M. Cyr. Chaperone functions of the e3 ubiquitin ligase CHIP. *Journal of Biological Chemistry*, 282(31):22267–22277, jun 2007.
- [137] J. Yan. AtCHIP, a u-box-containing e3 ubiquitin ligase, plays a critical role in temperature stress tolerance in arabidopsis. *PLANT PHYSIOLOGY*, 132(2):861–869, may 2003.
- [138] Jan Wilschut, Nejat Duzgunes, Robert Fraley, and Demetrios Papahadjopoulos. Studies on the mechanism of membrane fusion: kinetics of calcium ion induced fusion of phosphatidylserine vesicles followed by a new assay for mixing of aqueous vesicle contents. *Biochemistry*, 19(26):6011–6021, dec 1980.
- [139] Zhijian J. Chen. Ubiquitin signalling in the NF- κ pathway. *Nature Cell Biology*, 7(8):758–765, aug 2005.

- [140] Zhijian J. Chen and Serge Y. Fuchs. Ubiquitin-dependent activation of NF-kappaB: K63-linked ubiquitin chains—a link to cancer? *Cancer Biology & Therapy*, 3(3):286–288, mar 2004.
- [141] Peter Tsvetkov, Yaarit Adamovich, Evan Elliott, and Yosef Shaul. E3 ligase STUB1/CHIP regulates NAD(p)h:quinone oxidoreductase 1 (NQO1) accumulation in aged brain, a process impaired in certain alzheimer disease patients. *Journal of Biological Chemistry*, 286(11):8839–8845, jan 2011.
- [142] Concetta Giancola, Cira De Sena, Dimitrios Fessas, Giuseppe Graziano, and Guido Barone. DSC studies on bovine serum albumin denaturation effects of ionic strength and SDS concentration. *International Journal of Biological Macromolecules*, 20(3):193–204, jun 1997.
- [143] Esperanza Arias and Ana Maria Cuervo. Chaperone-mediated autophagy in protein quality control. *Current Opinion in Cell Biology*, 23(2):184–189, apr 2011.
- [144] Adrián Martínez-Limón, Marion Alriquet, Wei-Han Lang, Giulia Calloni, Ilka Wittig, and R. Martin Vabulas. Recognition of enzymes lacking bound cofactor by protein quality control. *Proceedings of the National Academy of Sciences*, 113(43):12156–12161, oct 2016.
- [145] Matthew D. Buschman, Mengke Xing, and Seth J. Field. The GOLPH3 pathway regulates golgi shape and function and is activated by DNA damage. *Frontiers in Neuroscience*, 9, oct 2015.
- [146] Neggy Rismanchi, Cynthia Soderblom, Julia Stadler, Peng-Peng Zhu, and Craig Blackstone. Atlastin GTPases are required for golgi apparatus and ER morphogenesis. *Human Molecular Genetics*, 17(11):1591–1604, feb 2008.
- [147] Armen Petrosyan and Pi-Wan Cheng. Golgi fragmentation induced by heat shock or inhibition of heat shock proteins is mediated by non-muscle myosin IIA via its interaction with glycosyltransferases. *Cell Stress and Chaperones*, 19(2):241–254, aug 2013.
- [148] Xue-Chao Gao, Chen-Jie Zhou, Zi-Ren Zhou, Meng Wu, Chun-Yang Cao, and Hong-Yu Hu. The c-terminal helices of heat shock protein 70 are essential for j-domain binding and ATPase activation. *Journal of Biological Chemistry*, 287(8):6044–6052, jan 2012.
- [149] Annemieke A. Michels, Bart Kanon, Olivier Bensaude, and Harm H. Kampinga. Heat shock protein (hsp) 40 mutants inhibit hsp70 in mammalian cells. *Journal of Biological Chemistry*, 274(51):36757–36763, dec 1999.

- [150] Jennifer Lippincott-Schwartz, Theresa H. Roberts, and Koret Hirschberg. Secretory protein trafficking and organelle dynamics in living cells. *Annual Review of Cell and Developmental Biology*, 16(1):557–589, nov 2000.
- [151] J S Lee, T W Seo, J H Yi, K S Shin, and S J Yoo. CHIP has a protective role against oxidative stress-induced cell death through specific regulation of endonuclease g. *Cell Death and Disease*, 4(6):e666, jun 2013.
- [152] Lang Yoo and Kwang Chul Chung. The ubiquitin e3 ligase CHIP promotes proteasomal degradation of the serine/threonine protein kinase PINK1 during staurosporine-induced cell death. *Journal of Biological Chemistry*, 293(4):1286–1297, dec 2017.
- [153] Stuart W. Hicks and Carolyn E. Machamer. Golgi structure in stress sensing and apoptosis. *Biochimica et Biophysica Acta (BBA) - Molecular Cell Research*, 1744(3):406–414, jul 2005.
- [154] Felipe Cabral Miranda, Juliana Adão-Novaes, William W. Hauswirth, Rafael Linden, Hilda Petrs-Silva, and Luciana B. Chiarini. CHIP, a carboxy terminus HSP-70 interacting protein, prevents cell death induced by endoplasmic reticulum stress in the central nervous system. *Frontiers in Cellular Neuroscience*, 8, jan 2015.
- [155] Kyoung-Jae Won, Joo-Young Im, Bo-Kyung Kim, Hyun Seung Ban, Young-Jin Jung, Kyeong Eun Jung, and Misun Won. Stability of the cancer target DDIAS is regulated by the CHIP/HSP70 pathway in lung cancer cells. *Cell Death & Disease*, 8(1):e2554–e2554, jan 2017.
- [156] Tsukasa Okiyoneda, Pirjo M Apaja, and Gergely L Lukacs. Protein quality control at the plasma membrane. *Current Opinion in Cell Biology*, 23(4):483–491, aug 2011.
- [157] T. Okiyoneda, H. Barriere, M. Bagdany, W. M. Rabeh, K. Du, J. Hohfeld, J. C. Young, and G. L. Lukacs. Peripheral protein quality control removes unfolded CFTR from the plasma membrane. *Science*, 329(5993):805–810, jul 2010.
- [158] Pirjo M. Apaja, Haijin Xu, and Gergely L. Lukacs. Quality control for unfolded proteins at the plasma membrane. *The Journal of Cell Biology*, 191(3):553–570, oct 2010.
- [159] R Postina, E Ufer, R Pfeiffer, N V Knoers, and F Fahrenholz. Misfolded vasopressin v2 receptors caused by extracellular point mutations entail congenital nephrogenic diabetes insipidus. *Molecular and cellular endocrinology*, 164:31–39, June 2000.

- [160] Huaqun Zhang, Cameron McGlone, Matthew M. Mannion, and Richard C. Page. ¹h, ¹⁵n and ¹³c resonance assignments for free and ieevd peptide-bound forms of the tetratricopeptide repeat domain from the human e3 ubiquitin ligase chip. *Biomolecular NMR Assignments*, 11(1):5–9, Apr 2017.
- [161] Lenka Kundrat and Lynne Regan. Balance between folding and degradation for hsp90-dependent client proteins: A key role for CHIP. *Biochemistry*, 49(35):7428–7438, sep 2010.
- [162] Korana Radovanac, Jessica Morgner, Jan-Niklas Schulz, Katrin Blumbach, Cam Patterson, Tamar Geiger, Matthias Mann, Thomas Krieg, Beate Eckes, Reinhard Fässler, and Sara A Wickström. Stabilization of integrin-linked kinase by the hsp90-CHIP axis impacts cellular force generation, migration and the fibrotic response. *The EMBO Journal*, 32(10):1409–1424, apr 2013.
- [163] Alex J. Laude and Ian A. Prior. Plasma membrane microdomains: Organization, function and trafficking (review). *Molecular Membrane Biology*, 21(3):193–205, jan 2004.
- [164] Dylan M. Owen, editor. *Methods in Membrane Lipids*. Number Pages 55-64. Springer-Verlag GmbH, 2014. Preparation of Detergent-Resistant Membranes (DRMs) from Cultured Mammalian Cells Deborah A. Brown Pages 55-64.
- [165] Kenji A K Tanaka, Kenichi G N Suzuki, Yuki M Shirai, Shusaku T Shibutani, Manami S H Miyahara, Hisae Tsuboi, Miyako Yahara, Akihiko Yoshimura, Satyajit Mayor, Takahiro K Fujiwara, and Akihiro Kusumi. Membrane molecules mobile even after chemical fixation. *Nature Methods*, 7(11):865–866, oct 2010.
- [166] Katharina N Richter, Natalia H Revelo, Katharina J Seitz, Martin S Helm, Deblina Sarkar, Rebecca S Saleeb, Elisa D'Este, Jessica Eberle, Eva Wagner, Christian Vogl, Diana F Lazaro, Frank Richter, Javier Coy-Vergara, Giovanna Coceano, Edward S Boyden, Rory R Duncan, Stefan W Hell, Marcel A Lauterbach, Stephan E Lehnart, Tobias Moser, Tiago F Outeiro, Peter Rehling, Blanche Schwappach, Ilaria Testa, Bolek Zapiec, and Silvio O Rizzoli. Glyoxal as an alternative fixative to formaldehyde in immunostaining and super-resolution microscopy. *The EMBO Journal*, 37(1):139–159, nov 2017.
- [167] Michael Mishkind, Joop E.M. Vermeer, Essam Darwish, and Teun Munnik. Heat stress activates phospholipase d and triggers PIP₂ accumulation at the plasma membrane and nucleus. *The Plant Journal*, 60(1):10–21, oct 2009.
- [168] Wang X., Devaiah S., Zhang W., and Welti R. Signaling functions of phosphatidic acid. *Progress in Lipid Research*, 45(3):250–278, may 2006.

- [169] A A Spector and M A Yorek. Membrane lipid composition and cellular function. *Journal of lipid research*, 26:1015–1035, September 1985.
- [170] G. van Meer and A. I. P. M. de Kroon. Lipid map of the mammalian cell. *Journal of Cell Science*, 124(1):5–8, dec 2010.
- [171] Yong Kim, Jung-Eun Kim, Sang Do Lee, Taehoon G. Lee, Jae Ho Kim, Jong Bae Park, Jung Min Han, Sung Key Jang, Pann-Ghill Suh, and Sung Ho Ryu. Phospholipase d1 is located and activated by protein kinase α in the plasma membrane in 3y1 fibroblast cell. *Biochimica et Biophysica Acta (BBA) - Molecular and Cell Biology of Lipids*, 1436(3):319–330, jan 1999.
- [172] Fraser D. Brown, Nicola Thompson, Khalid M. Saqib, Joanna M. Clark, Dale Powner, Neil T. Thompson, Roberto Solari, and Michael J.O. Wakelam. Phospholipase d1 localises to secretory granules and lysosomes and is plasma-membrane translocated on cellular stimulation. *Current Biology*, 8(14):835–838, jul 1998.
- [173] Michael A. Frohman. The phospholipase d superfamily as therapeutic targets. *Trends in Pharmacological Sciences*, 36(3):137–144, mar 2015.
- [174] Y. Fang. Phosphatidic acid-mediated mitogenic activation of mTOR signaling. *Science*, 294(5548):1942–1945, nov 2001.
- [175] Gilbert Di Paolo and Pietro De Camilli. Phosphoinositides in cell regulation and membrane dynamics. *Nature*, 443(7112):651–657, oct 2006.
- [176] Gerald R.V. Hammond and Tamas Balla. Polyphosphoinositide binding domains: Key to inositol lipid biology. *Biochimica et Biophysica Acta (BBA) - Molecular and Cell Biology of Lipids*, 1851(6):746–758, jun 2015.
- [177] Gregory J. Downing, Stanley Kim, Satoshi Nakanishi, Kevin J. Catt, and Tamas Balla. Characterization of a soluble adrenal phosphatidylinositol 4-kinase reveals wortmannin sensitivity of type III phosphatidylinositol kinases \dagger . *Biochemistry*, 35(11):3587–3594, jan 1996.
- [178] Joëlle Bigay, Jean-François Casella, Guillaume Drin, Bruno Mesmin, and Bruno Antonny. ArfGAP1 responds to membrane curvature through the folding of a lipid packing sensor motif. *The EMBO Journal*, 24(13):2244–2253, jun 2005.
- [179] H. Zhao and P. Lappalainen. A simple guide to biochemical approaches for analyzing protein-lipid interactions. *Molecular Biology of the Cell*, 23(15):2823–2830, jul 2012.
- [180] F. A. Heberle and G. W. Feigenson. Phase separation in lipid membranes. *Cold Spring Harbor Perspectives in Biology*, 3(4):a004630–a004630, mar 2011.

- [181] Gerrit van Meer, Dennis R. Voelker, and Gerald W. Feigenson. Membrane lipids: where they are and how they behave. *Nature Reviews Molecular Cell Biology*, 9(2):112–124, feb 2008.
- [182] Nam-Joon Cho, Lisa Hwang, Johan Solandt, and Curtis Frank. Comparison of extruded and sonicated vesicles for planar bilayer self-assembly. *Materials*, 6(8):3294–3308, aug 2013.
- [183] Hassan Y. Naim. Limited proteolysis in the study of membrane proteins. In *Proteolytic Enzymes*, pages 281–297. Springer Berlin Heidelberg, 1999.
- [184] Yasaman Pakdaman, Monica Sanchez-Guixé, Rune Kleppe, Sigrid Erdal, Helene J. Bustad, Lise Bjørkhaug, Kristoffer Haugarvoll, Charalampos Tzoulis, Ketil Heimdal, Per M. Knappskog, Stefan Johansson, and Ingvild Aukrust. In vitro characterization of six STUB1 variants in spinocerebellar ataxia 16 reveals altered structural properties for the encoded CHIP proteins. *Bioscience Reports*, 37(2):BSR20170251, apr 2017.
- [185] Jingjin Ding, Kun Wang, Wang Liu, Yang She, Qi Sun, Jianjin Shi, Hanzi Sun, Da-Cheng Wang, and Feng Shao. Pore-forming activity and structural autoinhibition of the gasdermin family. *Nature*, 535(7610):111–116, jun 2016.
- [186] Bijie Jiang, Hong Shen, Zheng Chen, Lei Yin, Linsen Zan, and Liangyou Rui. Carboxyl terminus of HSC70-interacting protein (CHIP) down-regulates NF- κ b-inducing kinase (NIK) and suppresses NIK-induced liver injury. *Journal of Biological Chemistry*, 290(18):11704–11714, mar 2015.
- [187] Spencer Hill and Gary Kleiger. Self-regulating ubiquitin ligases. *The EMBO Journal*, 36(4):392–393, jan 2017.
- [188] Dong-Hoon Hyun, Joe O. Hernandez, Mark P. Mattson, and Rafael de Cabo. The plasma membrane redox system in aging. *Ageing Research Reviews*, 5(2):209–220, may 2006.
- [189] V Natarajan, M M Taher, B Roehm, N L Parinandi, H H Schmid, Z Kiss, and J G Garcia. Activation of endothelial cell phospholipase d by hydrogen peroxide and fatty acid hydroperoxide. *The Journal of biological chemistry*, 268:930–937, January 1993.
- [190] Maria A. De Matteis, Cathal Wilson, and Giovanni D'Angelo. Phosphatidylinositol-4-phosphate: The golgi and beyond. *BioEssays*, 35(7):612–622, may 2013.

- [191] Mark S. Ladinsky, David N. Mastronarde, J. Richard McIntosh, Kathryn E. Howell, and L. Andrew Staehelin. Golgi structure in three dimensions: Functional insights from the normal rat kidney cell. *The Journal of Cell Biology*, 144(6):1135–1149, mar 1999.
- [192] J. Klumperman. Architecture of the mammalian golgi. *Cold Spring Harbor Perspectives in Biology*, 3(7):a005181–a005181, apr 2011.
- [193] A Stieber, Z Mourelatos, and N K Gonatas. In alzheimer’s disease the golgi apparatus of a population of neurons without neurofibrillary tangles is fragmented and atrophic. *The American journal of pathology*, 148:415–426, February 1996.
- [194] Z Mourelatos, N K Gonatas, A Stieber, M E Gurney, and M C Dal Canto. The golgi apparatus of spinal cord motor neurons in transgenic mice expressing mutant cu,zn superoxide dismutase becomes fragmented in early, preclinical stages of the disease. *Proceedings of the National Academy of Sciences of the United States of America*, 93:5472–5477, May 1996.
- [195] Yukio Fujita and Koichi Okamoto. Golgi apparatus of the motor neurons in patients with amyotrophic lateral sclerosis and in mice models of amyotrophic lateral sclerosis. *Neuropathology*, 25(4):388–394, dec 2005.
- [196] P. Hilditch-Maguire. Huntingtin: an iron-regulated protein essential for normal nuclear and perinuclear organelles. *Human Molecular Genetics*, 9(19):2789–2797, nov 2000.
- [197] Saya Nakagomi, Mark J. Barsoum, Ella Bossy-Wetzel, Christine Sütterlin, Vivek Malhotra, and Stuart A. Lipton. A golgi fragmentation pathway in neurodegeneration. *Neurobiology of Disease*, 29(2):221–231, feb 2008.
- [198] Pravir Kumar, Rashmi K. Ambasta, Vimal Veereshwarayya, Kenneth M. Rosen, Ken S. Kosik, Hamid Band, Ruben Mestril, Cam Patterson, and Henry W. Querfurth. CHIP and HSPs interact with β -APP in a proteasome-dependent manner and influence a β metabolism. *Human Molecular Genetics*, 16(7):848–864, feb 2007.
- [199] Hideki Shimura, Daniel Schwartz, Steven P. Gygi, and Kenneth S. Kosik. CHIP-hsc70 complex ubiquitinates phosphorylated tau and enhances cell survival. *Journal of Biological Chemistry*, 279(6):4869–4876, nov 2003.
- [200] Makoto Urushitani, Junko Kurisu, Minako Tateno, Shigetsugu Hatakeyama, Kei-ichi Nakayama, Shinsuke Kato, and Ryosuke Takahashi. CHIP promotes proteasomal degradation of familial ALS-linked mutant SOD1 by ubiquitinating hsp/hsc70. *Journal of Neurochemistry*, 90(1):231–244, jun 2004.

- [201] Jinho Seo, Eun-Woo Lee, Hyerim Sung, Daehyeon Seong, Yves Dondelinger, Ji-hye Shin, Manhyung Jeong, Hae-Kyung Lee, Jung-Hoon Kim, Su Yeon Han, Cheolju Lee, Je Kyung Seong, Peter Vandenabeele, and Jaewhan Song. CHIP controls necroptosis through ubiquitylation- and lysosome-dependent degradation of RIPK3. *Nature Cell Biology*, 18(3):291–302, feb 2016.
- [202] Pengcheng Zhou, Norvin Fernandes, Ingrid L. Dodge, Alagarsamy Lakku Reddi, Navin Rao, Howard Safran, Thomas A. DiPetrillo, David E. Wazer, Vimla Band, and Hamid Band. ErbB2 degradation mediated by the co-chaperone protein CHIP. *Journal of Biological Chemistry*, 278(16):13829–13837, feb 2003.
- [203] João Vasco Ferreira, Hugo Fôfo, Eloy Bejarano, Carla Figueira Bento, José S. Ramalho, Henrique Girão, and Paulo Pereira. STUB1/CHIP is required for HIF1a degradation by chaperone-mediated autophagy. *Autophagy*, 9(9):1349–1366, sep 2013.
- [204] S Rais, E Pédruzzi, M C Dang, J P Giroud, J Hakim, and A Périanin. Priming of phosphatidic acid production by staurosporine in f-met-leu-phe-stimulated human neutrophils—correlation with respiratory burst. *Cellular signalling*, 10:121–129, February 1998.

Appendix

5.1 Vector maps

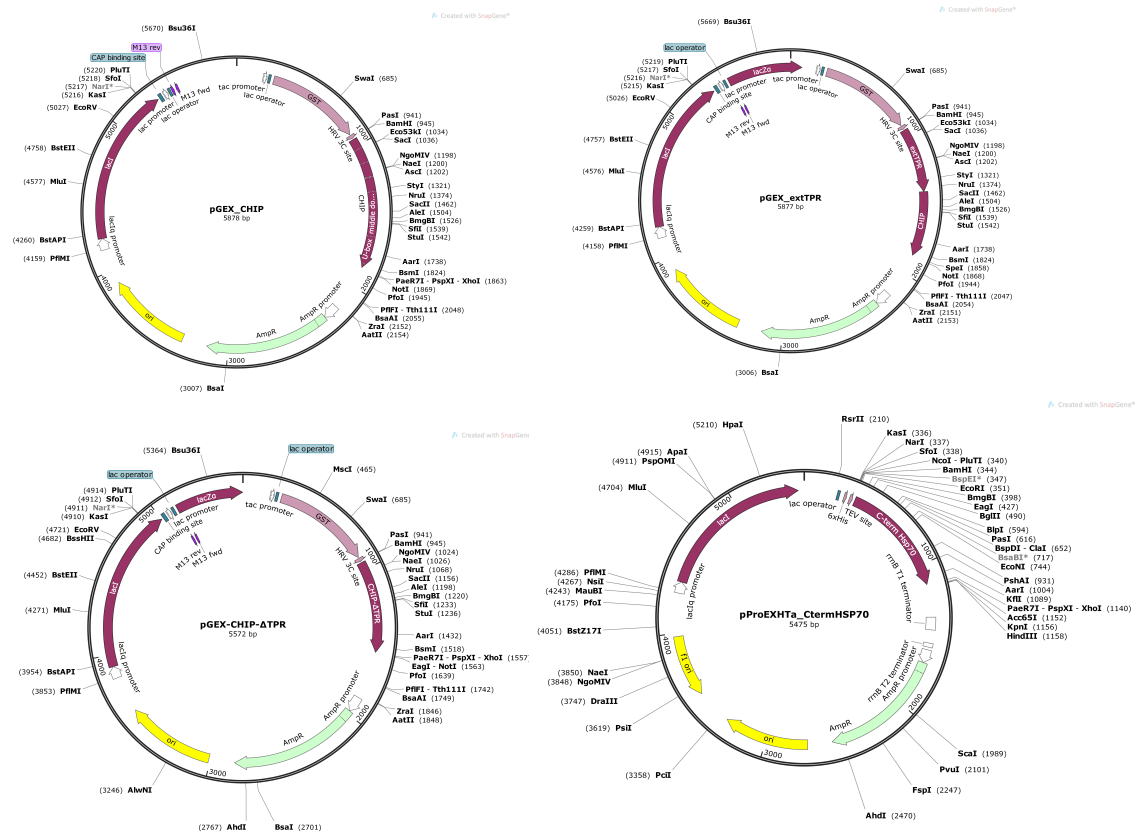


Figure 52. Bacterial expression vectors. Feature annotations and restriction enzyme annotations were generated with SnapGene Viewer.

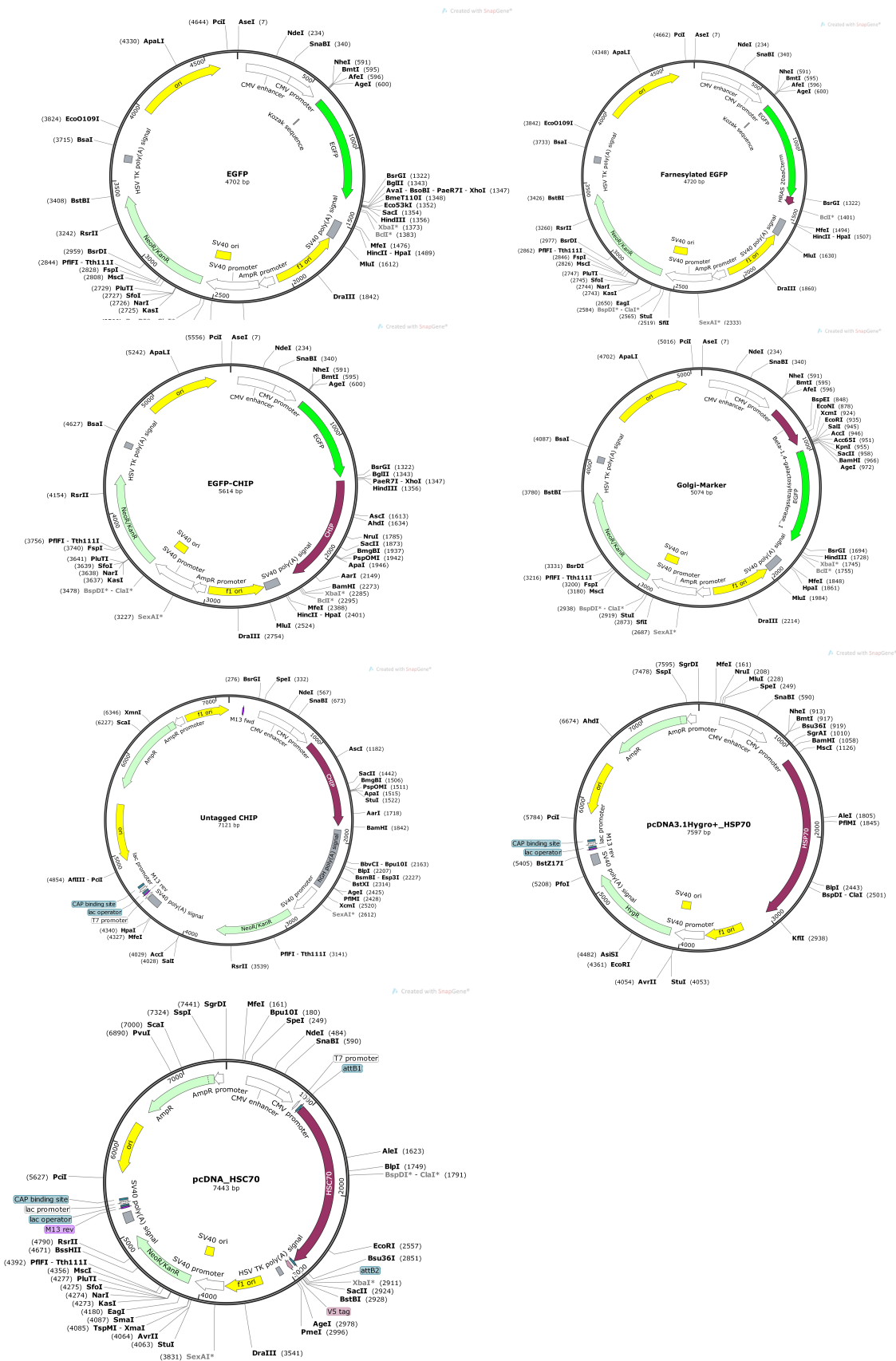


Figure 53. Mammalian expression vectors. Feature annotations and restriction enzyme annotations were generated with SnapGene Viewer.

5.2 Recombinant Protein Purifications

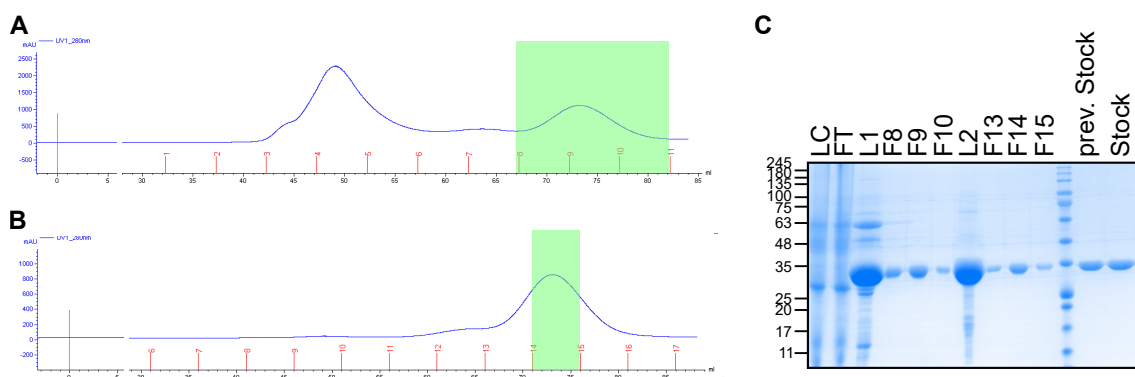


Figure 54. Purification of GST-CHIP. (A) HiLoad Superdex 200 column injected with 2ml GST-cut eluate at a flow rate of 1ml/min in HSP70 buffer. (B) HiLoad Superdex 200 column injected with 2ml pooled fractions (F8, F9, F10) at a flow rate of 1ml/min in HSP70 buffer. Framed in green are fractions that were pooled for processing. (C) Coomassie blue stained gel of the respective purification steps. LC, culture lysate; FT, flow through after GST-agarose incubation; L1, initial loading on Superdex 200; F, fractions 5ml each; L2, second loading on Superdex 200; stock, purified recombinant protein frozen as stock solution.

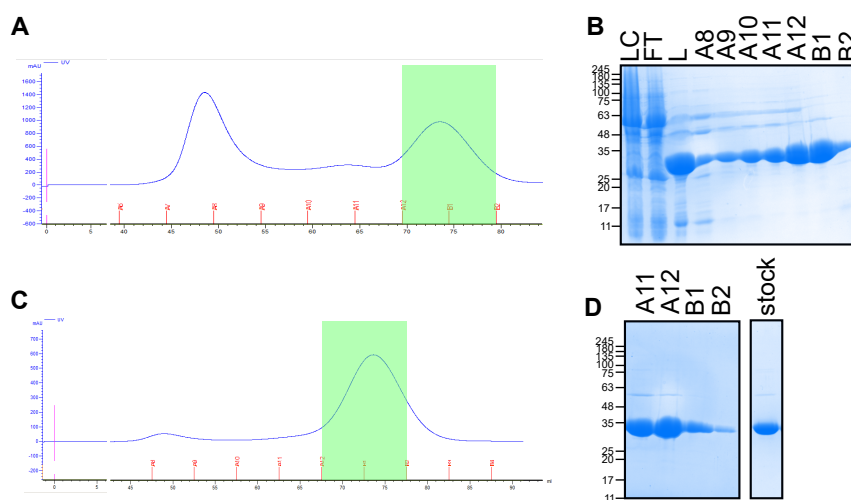


Figure 55. Purification of GST-CHIP-K30A. (A) HiLoad Superdex 200 column injected with 2ml GST-cut eluate at a flow rate of 1ml/min in HSP70 buffer. (B) HiLoad Superdex 200 column injected with 2ml pooled fractions (A12, B1) at a flow rate of 1ml/min in HSP70 buffer. Framed in green are fractions that were pooled for processing. (C) Coomassie blue stained gel of the first purification steps. LC, culture lysate; FT, flow through after GST-agarose incubation; L, loading on Superdex 200; A/B, fractions 5ml each. (D) Coomassie blue stained gel after the second SEC and final stock for storage. A/B, fractions 5ml each.

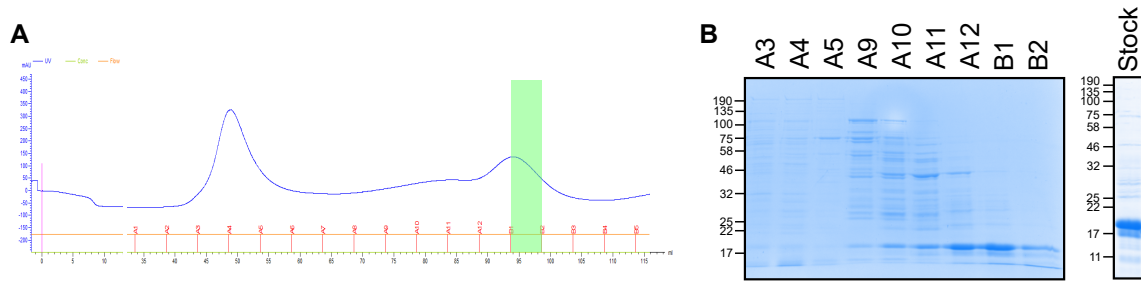


Figure 56. Purification of the His-Ube2W. (A) HiLoad Superdex 200 column injected with 2ml HisTrap eluate at a flow rate of 1ml/min in HSP70 buffer. (B) Coomassie blue stained gel of final SEC before freezing the stock. A/B, fractions 5ml each.

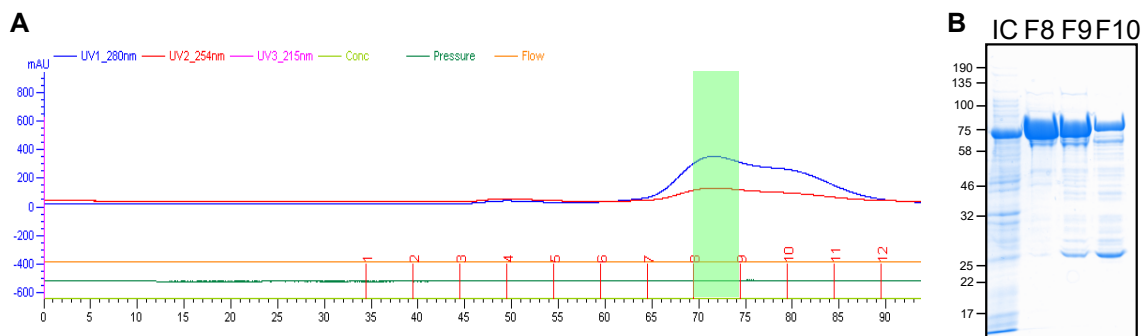


Figure 57. Purification of His-HSP70. (A) Final run of HiLoad Superdex 200 column injected with 1ml concentrated fractions from a previous SEC which was loaded with the HisTrap eluate. Flow rate of 1ml/min in HSP70 buffer. Framed in green are fractions that were pooled for freezing. (B) Coomassie blue stained gel of fractions from final SEC before freezing F8. IC, induced culture; F, fractions with each 5ml.

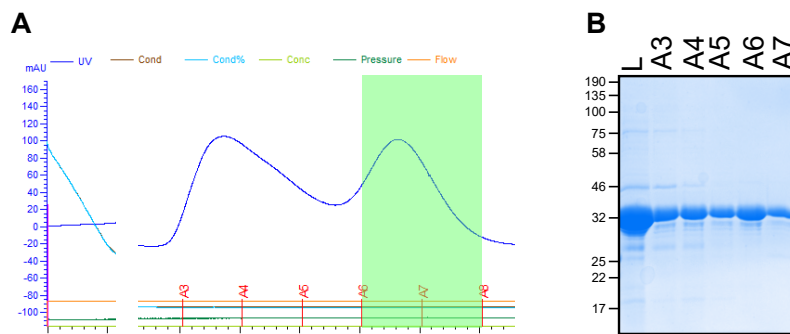


Figure 58. Purification of his-tagged C-terminal HSP70. (A) After initial elution from HisTrap and SEC on HiLoad Superdex 200 column, c-terminal HSP70 was unfolded with 4M Urea and refolded by dialysis O/N at 4°C. Substrate-free c-terminal HSP70 was injected on Superdex75 at a flow rate of 1ml/min in HSP70 buffer. Framed in green are fractions that were pooled for freezing. (B) Coomassie blue stained gel of final SEC for freezing the stock. L, pooled fractions loaded on superdex75; A, fractions A6+A7 pooled for freezing.

5.3 FACS

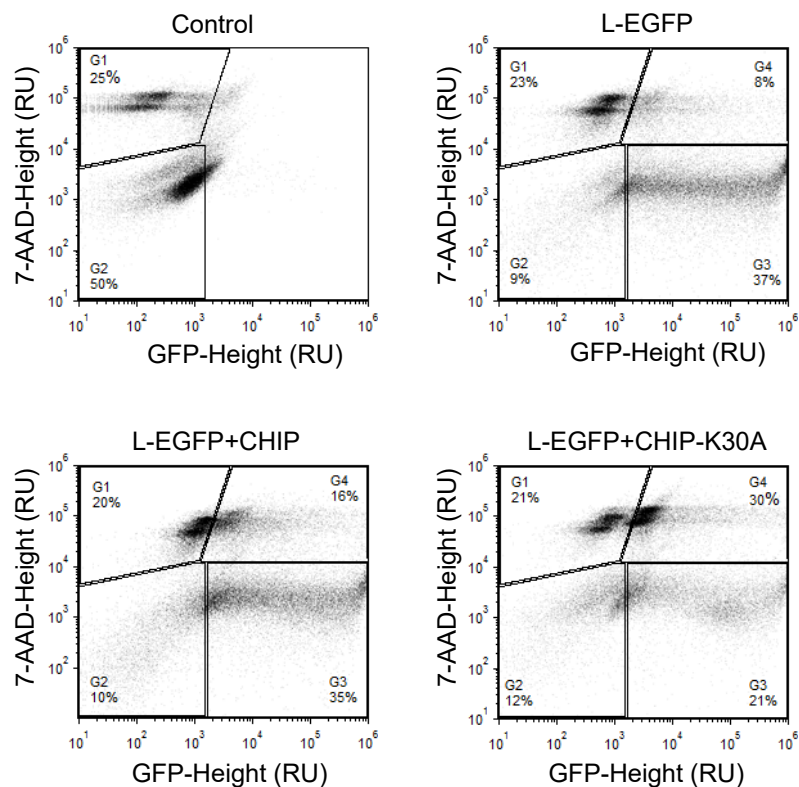


Figure 59. Cell death in CHIP transfected Hek293T (Fig51).

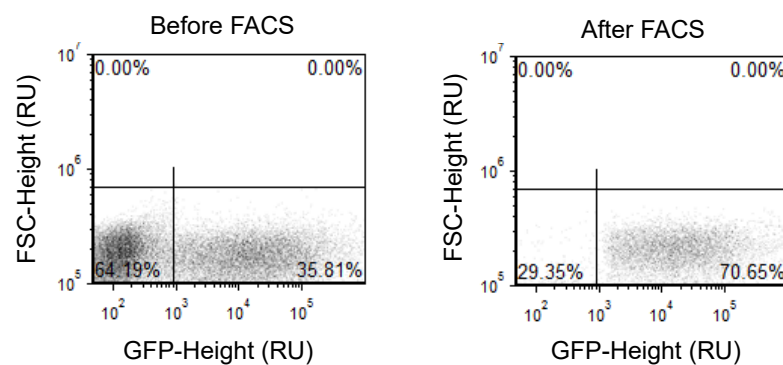


Figure 60. FACS sorting for MS interactome analysis of CHIP (Fig45).

5.4 Microscopy quantification

Table 14. Average cell numbers for quantification

Figure	Condition	av. Count
Fig.11 A	37°C	92,7
	43°C	92,7
Fig.11 A EGFP	37°C	108,3
	43°C	71,7
Fig.12	NT	149,0
	HSP70 inhibitor	108,7
	HSP90 inhibitor	117,0
Fig.13	CHIP	126,3
	CHIP+HSC70	119,3
Fig.14	NT	155,0
	Arsenite	142,0
Fig.18 A	CHIP	157,3
	K30A	126,7
Fig.24 A	control	150,0
	FIPI	128,8
	VU0155069	123,8
	CAY10594	116,3
Fig.24 A EGFP-F	NT	150
	FIPI	128,8
	VU0155069	123,8
	CAY10594	116,3
Fig.24 B	0.1µM 10min	40,33
	0.1µM 20min	40,00
	10µM 10min	45,67
	10µM 20min	46,67
Fig.24 C	K30A NT	93,7
	K30A+IN-10	89,7
	EGFP-F NT	67,7
	EGFP-F+IN-10	65,0
Fig.31	K30A	88,0
	m1	132,0
	m2	32,0
Fig.46 A	control	200,7

	CHIP	211,0
Fig.46 B	MEF WT NT	306,0
	MEF K.O. NT	242,7
	MEF WT HS	222,7
	MEF K.O. HS	196,7
Fig.47 A	control	152,3
	CHIP	146,0
	CHIP+HSP70	131,0
	CHIP+HSP70 Δ D	119,7
Fig.47 B	control	230,3
	CHIP	177,7
	CHIP Δ m2	230,3

Lebenslauf



Name: Dr.* Kopp Yannick
(*laufendes Promotionsverfahren)

Adresse: Burgweg 59, 64807 Dieburg

Geburtsdatum/-ort: 23.04.89, Dudweiler Saarbrücken

Mobil: 0177 3847749

E-Mail: ykopp52@gmail.com

Ausbildung und Studium:

- 01.11.14 – 31.12.19 **(Dr. phil. nat.*) in Biochemie**
Goethe-Universität Frankfurt am Main, Dr. Martin Vabulas
Entdeckung und Charakterisierung der Membraninteraktionen der E3-ligase CHIP und deren physiologischen Auswirkungen.
- 28.08.12 – 30.09.14 **Master of Science (1,4)**
Molekulare Biotechnologie, Goethe-Universität Frankfurt am Main
Masterthesis bei Prof. Dr. H. Bode.
Konstruktion eines kontinuierlichen Bioreaktors und Entwicklung eines spezialisierten Wachstumsmediums für die bakterielle Naturstoffproduktion.
- 04.10.09 – 28.08.12 **Bachelor of Science (1,5)**
Biotechnologie, Hochschule Darmstadt
Externe Bachelorthesis bei Prof. Dr. H. Bode.
Präparation von Naturstoffen aus bakteriellen Extrakten und Strukturaufklärung mittels HPLC-MS und NMR.
- 01.08.08 – 30.06.09 **Zivildienst**
Gustav-Heinemann Schule für praktisch Bildbare, 64807 Dieburg
Pflege und Förderung von geistig und körperlich beeinträchtigten Kindern im Klassenverband und in Einzelbetreuung.

Berufserfahrung:

- 01.11.14 – 31.12.19 **Doktorand, Arbeitsgruppe: „Protein Aggregation“**
Buchmann Institute for Molecular Life Science, Frankfurt am Main bei Dr. Martin Vabulas
Neben meiner Forschungstätigkeit war ich für die Verwaltung der Zelllinien, die Entsorgung der chem. Abfälle und die Gerätebetreuung und Wartung des Fluorescence-assisted-cell-sorter (FACS) zuständig. Desweiteren habe ich mehrere studentische Praktikanten in 2- bis 3-monatigen Praktika betreut.
- 01.07.12 – 30.06.14 **Studentischer Mitarbeiter, Zytotoxizität, Harlan CCR Roßdorf**
Mikroskopische Auswertung zellbasierter Zytotoxizitätstests und Probenvorbereitung in einem GMP-Umfeld. Desweiteren arbeitete ich den angestellten Tierpfleger bei der Pflege der Versuchstiere zu.



Auszeichnungen und Fortbildungen:

- 01.10.12 – 30.09.14 **Deutschland-Stipendium** der Goethe-Universität Frankfurt am Main
- 28.08.14 – 29.08.14 **Workshop:** Intercultural collaboration and communication von hm.cc creative consulting
Verbesserung der Teamfähigkeit durch mehr Verständnis und Toleranz für unterschiedliche Kommunikations- und Arbeitsweisen.
- 30.08.11 – 23.09.11 **Freiwillige Studienarbeit** bei Prof. Dr. Meyer-Almes an der Hochschule Darmstadt.
Inbetriebnahme und Methodenentwicklung eines Fluoreszenzdetektionssystems von LI-COR.
- 01.06.11 – 31.07.11 **Freiwillige Studienarbeit** bei Prof. Dr. Hüttenhain an der Hochschule Darmstadt.
Eigenständige Projektarbeit zur Optimierung enzymatischer Fettsäurenkatalyse und Analytik (GC-MS).

Sprachkenntnisse:

Englisch: Verhandlungssicher

Französisch: Konversationssicher

Mandarin: Grundkenntnisse

Publikationen:

- **CHIP as a membrane-shuttling proteostasis sensor.**
Kopp Y, Lang WH, Schuster TB, Martínez-Limón A, Hofbauer HF, Ernst R, Calloni G, Vabulas RM. *Elife*. 2017 Nov 1;6. pii: e29388. doi: 10.7554/eLife.29388.
- **Pyrones as bacterial signaling molecules.**
Brachmann AO, Brameyer S, Kresovic D, Hitkova I, Kopp Y, Manske C, Schubert K, Bode HB, Heermann R. *Nat Chem Biol*. 2013 Sep;9(9):573-8. doi: 10.1038/nchembio.1295. Epub 2013 Jul 14.
- **Reciprocal cross talk between fatty acid and antibiotic biosynthesis in a nematode symbiont.** Brachmann AO, Reimer D, Lorenzen W, Augusto Alonso E, Kopp Y, Piel J, Bode HB. *Angew Chem Int Ed Engl*. 2012 Nov 26;51(48):12086-9. doi: 10.1002/anie.201205384. Epub 2012 Oct 24.

Hobbys:

Ich spiele Klarinette und Saxophon in zwei projektbezogenen Orchestern und wirke regelmäßig bei der Organisation von Muscialprojekten der angeschlossenen Theater/Sängergruppen (OnStage, Bad König/MusicalFractory, Groß-Umstadt) mit.